ENGINEERING RESEARCH INSTITUTE
UNIVERSITY OF MICHIGAN
ANN ARBOR

THE INSERTION MAGNETRON

A NEW EXTERNAL-CAVITY MAGNETRON FOR LOW-POWER ELECTRONICALLY-TUNABLE OPERATION IN THE 10 TO 20-CM WAVELENGTH RANGE

Technical Report No. 11
Electron Tube Laboratory
Department of Electrical Engineering

BY

JULES S. NEEDLE

Approved by: W. G. DOW

G. HOK

Project M921

CONTRACT NO. DA-36-039 sc-5423
SIGNAL CORPS, DEPARTMENT OF THE ARMY
DEPARTMENT OF ARMY PROJECT NO. 3-99-13-022
SIGNAL CORPS PROJECT 27-112B-0

Submitted in partial fulfillment of the requirements for the Degree of Doctor of Philosphy in the University of Michigan.

August, 1951

ABSTRACT

In this report we consider the design, construction, and performance of a new type of low-power, external-cavity, multianode magnetron for operation in the 10 to 20-cm wavelength range. Special attention is given to the problem of wide-range tunability using either mechanical or electrical methods.

The basic structure of this new magnetron consists of a short hermetically-sealed section of coaxial transmission line which can be used with an external cavity. The sealed-off section contains a multianode structure consisting of six equally spaced radial vanes extending from the inner wall of the outer coaxial cylinder into six longitudinal slots in the inner coaxial cylinder. The cathode is symmetrically located within the inner coaxial cylinder at the position of the multianode structure. This sealed-off structure is used to excite a TEM mode in an external coaxial circuit.

Design equations for a mechanically-tunable coaxial-line resonator are derived and are utilized in the design and construction of a prototype resonator.

Experimental observations of mechanical and electronic tunability are reported for a number of tubes with particular emphasis on the electronic or voltage-tuning aspects. These experimental observations are interpreted in terms of computed circuit properties.

ACKNOWLEDGMENTS

The author wishes to express his appreciation to the members of the University of Michigan Tube Laboratory who have assisted him in the course of this investigation. He is most grateful to Mr. Gunnar Hok for his valuable suggestions resulting from many hours of patient consultation. Thanks are given to Professor W. G. Dow and Mr. H. W. Welch for their encouragement and advice. He is appreciative of the conscientious efforts of Mr. R. F. Steiner in the assembly of the tubes, and is indebted to Mr. N. Navarre for his work on the illustrations.

Personnel of the Laboratory

H. W. Welch	Research Engineers
J. R. Black	
G. Hok	
G. R. Brewer	
J. S. Needle	Instructor of Electrical Engineering
S. Ruthberg	Research Associate
V. R. Burris	Machine Shop Foreman
R. R. Steiner	Assembly Technicians
J. W. Van Natter	
R. F. Denning	Laboratory Machinists
D. L. McCormick	
T. G. Keith	
E. A. Kayser	
N. Navarre	Draftsman
S. Spiegelman	Stenographers
J. Long	

TABLE OF CONTENTS

LIST OF ILLUSTRATIONS

LIST OF ILLUSTRATIONS (Cont'd.)

LIST OF ILLUSTRATIONS (Cont'd.)

LIST OF ILLUSTRATIONS (Cont'd.)

CHAPTER I

INTRODUCTION

1.1 Scope of the Investigation

One of the most serious obstacles in the development of microwave systems and measurement techniques has been the lack of adequate sources of continuously tunable radio-frequency power. The problem dealt with here is aimed toward a partial amelioration of this situation.

In this paper, we consider the design, construction, and performance of a new type of external-resonator multianode magnetron oscillator for producing low-level continuous radio-frequency power in the 10 to 20-cm wavelength region. Special attention is given to the problem of wide-range tunability using either mechanical or electrical methods. Design equations for a mechanically tunable resonator are derived and are utilized in the design and construction of a prototype tunable resonator. Experimental observations of mechanical and electronic tunability are reported for a number of tubes with particular emphasis on the electronic or voltage-tuning aspects. An attempt is made to interpret these experimental observations in terms of computed circuit properties. The usefulness of this new structure as a tool for the study of certain aspects of magnetron operation is demonstrated.

1.2 Limitations of Conventional Microwave Signal Generators

There are two classes of tubes which are commonly employed as microwave signal generators in the 10 to 20-cm wavelength range. These are the disk-seal or lighthouse tube, and the klystron. Both classes of tubes have serious limitations when used as microwave oscillators.

The disk-seal tube is a planar triode in which the connections to the electrodes take the form of disks. This electrode arrangement results in low lead inductance; consequently higher frequency operation is attainable with these tubes than with structures having single or even double wire leads. In addition, the disk seal geometry permits this tube type to be used conveniently in coaxial resonators.

Lighthouse tubes, in conjunction with coaxial-line resonators, are capable of producing continuous power outputs of a few watts at wavelengths as low as 10 cm. Oscillation is obtained by class-C operation utilizing some form of feedback arrangement. The load impedance has an important bearing upon power output and efficiency and, in practice, the coupling between the load and the resonant circuit is adjusted experimentally to give maximum output. Amplitude modulation of disk-seal oscillators may be accomplished by conventional modulation procedures. Frequency modulation is feasible mechanically but not electrically.

When oscillator operation is extended into the higher microwave frequencies electron transit delay increases the input conductance and also introduces a phase shift between the maximum plate current and minimum plate voltage. Within practical limits of design, these effects, together with the increased cavity losses, result in reduced power output and efficiency as the frequency is increased.

The upper frequency limit of the lighthouse tube and similar parallel-plane structures is governed by the relation between interelectrode spacing and electron transit time. In practice, optimum performance of these types is dependent upon the critical adjustment of resonator feedback and loading circuits with resultant operational difficulties. One of the most disturbing features in the operation of disk-seal structures in coaxial wide-range tunable resonator systems is the instability caused by the inherent mode characteristics of the resonator system.

There are two types of velocity-modulation tubes employed as low-power microwave generators. They are, respectively, the double-cavity klystron and the single-cavity or reflex klystron oscillator. The double-cavity klystron, as the name implies, utilizes two resonators; one for electronic bunching, and the other for the conversion of electron energy into radio-frequency power. The reflex klystron, on the other hand, employs a single resonator for both the bunching and the energy conversion processes. The operation of velocity-modulation tubes utilizes electron transit time as a means of bunching electrons, as well as for the production of r-f power. Since electron transit time is a function of both the electrode spacing and the electrode potentials, the operation of velocity-modulated tubes calls for the adjustment of a number of parameters as the frequency is changed. For instance, in the double-cavity klystron, it is necessary to adjust the grid voltage, d-c accelerating voltage, and the tuning of two resonators. The reflex klystron is much simpler to operate than the double-cavity klystron. Oscillations may usually be obtained by adjusting only the accelerator and reflector potentials. The resonance frequency of the cavity is controlled by changing the spacing between the grids of the

resonator. Small frequency variation may be obtained by varying the accelerator and/or the reflector voltage. Frequency variation of the order of 10 to 40 megacycles at 3000 megacycles is obtainable by varying the reflector voltage without retuning the resonator.

The most serious operational difficulties experienced with klystron power sources may be summarized as resulting from (a) the number of variables requiring adjustment, (b) the narrow frequency range covered by self-contained cavity types, (c) the inadequate power output in the case of most reflex oscillators.

A knowledge of the foregoing limitations of the existing low-power microwave sources was largely responsible for the initial impetus to the investigation described herein. The magnetron was the only known type of generator which could possibly satisfy the requirements of adequate continuous radio-frequency power and wide-range tunability in the microwave region with a minimum of operational obstacles. The initial problem was that of deciding on the magnetron structure most suitable for wide-range tunability. In the next section we present the history of magnetron oscillators leading up to the structure chosen for this investigation.

1.3 The Historical Background of the Insertion Magnetron

In 1921 the behavior of electrons in a cylindrical diode in the presence of a magnetic field was investigated by A. W. Hull[1]. The work of Hull provided the basis for much of the theory of magnetron operation. No further significant progress was made until 1924, when Habann[2] showed that a coaxial diode with an axial magnetic field and an anode split into two halves parallel to the axis could be used to produce r-f power. The r-f circuit was attached between the two anode segments and operation as an

oscillator was obtained by virtue of the static negative resistance characteristic of the device. If the transit time of the electrons from cathode to anode is small relative to the period of r-f oscillation, then under certain conditions, the orbits of the majority of electrons terminate on the anode segment of lower potential, irrespective of the segment toward which they start[3]. The electrons are therefore capable of gaining energy from the d-c field and traveling against the r-f field, thereby giving energy to the r-f field. Efficiencies of the order of 25 per cent, and r-f outputs as large as 100 watts at 600 megacycles have been attained. This type of magnetron requires the use of a high magnetic field for operation in the microwave region and is therefore less desirable than other types.

In 1924, A. Zacek[4] disclosed that oscillations between the anode and cathode of a smooth-bore d-c magnetron could be obtained with magnetic fields near the cutoff value of magnetic field. These oscillations occur at a frequency termed the cyclotron frequency, which is given by the relation

$$\omega_c = \frac{eB}{m} , \qquad (1.1)$$

where

ω_c = The cyclotron angular frequency

e = the electronic charge in coulombs,

B = the magnetic field in webers per square meter, and

m = the electronic mass in kilograms.

Cyclotron-frequency magnetrons were later built with split anodes with the same criterion for oscillation, that is, a resonance between the r-f field and the rotational component of the electron motion. Efficiencies of 10 to 15 per cent have been obtained and wavelengths as low as 6.4 millimeters

have been reached[5]. The inherent drawback in the cyclotron-frequency oscillator is the difficulty of removing electrons from the interaction space after they gradually fall out of phase with the r-f field. If the electrons are not removed from the interaction space after falling out of phase with the r-f field, they begin to take energy from the a-c field and never reach the anode.

In a paper[6] by K. Posthumus in 1935, a third type of magnetron oscillation similar to negative-resistance oscillation was disclosed. This new type of oscillation, termed traveling-wave oscillation, differs from the negative-resistance type only in the ratio of angular frequency of the r-f traveling wave around the anode structure to that of the cyclotron frequency given by $\omega_c = eB/m$. In the negative-resistance oscillator, the ratio of the angular frequency of the traveling wave is small relative to the cyclotron frequency; therefore, in terms of a cyclotron-frequency time scale, the traveling wave is essentially stationary. In the traveling-wave magnetron, the magnetic field required for the generation of a particular frequency is much lower than that needed to produce negative-resistance oscillations. Posthumus[6] attained efficiencies as high as 60 to 70 per cent with a four-anode traveling-wave magnetron and presented the first theory of the traveling-wave magnetron. The basic relation given by Posthumus for the conditions in a traveling-wave magnetron between the electrons and the r-f field is

$$\frac{\omega r_a}{n} = \frac{E_a}{\frac{r_a}{2} B} \qquad (1.2)$$

Here

ω = 2π x frequency,

n = the number of pairs of anodes,

F_a = the anode potential, (volts)

r_a = the radius, (meters)

B = the magnetic field, (webers/meter^2).

Thus, the mean translational velocity of the electrons should be in close agreement with the linear velocity of the rotating wave.

In a paper[7] by F. Herringer and F. Hülster, the effect of the radial component of the traveling-wave r-f electric field was recognized as the agent which maintains the proper phase between the electrons and the wave.

The most noteworthy development after the discovery of traveling-wave oscillation took place during the early part of World War II when the British constructed a self-contained multianode, multicavity traveling-wave magnetron for 10-cm operation. Thereafter, a feverish development program began on this type of magnetron in order to satisfy the requirements of microwave high-definition radar systems. Many excellent papers[8] on both the theory and performance of multianode, multicavity magnetrons appeared in the form of classified reports during the war and have since been assimilated and put into texts[9]. Hartree, Stoner, Slater, Brillouin, and Rieke are generally associated with the major developments in the theory and concepts of traveling-wave magnetron operation. Pulsed and c-w magnetron development continued after World War II with the emphasis directed toward more efficient and more widely tunable multianode, multicavity magnetrons.

The first departure from the multicavity magnetron structure occurred during the early part of World War II when the British developed an interdigital magnetron (See Fig. 1.1) for pulsed communication. Development of a similar structure in the United States, under the name Donutron, or interdigital magnetron, took place during the war development program and is still being continued.

An interdigital magnetron, using an external cavity, was produced by the Sylvania Electric Company[10] and work is being conducted on a tunable interdigital magnetron at the University of Illinois.

In March, 1944, R. J. Bondley of the General Electric Company applied for a patent[11] on a new type of magnetron structure. This magnetron utilized a single-resonator cavity which was formed by a coaxial line closed at each end. The resonator was excited by a system of vanes extending from the inner wall of the outer conductor into slots in a tubular coaxial center conductor. The cathode was located within the tubular center conductor and was symmetrically located with respect to the vane and slot system.

In August, 1948, G. Hok, of the University of Michigan, proposed a structure physically similar to that of Bondley's but in which a different principle of operation was indicated. The first self-contained non-tunable magnetron of this type was designed by H. W. Welch of the University of Michigan Engineering Research Institute, and several models were built and tested. Power outputs at 14 cm in the order of 100 to 250 watts at efficiencies of 50 to 60 per cent were attained with these structures[12]. In May, 1950, Mr. Welch suggested the application of this structure to the present investigation and consideration was thereafter given to

the design and construction of such a low-power external-cavity magnetron tunable from 10 to 20 cm.

At about this time, Wilbur and his collaborators at General Electric, reported[13] on a new type of magnetron operation which was named voltage-tunable operation. This is an electronic method of frequency control accomplished by utilizing a low-Q resonator and operating the cathode under temperature-limited conditions. The magnetron anode structures employed were of the split-anode variety, operating into a parallel transmission-line resonator in the frequency range below 1000 megacycles per second. After the appearance of the report by the General Electric Group on the voltage-tuning phenomenon, the decision was made to attempt, in this investigation, to extend the frequency range of this type of operation into the microwave region.

1.4 Description of Traveling-Wave Magnetron Operation

Before considering the concepts of traveling-wave operation it is convenient to classify the magnetron structures which are now in existence. A traveling-wave magnetron may be defined as a two-element vacuum tube, usually of cylindrical geometry, which is operated with a constant and substantially uniform axial magnetic field and a radial d-c electric field. Magnetron cathodes are made in either the directly or indirectly heated variety and, in practically all instances, are constructed so as to emit electrons radially outward. All magnetron anodes have in common a cylindrically symmetric system of axially-directed, equally-spaced bars.

The anode bars, or segments, form part of a r-f circuit and serve as its input terminals as well as the boundary for the interaction space

between the anode and cathode. The major distinction between different traveling-wave magnetrons lies in the form of the resonator employed.

Magnetrons are classified in accordance with the resonator employed as follows:

(a) split-anode magnetrons,

(b) multicavity, multianode magnetrons, and

(c) interdigital multianode magnetrons

Multicavity magnetrons are further subdivided into types insofar as their resonator geometries differ. Fig. 1.1 schematically illustrates the different classes mentioned above, in addition to the subclasses of the multicavity magnetron. The vane magnetron system will be particularly important in a subsequent section of this paper. Both the split-anode and interdigital magnetrons are easily adaptable for external resonator use and are therefore readily applicable to wide-range tunable operation. The structure which forms the basis of this investigation has been given the name vane-and-bar magnetron. The essential features of the geometry are shown in Fig. 1.2. The vane-and-bar system may be thought of as an excitation unit for an external coaxial-line resonator.

The basic concepts pertaining to the electron to r-f field interaction, in a traveling-wave magnetron, are identical for all of the magnetron classes listed above. Thus, if two magnetrons have the same cathode radius, anode radius, and cathode-emitting length and if both have an identical number of anode segments and spacing between anodes, then the electron to r-f field interaction equations for both will be identical. The significant differences between the two oscillators will be caused by

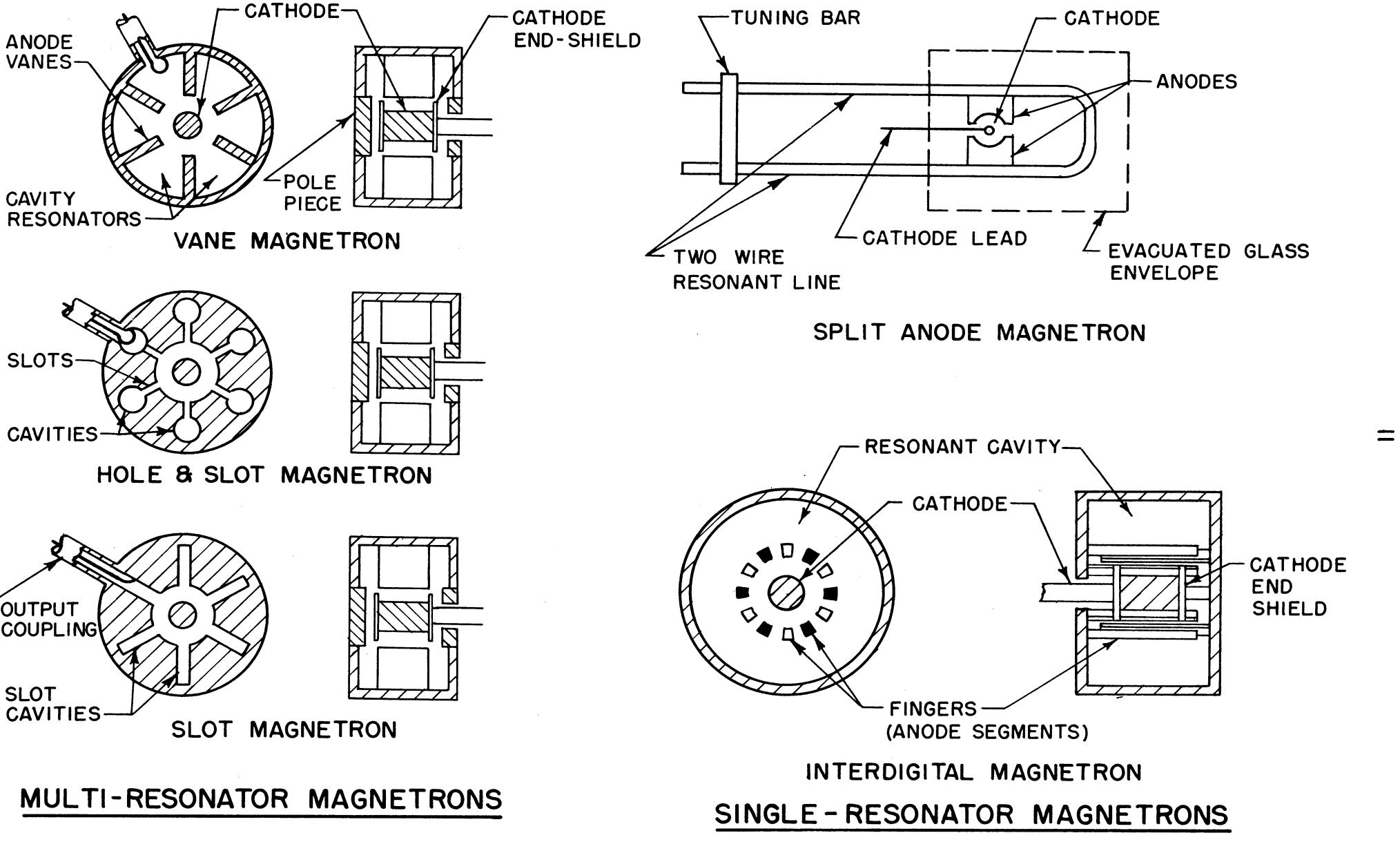

FIG. 1.1 TRAVELING WAVE MAGNETRONS

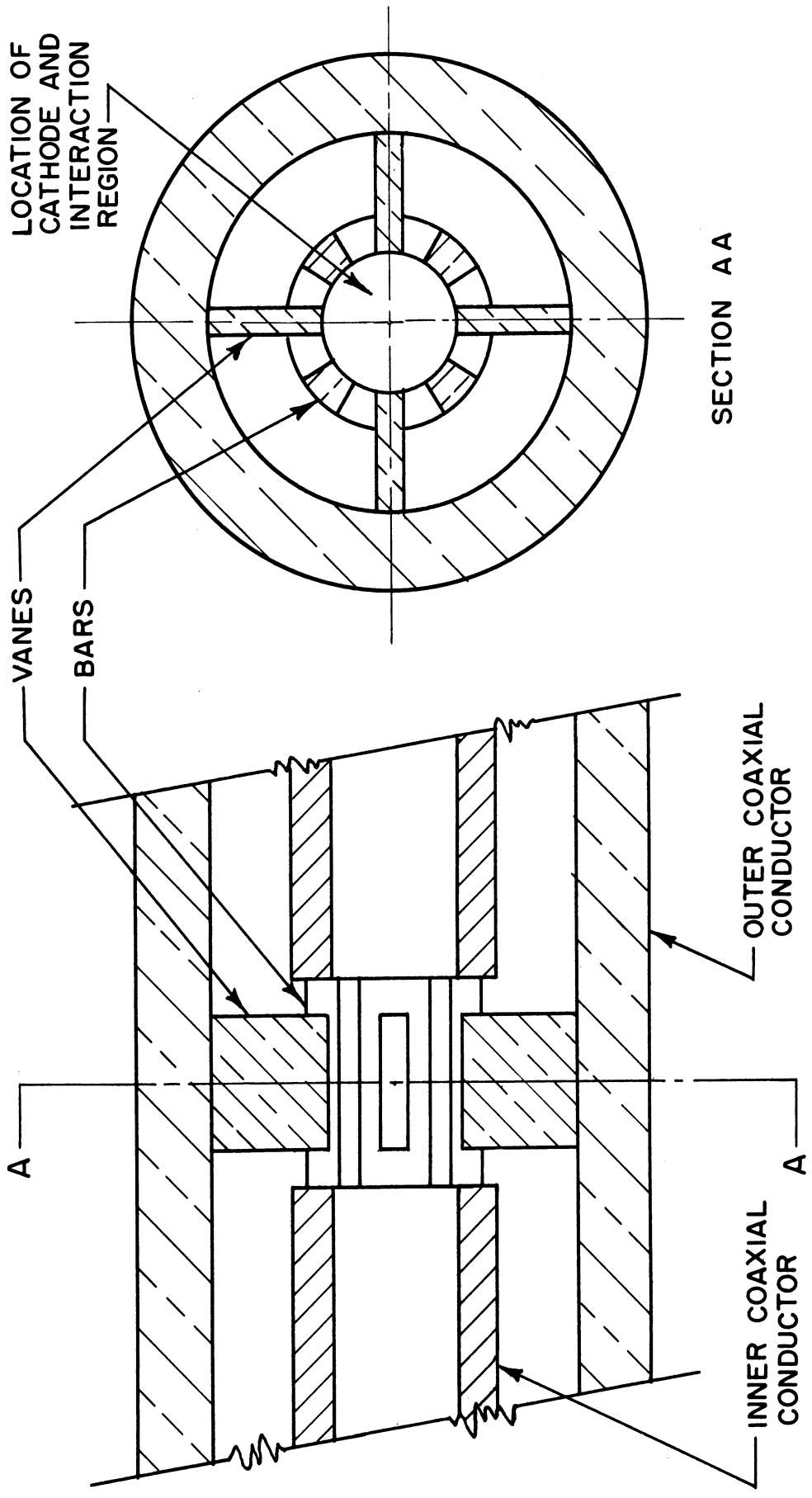

FIG. 1.2
THE VANE-AND-BAR MAGNETRON GEOMETRY

the properties of their respective resonators. In this section, we consider those relations which pertain to the operation of all traveling-wave magnetrons insofar as the interaction space or region between the cathode and anode alone is concerned.

If radio-frequency effects are omitted then the interaction space is a region in which the electrons emitted from the cathode are acted upon by a radial d-c electric field and a constant and uniform axial magnetic field. One may obtain a concept of the situation in the non-oscillating cylindrical diode magnetron by utilizing the results of the space-charge-free analysis for a planar diode magnetron[14]. The planar-magnetron analysis shows that the electron motion can be interpreted as a circular motion with angular velocity eB/m superposed on a rectilinear drift of velocity $\mathcal{E}/B$.

Here

e = absolute value of the electronic charge (coulombs)

m = electronic mass (kilograms)

B = magnetic flux density (webers/meter ^{2})

$\mathcal{E}$ = electric field intensity (volts/meter)

If the electrons start from the cathode with zero initial velocity, the orbits of the electrons are cycloids, and the maximum departure of the electrons from the cathode is given by $\frac{2m}{e}\frac{\mathcal{E}}{B^2}$. For initial velocities other than zero, the electron orbits are such trochoids that the radius of the circular motion, or rolling circle, is consistent with the conservation of the initial energy. These relations are applicable to the cylindrical space-charge-free magnetron when the ratio of cathode-to-anode radius is close to unity, but must of course be modified for smaller ratios. However,

the concepts of a drift velocity around the cathode and a maximum departure boundary for the electron orbits are correct even for small cathode-to-anode ratios. Inclusion of space-charge effects in the analysis changes the potential distribution and complicates the calculations of the actual electron orbits. There is still some question as to the actual electron orbits in a non-oscillating cylindrical magnetron. Two orbital solutions are given in the literature[15]. Circular orbits concentric with the cathode give the "single-stream" or Brillouin solution of the space-charge equations, whereas orbits of cycloidal character give the "double-stream" solution. "Double-stream" solution implies electron motion both toward and away from the cathode.

Other properties of the interaction space may be gleaned regardless of the exact nature of the electronic orbits. A relation for the potential at the edge of the space-charge cloud in the cylindrical diode magnetron may be derived by means of the laws of conservation of energy which are valid regardless of the potential distribution inside the cloud. Assuming there is no electron-electron interaction, the relation between the potential E_h at the space-charge boundary and the radius r_h of the space charge is:[16*]

$$E_h = \frac{eB^2 r_h^2}{8m} \left[1 - \left(\frac{r_c}{r_h} \right)^2 \right]^2 . \qquad (1.3)$$

Here

E_h = potential at radius r_h (volts)

r_h = radius to the space-charge boundary (meters)

r_c = cathode radius (meters)

* See Appendix A-1 for the derivation of this equation.

e = absolute value of the electronic charge (coulombs)

B = magnetic-flux density (webers/meter^2)

m = electronic mass (kilograms)

The electron energy was assumed to be zero at the cathode in this derivation. Equation (1.3), when $r_h = r$ and $E_h = E$, gives the potential distribution inside the space charge providing the electrons are restricted to concentric orbits, i.e., (no radial motion). The potential difference between cathode and anode for which current just begins to flow (Hull cutoff potential) is given by this relation if E_h is set equal to the anode potential E_a and r_h is set equal to the anode radius r_a. Normal oscillator operation of all multianode magnetrons takes place at voltages lower than the "Hull cutoff potential"for a fixed magnetic field, or at magnetic fields higher than that given by the Hull relation for a fixed voltage. The region of operation is illustrated in Fig. 1.3.

The concepts of the operation of an oscillating magnetron may be obtained from the following physical picture. Consider the magnetron interaction space as shown in Fig. 1.4. Let us assume that the space-charge density is negligible and that an r-f field already exists between the anode segments such that there is a phase difference of π radians between adjacent segments. This mode of operation of the anode structure is commonly referred to as the "π mode". The r-f field may then be considered either as a standing wave in space or as a combination of two traveling waves rotating in opposite directions. Fig. 1.4 shows qualitatively the trajectories for electrons leaving the cathode under three different conditions[17]. Orbit 1, which serves as a reference orbit, is for the case of zero r-f voltage, with d-c voltage and magnetic field, such as to give

below-cutoff operation. In orbit 2, the electron has entered the r-f field at a time such that it is accelerated by the field and returns to the cathode with an energy larger than its initial energy. The energy absorbed from the r-f field by this electron is therefore converted into heat energy at the cathode. The common terms applied to this situation are "back heating" or "back bombardment". Trajectory 3 represents the path taken by an electron which leaves the cathode at a time such that, on the average, it gives energy to the r-f field. The requirement here is that the electron move against the r-f field in order to give up energy and be collected on the anode. According to this simplified physical picture, the "phase" of the electron with reference to one of the component traveling waves, determines whether the electron shall remain in the interaction space and convert d-c energy into r-f energy, or whether it shall be forced back into the cathode as a result of the energy gained from the r-f field. It is of importance to note that for orbit 3, the kinetic energy of the electron at a particular point is less than the potential energy corresponding to the instantaneous potential. For instance, the kinetic energy at point R may be zero. The energy of the electron when it reaches the anode may be only a small fraction of that corresponding to the anode potential. The difference between the electron arrival energy and the energy corresponding to the anode potential is the energy transferred to the r-f field.

Although the details of the orbital picture given above are incorrect since space-charge effects are neglected, the concepts of electron-sorting and energy-conversion mechanisms are nevertheless applicable to the more complex situation which exists in the interaction space. It should

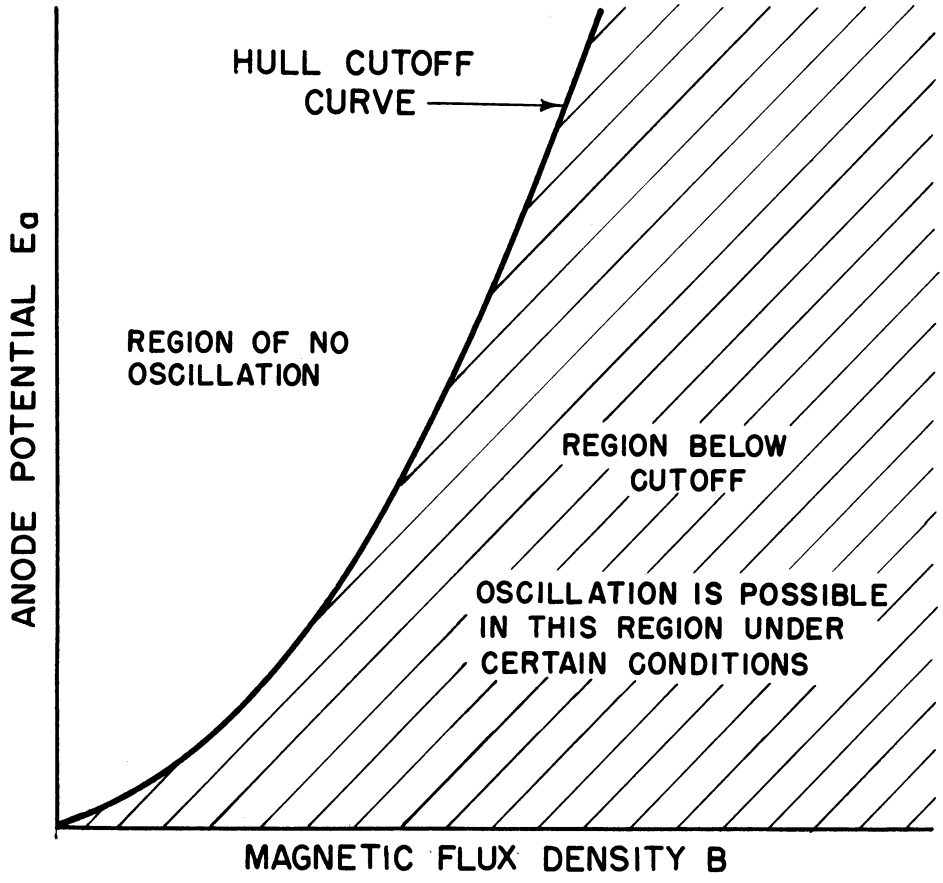

FIG. 1.3
SKETCH SHOWING THE HULL CUTOFF CURVE AND THE REGION IN WHICH OSCILLATION MAY BE OBTAINED.

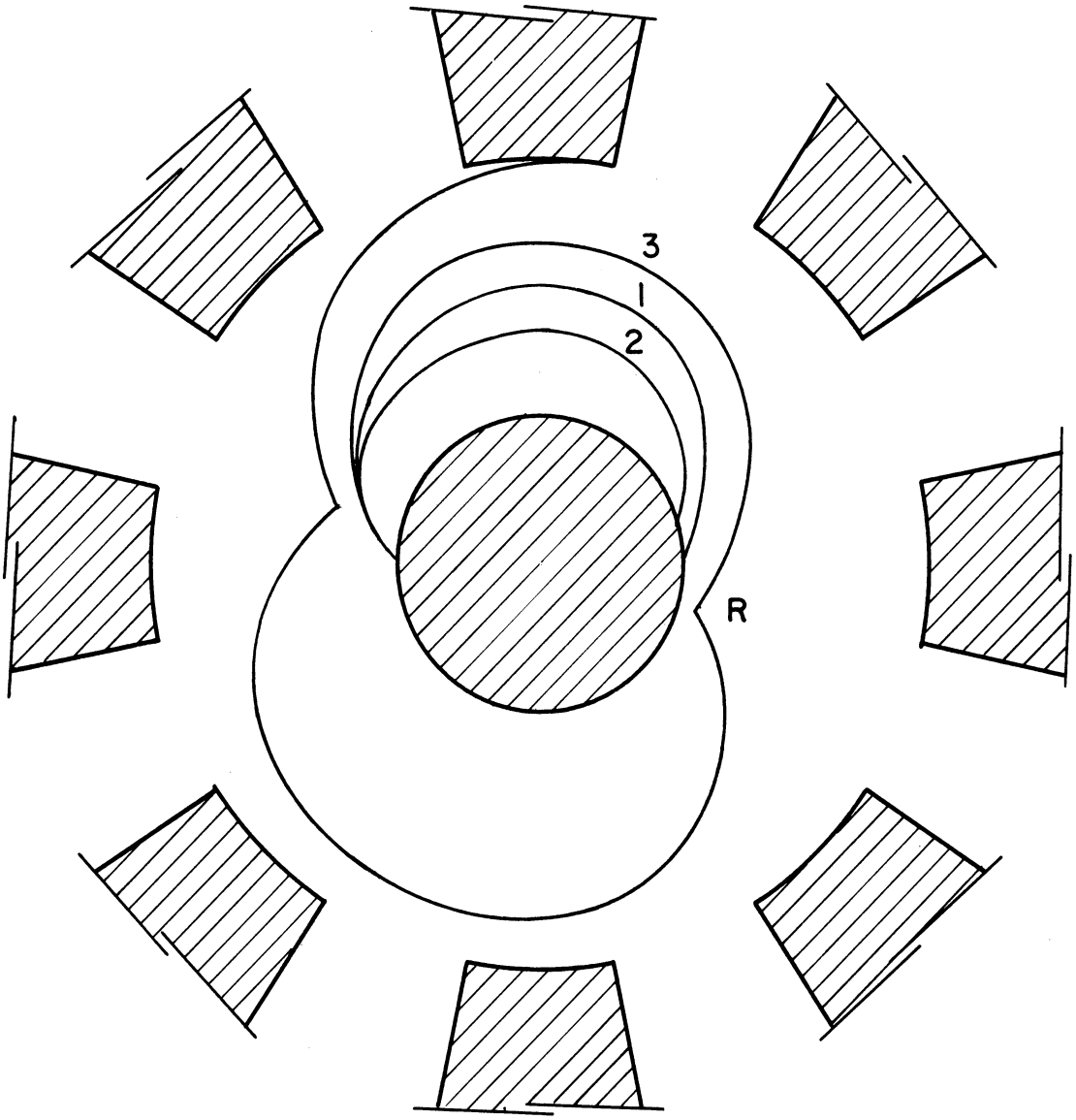

FIG. 1.4
SKETCH SHOWING TYPICAL ELECTRON ORBITS
IN A MAGNETRON. (SPACE CHARGE NEGLIGIBLE)
FROM WILLSHAW et al [17]

be clear that if the energy-conversion process is as indicated above, electrons may be able to reach the anode even though the magnetic field is significantly greater than the Hull cutoff value and the amplitudes of the rotating r-f field components are small.

Hartree is credited with the initial derivation of the threshold condition for oscillation in a traveling-wave magnetron. This derivation, which took space-charge effects into account resulted in the relation*

$$E_H = \frac{1}{2} eB\omega_n(r_a^2 - r_c^2) - \frac{1}{2} m\omega_n^2 r_a^2 . \qquad (1.4)$$

Here E_H = The threshold or Hartree potential. This is the anode potential below which oscillation cannot occur. (volts)

e = The absolute value of the electronic charge (coulombs)

m = The electronic mass (kilograms)

B = The magnetic-flux density (webers/m^2)

r_a = The anode radius (meters)

r_c = The cathode radius (meters)

ω_n = $\frac{2\pi f}{n}$ where f is the frequency in cycles per second and n is the mode number. The mode number n is the number of full interaction space wavelengths existing around the anode.

The Hartree equation will subsequently be employed in the discussion of the design of the magnetron that forms the nucleus of this investigation. It will also be important in the study of electronic tuning. For the latter application of the Hartree relation, we shall find it more convenient to write this equation in terms of the frequency. For one of the important cases, that for which the phase difference between r-f potentials of adjacent segments is π radians (the π mode), the mode number n

* See Appendix A2 for a derivation of this equation.

is equal to half the number of anode segments, or

$$n = \frac{N}{2} \tag{1.5}$$

The Hartree relation can be written as follows by using the binomial equation:

$$\omega_n = \frac{eB}{2m}\frac{(r_a^2 - r_c^2)}{r_a^2} \pm \sqrt{\left(\frac{eB}{2m}\right)^2 \left(\frac{r_a^2 - r_c^2}{r_a^2}\right)^2 - \frac{2e}{m}\frac{E_H}{r_a^2}} \tag{1.6}$$

The use of series expansion for the second term gives the following relation for frequency if all terms having potential to greater than the second power are dropped:

$$n\frac{\omega_n}{2\pi} = f \cong \frac{nE_H}{\pi(r_a^2 - r_c^2)B}\left[1 + \frac{2m}{e}\frac{r_a^2}{(r_a^2 - r_c^2)^2}\frac{E_H}{B^2}\right] \tag{1.7}$$

This procedure is justified since, for the range of magnetic fields and potentials considered here, the series converges rapidly. For large values of B the relation between frequency and anode potential is seen to be linear.

Wilbur and his collaborators[13] have shown that, for temperature-limited conditions, the frequency of a magnetron obeys the relation (1.4) providing the resonator employed is heavily loaded, i.e., low-Q operation.

A presentation of the basic principles of magnetron operation would not be complete without some discussion of the role of the radial component of the r-f field[7]. From Eq (A1-9), Appendix A-1, one readily finds that the important forces on the electron in typical magnetrons are those due to the magnetic field and the electric field. The centrifugal force

is of the order of a few per cent of the electric or magnetic forces. Thus the translation velocity of the "rolling circle", even in the cylindrical geometry, is given approximately by the relation

$$v_{trans} \cong \frac{\mathcal{E}}{B} \tag{1.8}$$

This is the component of electron velocity which interacts with the tangential component of the r-f field in the case of an oscillating magnetron. The relation above for velocity indicates that, since the d-c electric field is a function of the radius, in a cylindrical magnetron, the translational electron velocities will be different at different radii.

The effect of the radial component of the r-f field is easily shown with the aid of Fig. 1.5[18]. In a rotating frame of reference, an electron at point A will have a radial component of r-f field force acting on it in addition to that of the d-c electric field; the net effect being an increase in translational velocity. An electron at point B, on the other hand, will be acted upon by an instantaneous total electric field smaller than the d-c field and will therefore suffer a decrease in translational velocity. The net result of the radial components of the r-f field action upon electrons of different translational velocities is a grouping of electrons in region D which allows the electrons to transfer a maximum of energy to the r-f field by interaction with the tangential r-f components. The mechanism discussed above is often called "phase focusing".

The accepted physical picture[19] of the nature of the space-charge configuration is that of a hub of space charge surrounding the cathode, and a system of spokes, which travel in synchronism with one of the traveling-wave components of the r-f field. A sketch of the generally accepted

space-charge configuration in an oscillating magnetron is shown in Fig. 1.6.

For the customary type of magnetron operation, the frequency of operation is primarily determined by the resonant system of the circuit. There is an energy transfer from the electrons to the circuit (or field) when the electron translational velocities correspond to the velocity of one of the traveling-wave components of the r-f field. After the rotating electrons are brought into synchronism with the traveling wave, any further increase in anode d-c potential results in an increase in r-f voltage and an increase in d-c current into the magnetron. The r-f voltage is sufficient to maintain the synchronism in spite of the increase in d-c voltage, up to a maximum current called the upper-mode-boundary current. This maximum current is less than the "one-half Allis current"* and appears to be a function of many variables.

As the anode potential is raised, it is found that the power input and power output increase, and the frequency also increases. The frequency increase is generally known as pushing. The frequency increase per unit of d-c current is known as the pushing figure and is usually larger for more heavily loaded circuits.

Recently Wilbur and his collaborators at the General Electric Company have shown that, for operation with a temperature-limited cathode and low-Q circuit, the frequency of the magnetron can become independent of the resonant system and follow the voltage-frequency relation given by the Hartree equation. The frequency range which Wilbur et al covered in their investigations was below 1000 megacycles per second. The resonant

* See Appendix A, Sec. A.3.

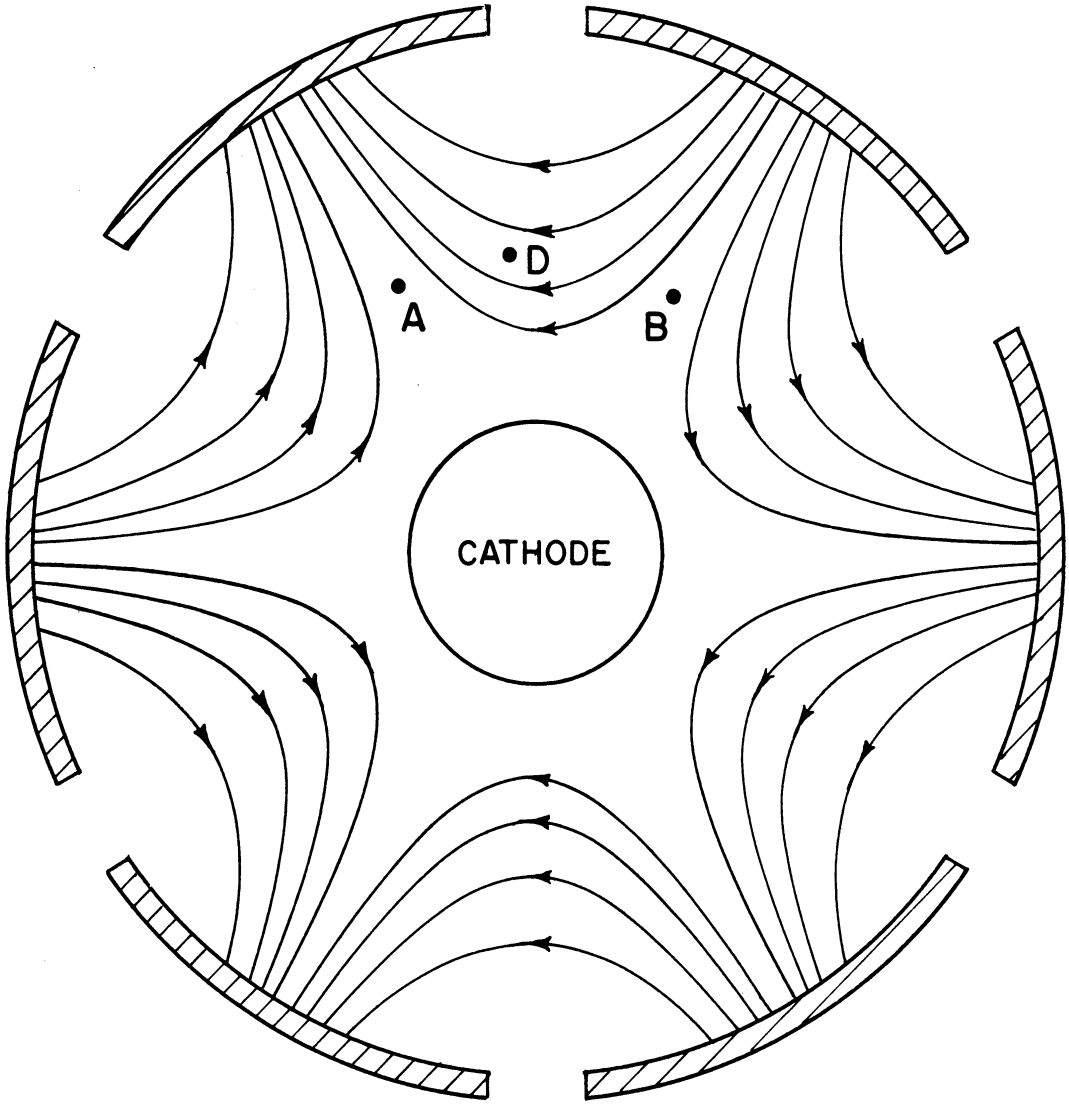

FIG. I.5

DIAGRAM TO SHOW THE PHASE FOCUSING ACTION OF THE RADIAL COMPONENT OF THE RF FIELD

ARROWS REPRESENT DIRECTION OF FORCE ON ELECTRON. DRIFT MOTION OF THE ELECTRONS IS IN CLOCKWISE DIRECTION.

FROM DOEHLER[18]

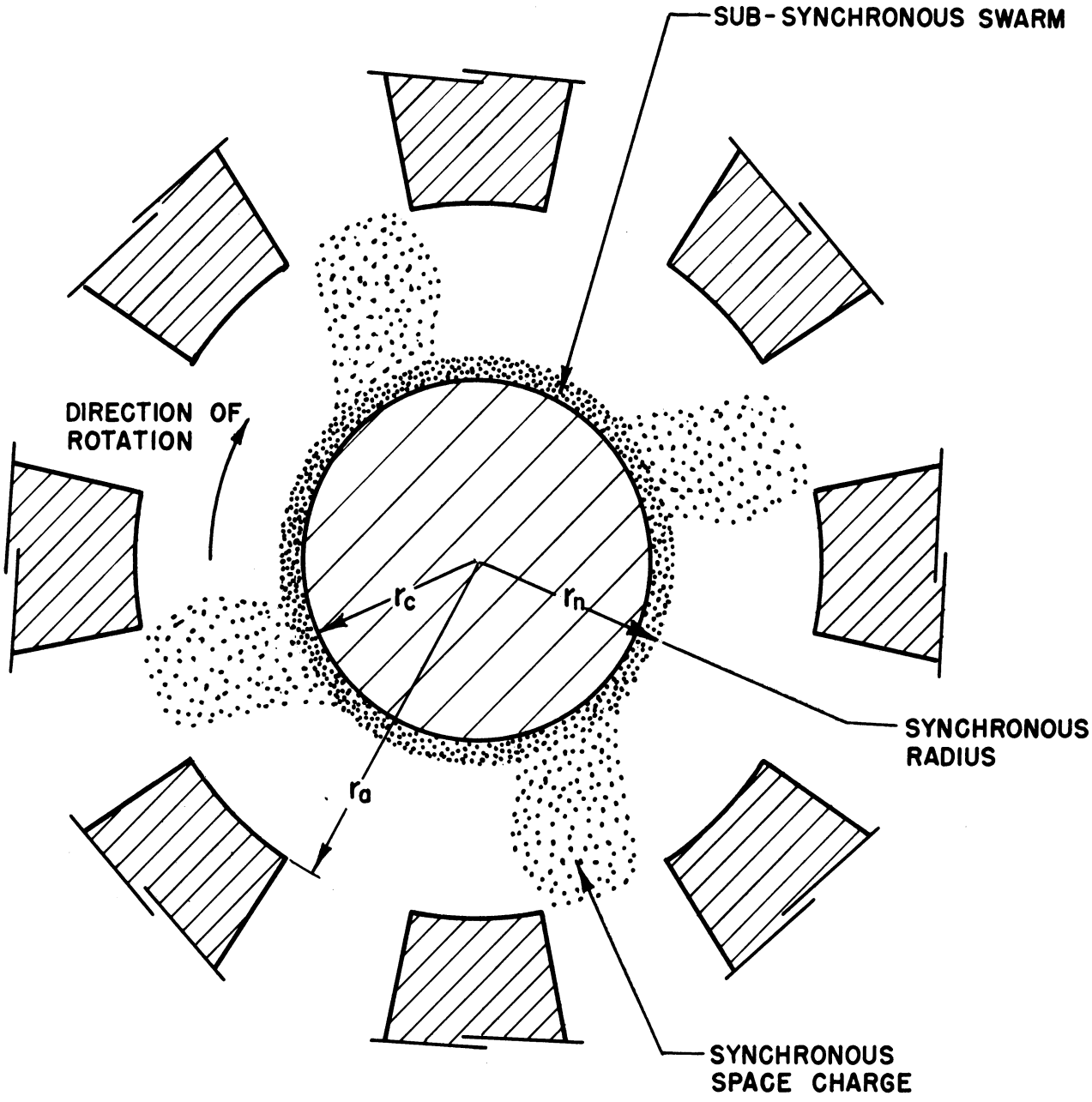

FIG. 1.6
GENERALLY ACCEPTED PHYSICAL PICTURE OF THE SPACE CHARGE CONFIGURATION IN AN OSCILLATING MAGNETRON (π MODE OPERATION)[19]

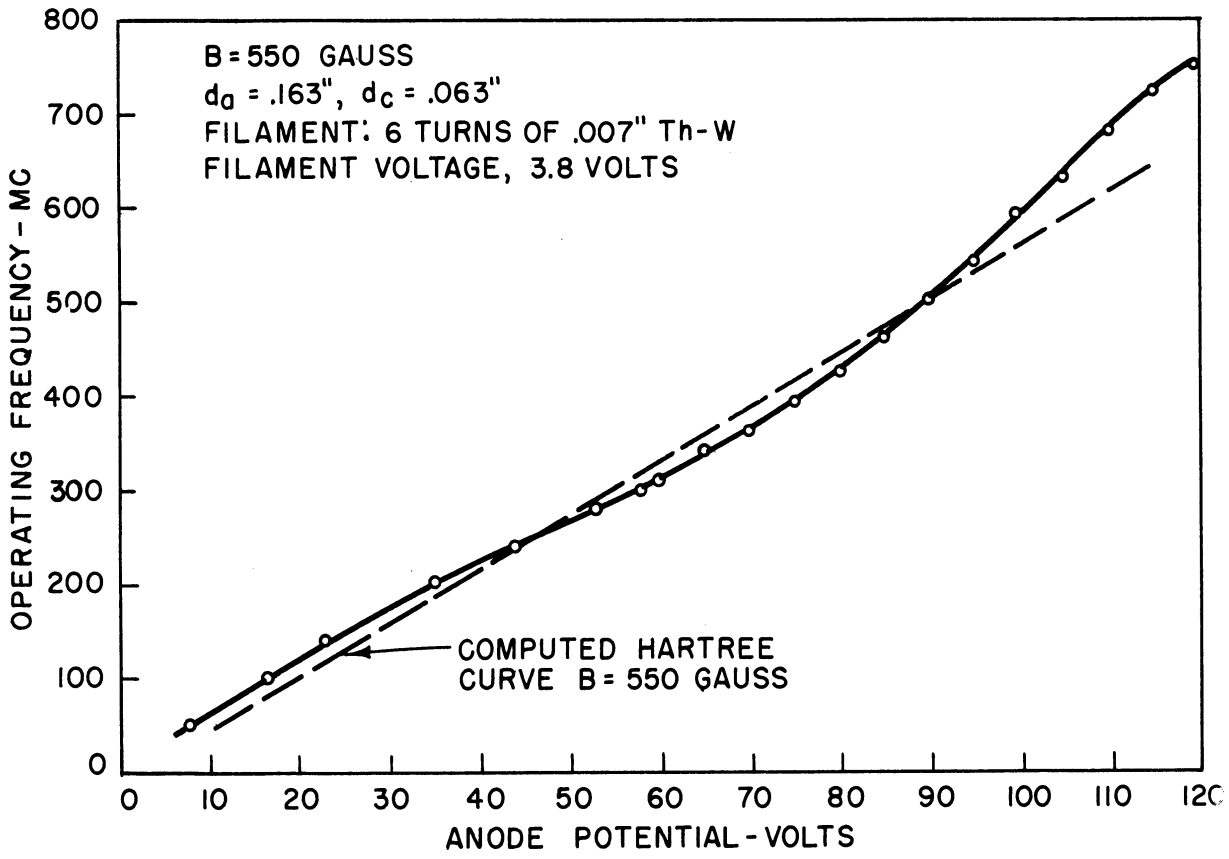

FIG. 1.7

G.E. 6-VANE MINIATURE MAGNETRON
VOLTAGE TUNING CHARACTERISTIC.

systems employed were two-wire lines with a resistive load consisting of carbon resistors. Fig. 1.7 shows the typical performance attained by Wilbur and his group with a multisegment anode structure and an external low-Q tank circuit. The correspondence between the experimental voltage-frequency characteristic and the theoretical Hartree relation is excellent over the frequency range considered.

The material which follows is presented in substantially the order in which the present investigation was conducted.

In Chapter II we discuss the procedure employed in the design of the interaction space of the insertion magnetron.

In Chapter III we consider the mechanical design of the first model of this magnetron and the modifications which were incorporated in subsequent models.

In Chapter IV we consider the thermal problems which are related to the maximum permissible power input to the magnetron.

The parameters of interest in the design of an external coaxial resonator for the insertion magnetron are determined in Chapter V. Two cases of interest are considered. These are:

(a) The case of a coaxial resonator system which is symmetrically disposed about the interaction space.

(b) The case of assymetrical disposition.

Experimental results for high-Q, low-Q, and intermediate-Q operation are presented in Chapter VI. The ranges of Q are divided as follows: (a) High-Q - larger than 100, (b) Intermediate-Q - between 100 and 10, (c) Low-Q - less than 10.

CHAPTER II

INTERACTION SPACE DESIGN OF THE LOW-POWER EXTERNAL-CAVITY MAGNETRON

The low-power external-cavity magnetron considered here will often be referred to as the Model 9 magnetron. In the initial phase of design the maximum power output, anode potential, and range of magnetic-flux density were chosen. The design of the interaction space* was based, in part, upon an assumed maximum power output of 10 watts at an anode potential of approximately 1000 volts with magnetic-flux densities of the order of 1000 to 2000 gauss. This voltage and range of magnetic field are typical for low-level multianode c-w magnetrons whose operating frequencies are in the vicinity of 3000 megacycles per second. The choice of 3000 megacycles as the highest operating frequency for the Model 9 magnetron was primarily due to the availability of test equipment in this frequency range. The number of anode segments and the ratio of the cathode-to-anode radii were chosen on the basis of the performance of known operable magnetrons. After due consideration of a number of existing magnetrons, the choice of 12 anode segments and a cathode-to-anode ratio of 0.6 was made. An anode radius of 0.318 cm was imposed by available Kovar** tubing dimensions. The remaining factors in the interaction space design were:

(a) cathode-emitting length required to satisfy the plate-current requirements for an overall maximum efficiency of 50 per cent,

---

* See Appendix A-3 --"Magnetron Scaling and Design".

** This is a special iron alloy for glass-to-metal hermetic seals.

(b) anode-segment length; this dimension was chosen as a compromise between the total cathode-emitting length, including cathode end-shields, and the lumped-constant properties of the anode segments with relation to the remainder of the resonator system. Listed below are some of the quantities of interest resulting from the design of the interaction space.

P_{in} = 20 watts (assumed maximum power input)

P_{out} = 10 watts (assumed maximum output)

η = 50% (assumed maximum overall efficiency)

r_a = 0.318 cm (prescribed by the availability of Kovar tubing)

r_c/r_a = 0.6 (based on existing-magnetrons)

N = 12 (number of anodes based on existing magnetrons)

λ = 10 cm (chosen to suit available test equipment)

E_a = 1000 volts (chosen as a reasonable operating potential for signal-generator application)

I_b = .020 amperes (required to satisfy the assumed maximum power input)

L_c = 0.508 cm (cathode-emitting length; chosen partly on the basis of the emission area required to give at least twice the plate current necessary under space-charge-limited conditions)

ℓ_s = 0.632 cm (anode-segment length; chosen to allow for cathode end-hat dimensions plus emission length of cathode).

The next step in the design procedure was to find the quantities E_o, B_o, and I_o,* and to determine the electronic efficiency. This resulted in:

---

* Defined in Appendix A-3.

E_o = 280 volts

B_o = 554 gauss

I_o = 0.45 amperes

λ = 10 cm

$n\lambda = N\lambda/2 = 60$

r_a = 0.318 cm

r_c/r_a = 0.6

If we let $E_a = 5E_o$ or 1400 volts, the electronic efficiency is

$$\eta_e = 1 - \frac{E_o}{5E_o} = 0.8 \text{ or } 80 \text{ per cent} \qquad (2.1)$$

and the circuit efficiency required for a total efficiency of 50 per cent (circuit efficiency times electronic efficiency) is therefore approximately 60 per cent. The magnetic-flux density required for operation at 10 cm with an anode potential of $5E_o$ is given by the Hartree relation

$$\frac{5E_o}{E_o} = 2\frac{B}{B_o} - 1 , \qquad (2.2)$$

therefore, the operating magnetic field is

$$B = 3B_o = 1662 \text{ gauss} . \qquad (2.3)$$

The quantities which are given above apply to only one point in the region of possible operation. A more complete picture of the possible voltages and associated magnetic fields is given in Fig. 2.1. The lines shown in this figure represent the theoretical operating ranges for particular wavelengths of oscillation. The line $n\lambda = 60$ corresponds to 10-cm π-mode operation. This mode of operation implies that a 10-cm resonator is

associated with the interaction-space anode segments. E_o and B_o are both functions of wavelength and are plotted versus $n\lambda$ in Fig. 2.2.

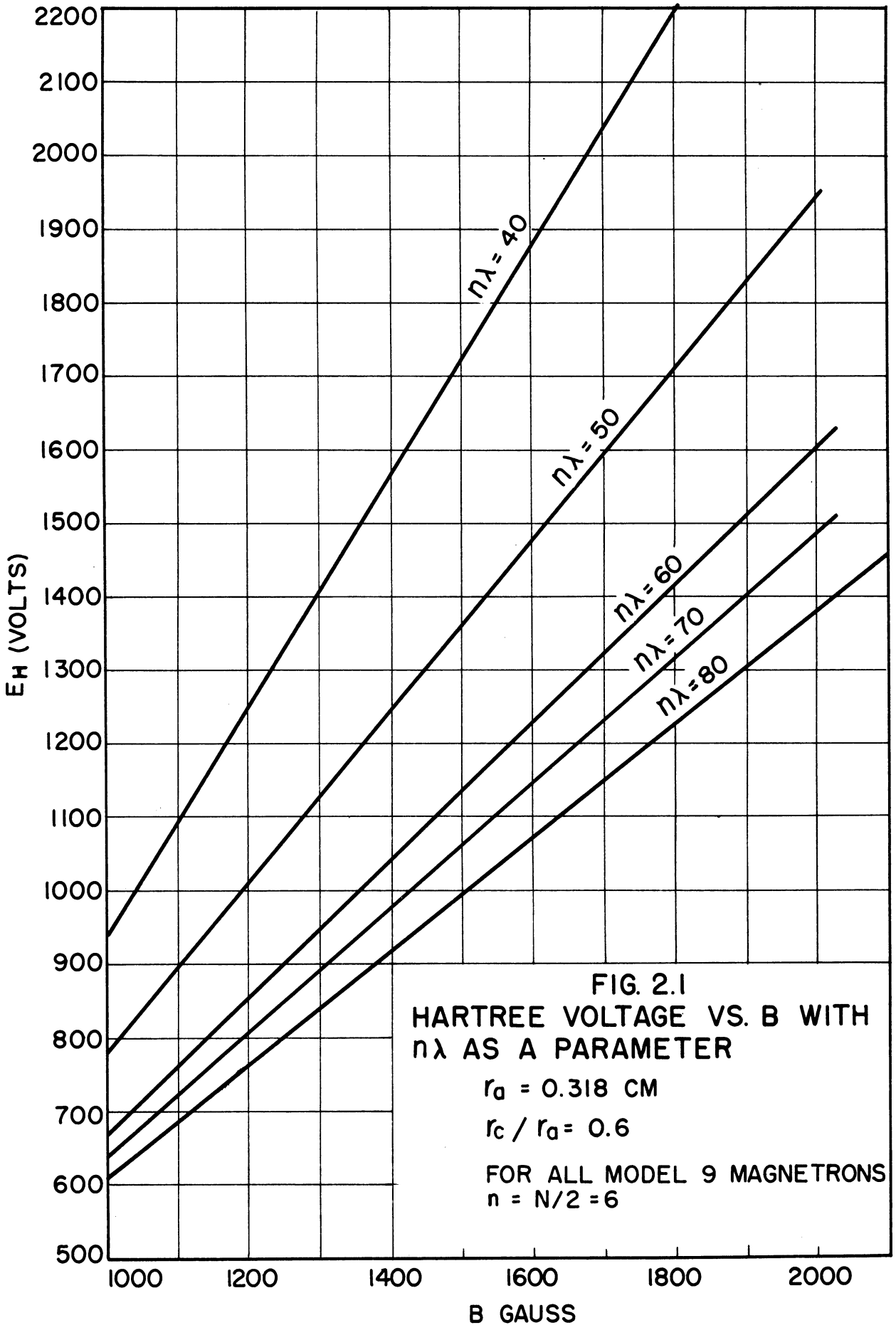

FIG. 2.1
HARTREE VOLTAGE VS. B WITH nλ AS A PARAMETER

r_a = 0.318 CM

r_c / r_a = 0.6

FOR ALL MODEL 9 MAGNETRONS
n = N/2 = 6

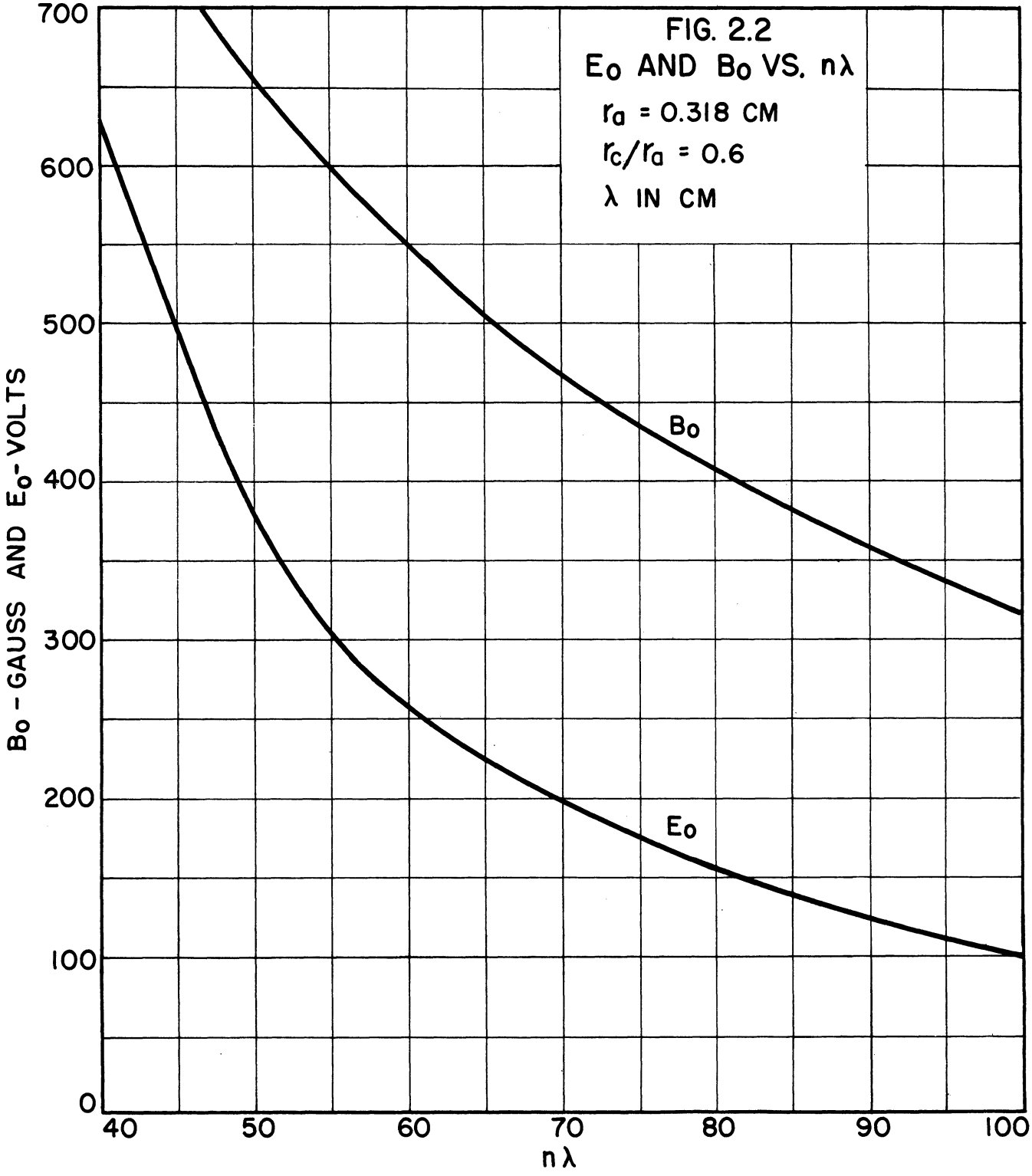
FIG. 2.2
E0 AND B0 VS. nλ
ra = 0.318 CM
rc/ra = 0.6
λ IN CM
B0
E0
B0 - GAUSS AND E0 - VOLTS
nλ
700
600
500
400
300
200
100
0
40
50
60
70
80
90
100

CHAPTER III

STRUCTURAL-DESIGN CONSIDERATIONS

The interaction-space design procedure described in the foregoing section required no previous knowledge of the associated microwave resonator system. For the mechanical design of the insertion tube, on the other hand, consideration had to be given to the types of resonators which might eventually be associated with the tube, the heat problems which might arise, and the magnetic-circuit requirements. In short, the mechanical design of the Model 9 vacuum envelope was the result of the consideration of many known or envisaged factors. Although the resonator circuit, cathode, and heat dissipation will be considered separately in this report, they were in reality inseparable in the initial planning.

The first step taken was to make the decision to utilize the vane-and-bar structure which had been investigated by the Electron Tube Laboratory of the University of Michigan.[12] With this structure as the starting point, and with a desire to make the first model as flexible and simple as possible, plans were drawn up for the first tube. An assembly sketch for this tube is shown in Fig. 3.1. Before the detail drawings had been completed for this model, modifications were made in cathode design. These modifications are embodied in the sketch of Fig. 3.2. The changes in cathode design resulted from a conversation with Mr. W. C. Brown of the Raytheon Manufacturing Company, who indicated that difficulty had been encountered with cathode structures similar to that shown in Fig. 3.1. Upon his recommendation, a new cathode was designed to eliminate the necessity

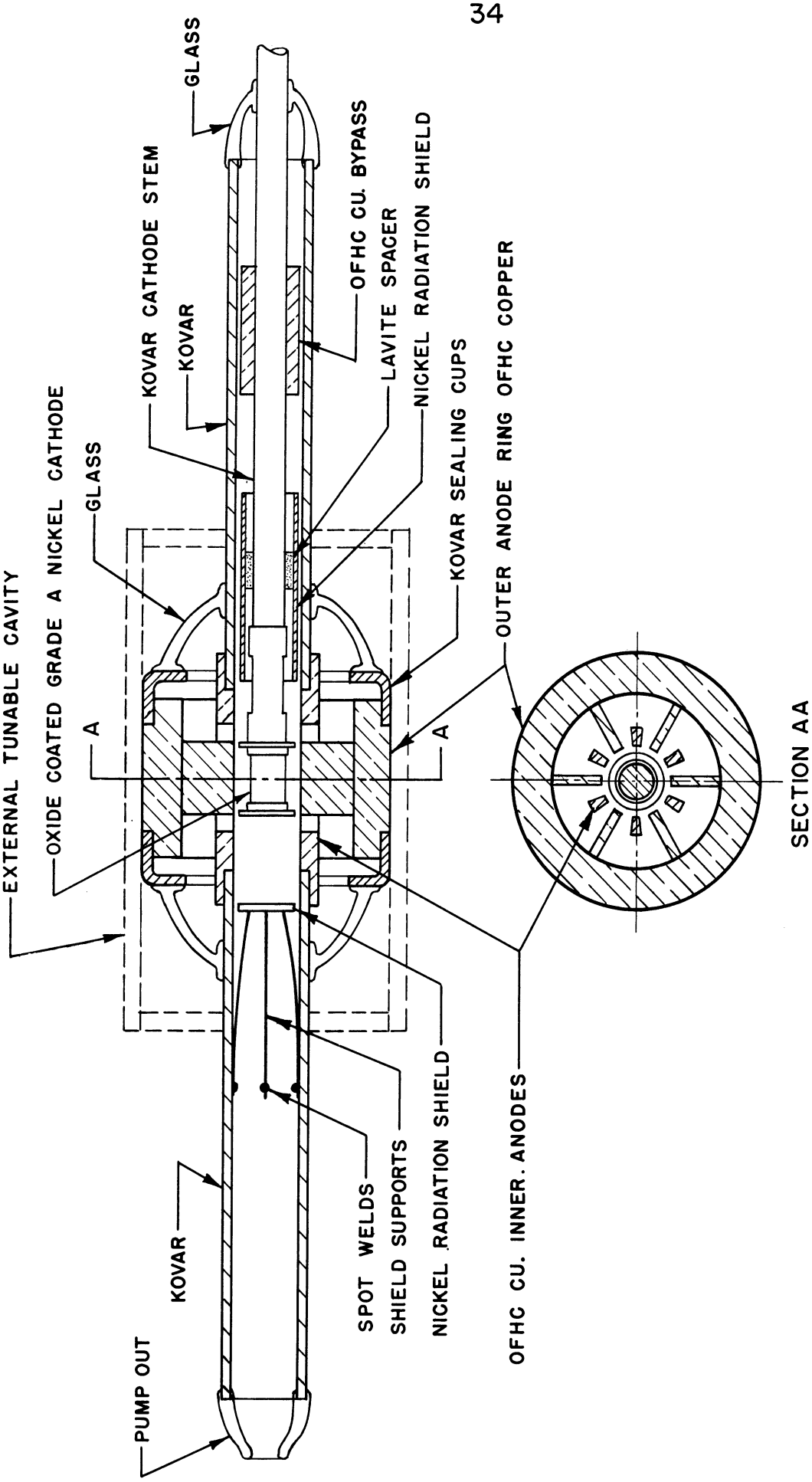

FIG. 3.1
SKETCH SHOWING THE FIRST PROPOSED MODEL
OF THE INSERTION MAGNETRON

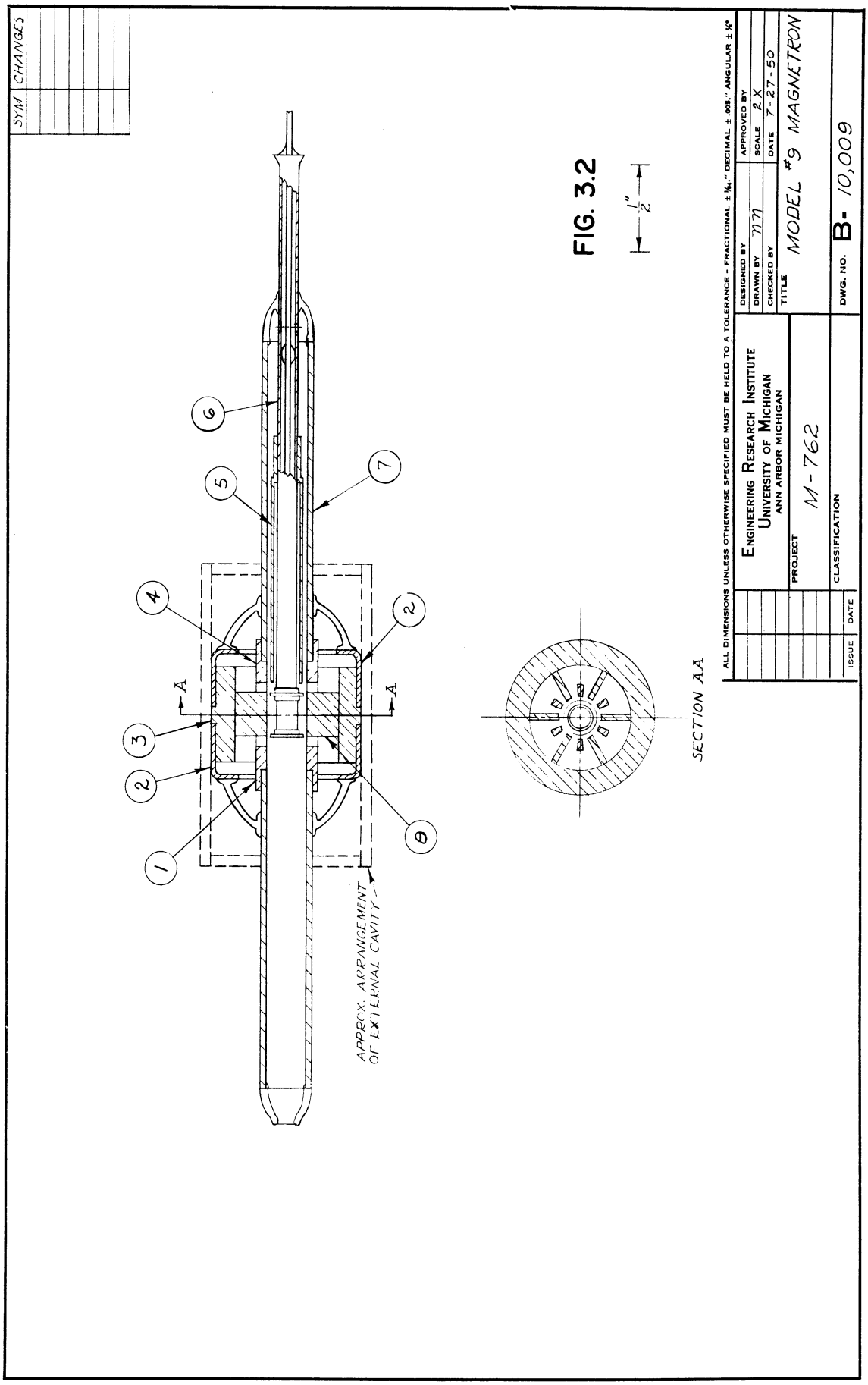
SYM | CHANGES
DWG. NO. B
1
2
3
4
5
6
7
8
A
A
APPROX. ARRANGEMENT OF EXTERNAL CAVITY
SECTION AA
FIG. 3.2
1/2"
ALL DIMENSIONS UNLESS OTHERWISE SPECIFIED MUST BE HELD TO A TOLERANCE - FRACTIONAL ± 1/64" DECIMAL ± .005" ANGULAR ± 1/2°
ENGINEERING RESEARCH INSTITUTE
UNIVERSITY OF MICHIGAN
ANN ARBOR MICHIGAN
PROJECT M-762
CLASSIFICATION
ISSUE | DATE
DESIGNED BY
DRAWN BY TTT
CHECKED BY
APPROVED BY
SCALE 2X
DATE 7-27-50
TITLE MODEL #9 MAGNETRON
DWG. NO. B- 10,009

of a braze joint near the heater region. The cathode line choke and by-pass capacitor (part No. 5, Fig. 3.2) was incorporated inside the evacuated envelope for the purpose of reducing power leakage out of the cathode. Processing of the first tube thereafter proceeded as far as the pumping stage, where a leak was detected between one of the glass seals and a Kovar sealing cup (part No. 2 of Fig. 3.2). All attempts to repair the leak were futile and this first model was discontinued. However, important information had been gained from the construction of this model. First of all, it was encouraging to know that the structure could even be assembled with the glassing equipment available. Second, the cost of machining the anode-bar segments was found to be quite high and steps were taken which reduced this machining time by a factor of at least 5. Fig. 3.3 is a detail drawing of the center conductor anode fingers for the first model of the insertion magnetron. It is apparent that each of the vertical bars requires individual vertical mill machining since the tapered geometry of the bars does not permit a saw cut across the diameter of the structure. The modification made on the anodes for subsequent models is also depicted in this figure, where it may be seen that a single saw cut across the anode ring can result in the simultaneous completion of the sides of two anodes.

The gold-copper brazes between the Kovar and copper pieces of the center conductor (parts 7 and 4 of Fig. 3.2), and the gold-copper brazes between the vanes and the vane anode ring (parts 8 and 3) were completed with little difficulty and the procedure used was continued in later models. During the process of glass sealing the inner conductor to the outer one, a great deal of difficulty was encountered in completing the second seal.

SYM	CHANGES
A	WAS .381
B	WAS .125
C	WAS .125
D	WAS .049
E	WAS 22½° TO EDGE OF VANE

DWG. NO. A

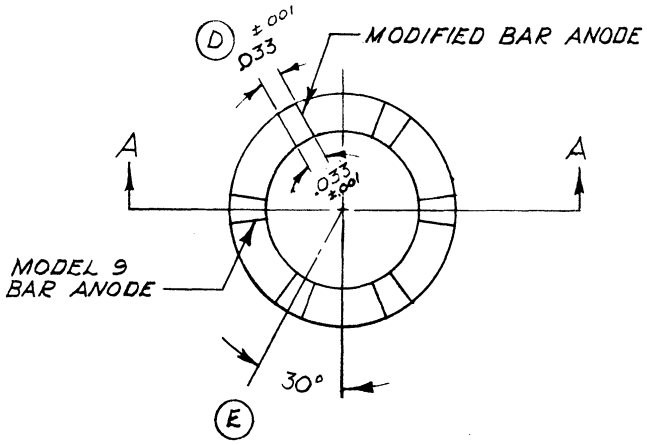

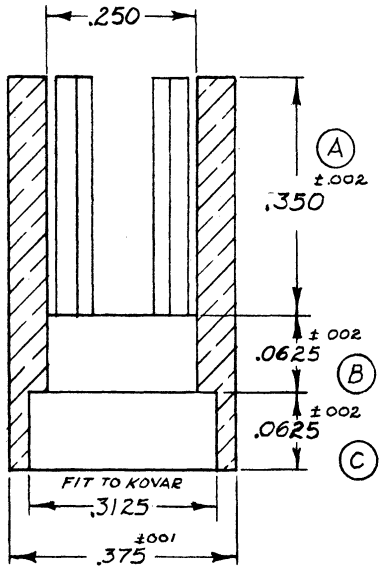

FIG. 3.3

SECTION AA

OFHC COPPER 1 REQ'D

ALL DIMENSIONS UNLESS OTHERWISE SPECIFIED MUST BE HELD TO A TOLERANCE - FRACTIONAL ± 1/64," DECIMAL ± .005," ANGULAR ± ½°

		ENGINEERING RESEARCH INSTITUTE UNIVERSITY OF MICHIGAN ANN ARBOR MICHIGAN	DESIGNED BY JN	APPROVED BY
			DRAWN BY MM	SCALE 4X
			CHECKED BY DPB	DATE 7-25-50
		PROJECT M-762	TITLE ANODE FINGERS (BAR ANODES)	
2	10-21-50	CLASSIFICATION	DWG. NO. A- 5021	
ISSUE	DATE			

DWG. NO. B

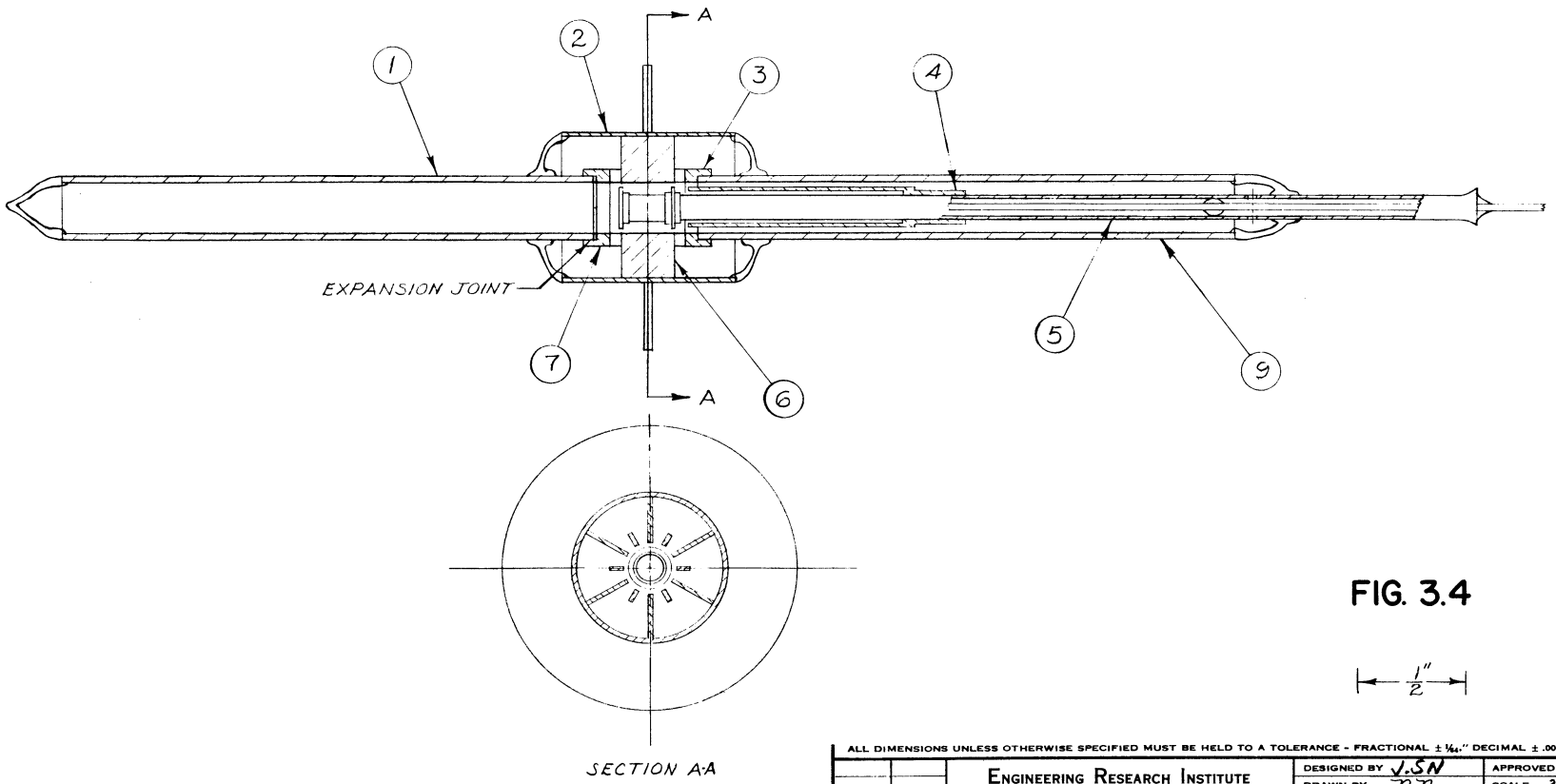

FIG. 3.4

1/2"

ALL DIMENSIONS UNLESS OTHERWISE SPECIFIED MUST BE HELD TO A TOLERANCE - FRACTIONAL ± 1/64" DECIMAL ± .005" ANGULAR ± ½°

ENGINEERING RESEARCH INSTITUTE UNIVERSITY OF MICHIGAN ANN ARBOR MICHIGAN		DESIGNED BY J.SN	APPROVED BY
		DRAWN BY NN	SCALE 2X
		CHECKED BY H.W.W	DATE 9-18-50
PROJECT M-762		TITLE LOW-POWER MAGNETRON MODEL 9A	
CLASSIFICATION		DWG. NO. B-10,009A	
ISSUE	DATE		

The heat transmitted through the copper vane-anode ring, from the final seal to the initial glass seal, was usually sufficient to crack the latter before completion of the glassing operation. Two factors of importance were recognized here. One was that the differential expansion between the inner and outer conductors was considerable during the glassing operation. The other factor was that it would be necessary to heat the first seal while the second seal was being completed. This model indicated in addition that, even if it could be successfully completed, it would be overly fragile due to the bulk of the vane-anode copper ring. This ring was employed partly to reduce r-f losses and partly to separate the Kovar sealing cups so that they would not distort the magnetic field. It was proposed to use the inner conductor Kovar tubes (part 7) to provide part of the magnetic-flux path into the interaction space since Kovar is magnetic. The question of magnetic-field distortion will be brought up again in connection with the experimental results.

The second model of the insertion magnetron, designated Model 9A, was made in accordance with the assembly drawing shown in Fig. 3.4. This design differs from the first model, i.e., the Model 9, in the following aspects:

(a) the length of the bar anodes, part 3, is shorter,

(b) the vane-anode ring, part 2, is a thin (.0508-cm wall) Kovar cylinder,

(c) an expansion joint is employed between the inner Kovar tube, part 1, and the bar-anode cap, part 7,

(d) a copper flange is soldered to the vane-anode, Kovar cylinder, part 2, to provide a means of connection to an external cavity.

This model was the first successfully completed tube of this type. Further discussion of the Model 9A appears in Chapter VI, "Presentation and Interpretation of Experimental Results". One mechanical improvement on the Model 9A, No. 39 tube was made; this was in the elimination of the soldered copper flange from the vane-anode Kovar cylinder. Experience with the Model 9A, No. 39 resulted in the design of the spring finger flange arrangement shown in Fig. 3.5. The advantage of the removable flange jacket over the soldered flange is two-fold; (a) the tubes do not require the additional machine and assembly time, and (b) the removable flange can be used interchangeably with any tube. All tubes built subsequent to the Model 9A, No. 39 were designed to employ the removable flange cavity connector.

Two other models were constructed; namely the Model 9B and 9C, drawings for which are given in Figs. 3.6 and 3.7, respectively. The Model 9B tube differs from the Model 9A primarily in the omission of the vacuum-sealed cathode choke and bypass. The reason for this omission stemmed from a desire to obtain information on the effect of the cathode circuit on tube performance. By leaving the cathode choke and bypass out of the evacuated portion of the tube, and by extending the length of the external portion of the cathode stem, it has been possible to employ a variable external cathode-line circuit.

The Model 9C structure utilizes a single glass seal, between the bar-anode and the vane-anode cylinders, rather than two glass seals. This limits the flexibility of the tube since it is impossible to use a symmetrically disposed coaxial-line tunable resonator with it. A complete set

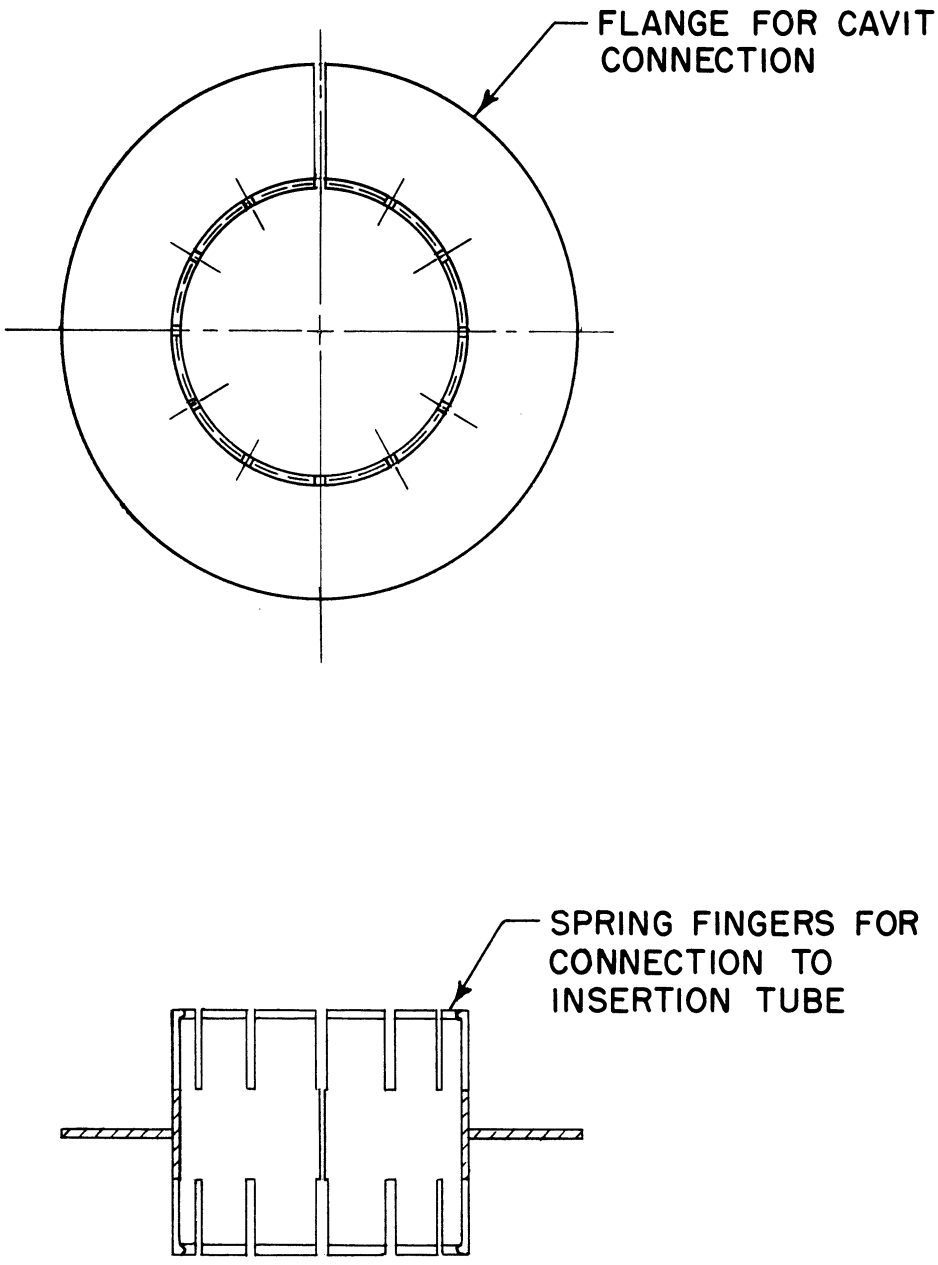

FIG. 3.5
SPRING-FINGER REMOVABLE-
CONNECTION FLANGE

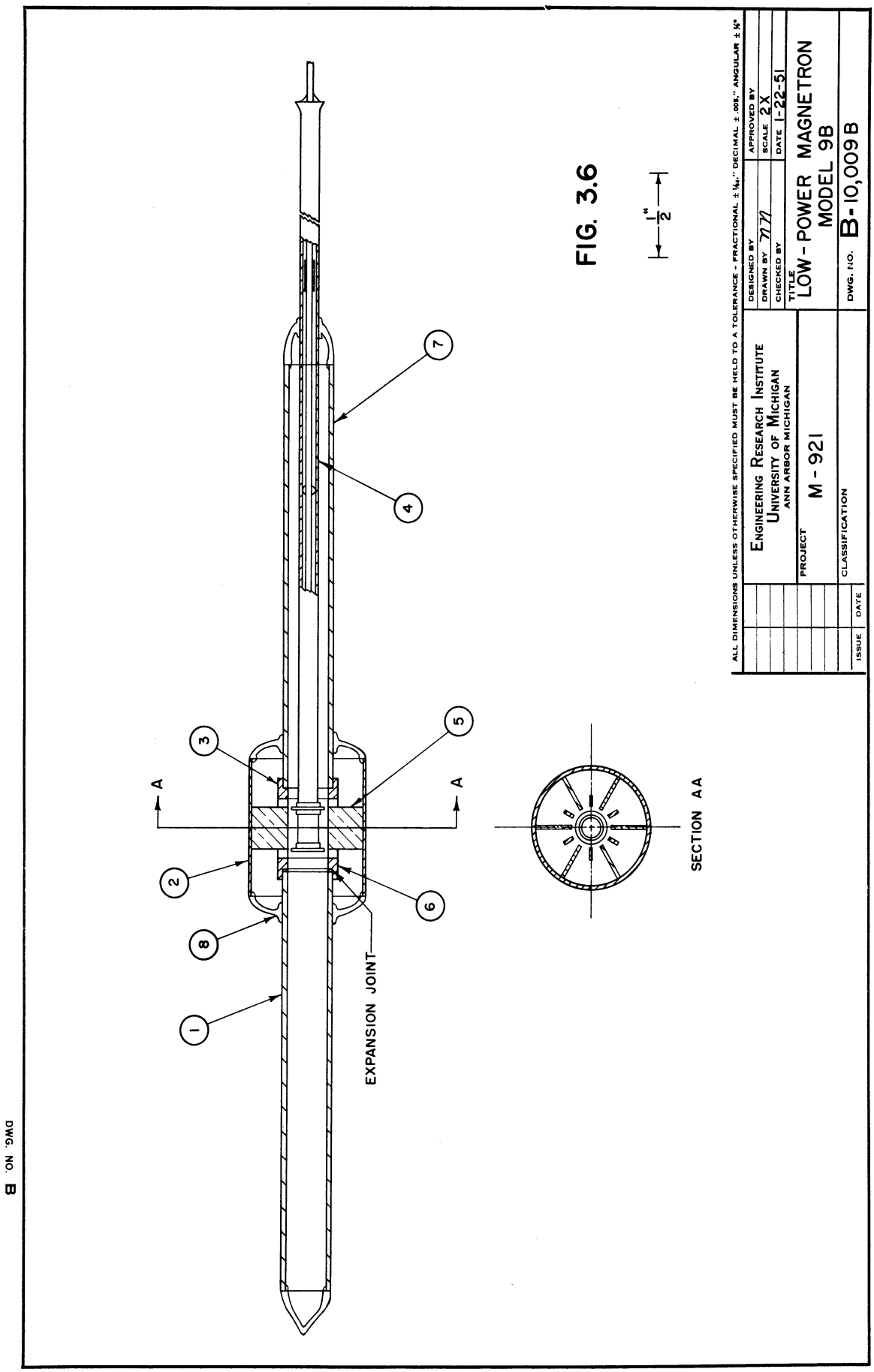
A
A
1
2
3
4
5
6
7
8
EXPANSION JOINT
SECTION AA
1"
2
ALL DIMENSIONS UNLESS OTHERWISE SPECIFIED MUST BE HELD TO A TOLERANCE - FRACTIONAL ± 1/64." DECIMAL ± .005." ANGULAR ± ½°
ENGINEERING RESEARCH INSTITUTE
UNIVERSITY OF MICHIGAN
ANN ARBOR MICHIGAN
PROJECT M-921
CLASSIFICATION
ISSUE
DATE
DESIGNED BY
DRAWN BY 7777
CHECKED BY
APPROVED BY
SCALE 2X
DATE 1-22-51
TITLE LOW-POWER MAGNETRON MODEL 9B
DWG. NO. B-10,009 B
DWG. NO. B

FIG. 3.6

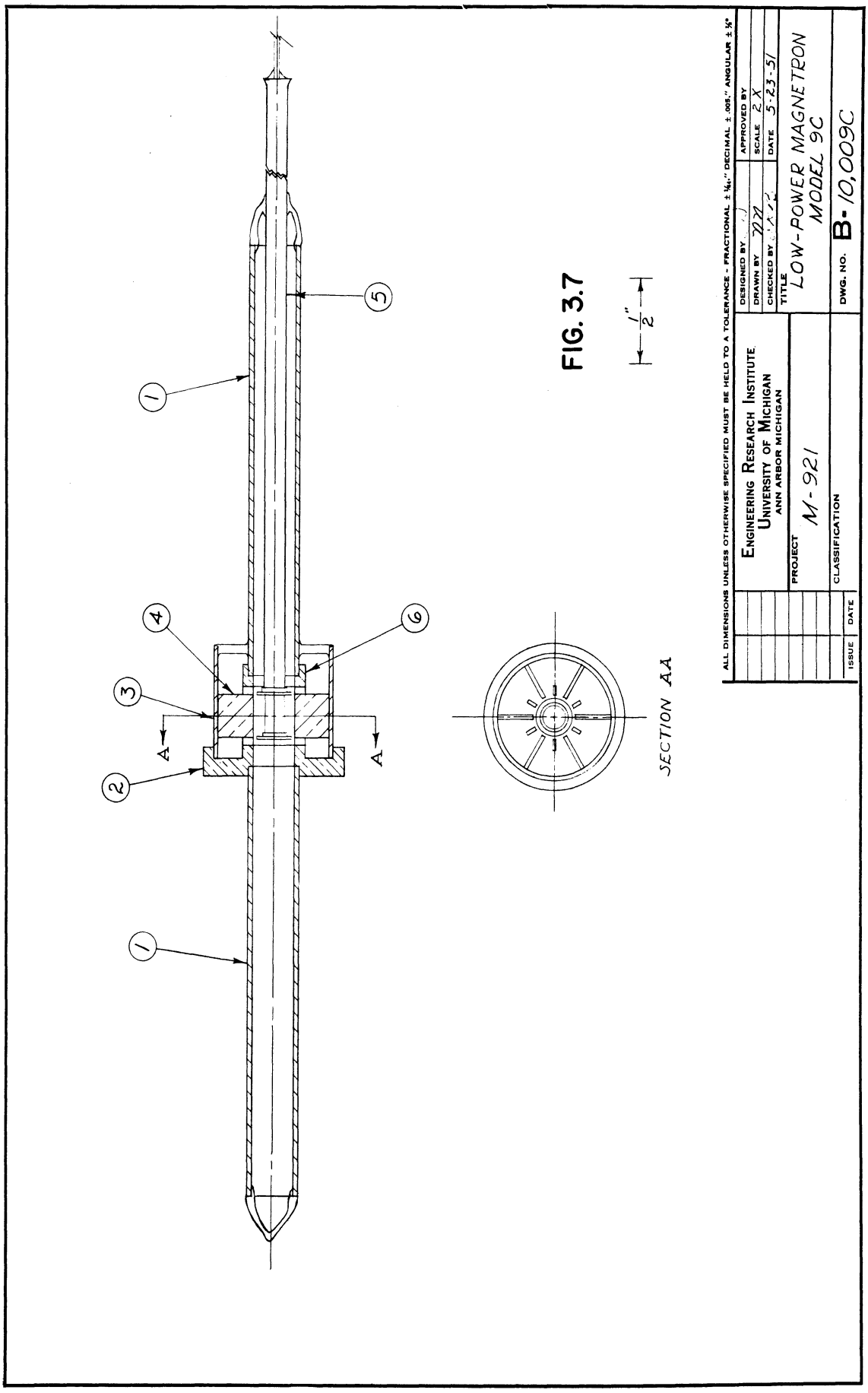
1
2
3
4
5
6
A
A
SECTION AA
1/2"
ALL DIMENSIONS UNLESS OTHERWISE SPECIFIED MUST BE HELD TO A TOLERANCE -- FRACTIONAL ± 1/64," DECIMAL ± .005," ANGULAR ± 1/2°
ENGINEERING RESEARCH INSTITUTE
UNIVERSITY OF MICHIGAN
ANN ARBOR MICHIGAN
PROJECT M-921
CLASSIFICATION
ISSUE
DATE
DESIGNED BY
DRAWN BY
CHECKED BY
APPROVED BY
SCALE 2 X
DATE 5-23-51
TITLE LOW-POWER MAGNETRON MODEL 9C
DWG. NO. B-10,009C
DWG. NO. B

FIG. 3.7

of detail drawings for the Model 9B structure is included in Appendix C. It is felt that this model is the simplest and most flexible of all the designs. Photographs of Model 9B, No. 43 and Model 9A, No. 39 appear in Figs. 3.8a and 3.8b, respectively.

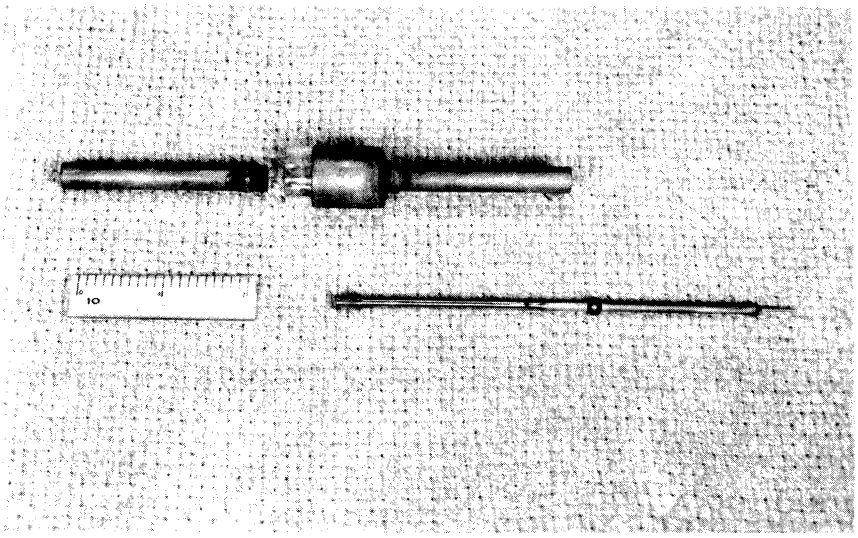

FIG. 3.8a
PARTIALLY ASSEMBLED MODEL 9B

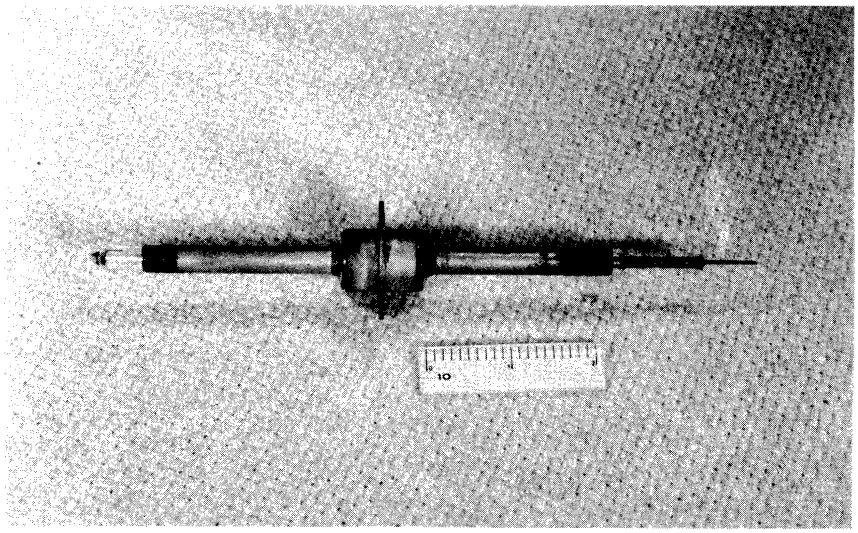

FIG. 3.8b
ASSEMBLED MODEL 9A

CHAPTER IV

THERMAL CONSIDERATIONS

The thermal problems which arose in the design of the insertion magnetrons were of particular significance since their successful solution, to a great extent, determined the feasibility of tube assembly as well as the operational life of the structure. The questions which required answers were:

(a) What power input would be necessary to maintain the cathode at the operating temperature required for the activation process?

(b) At what temperature would the cathode stem operate, at the position of the hermetic seal between it and the bar-anode Kovar cylinder?

(c) At what temperatures would the glass seals between the inner and outer Kovar cylinders operate under normal steady-state conditions?

Clogston[20] has considered the problem of heat balance for magnetron cathodes operating under the following conditions:

1. Heat is lost from the cathode almost entirely by radiation.
2. The whole cathode structure is at a nearly uniform temperature.
3. The heater construction is such that heater power and back-heating power may be considered thermally equivalent.

These conditions apply quite well to radially-mounted cathodes, in which only a small proportion of heat is lost through the supporting

leads. According to Clogston,[20] general mathematical relations cannot be established for end-mounted cathodes such as are employed in the insertion magnetrons. This is due to the complexity of the problem which requires the consideration of both radiation and conduction heat losses, in addition to back-heating effects.

4.1. Calculation of the Cathode-Power Input and the Temperature Variation Along the Cathode Stem

In order to obtain a reasonable estimate of both the cathode-power input requirements and the variation of temperature along the cathode stem, it is convenient to neglect the effects of back bombardment. The following method of calculation,* in which both the radiation and conduction losses have been considered, has been employed to obtain an estimate of the cathode power as well as the temperature variation along the cathode stem. The calculations are based on the cathode dimensions given in Appendix C. The quantities used in the calculations are:

A_c = $4.6\pi \times 10^{-3}$ sq in. (cross-sectional area of the Kovar stem)

A_s = $0.125 \times \pi \times 1$ sq in. (surface area per axial inch of length of stem)

e = 0.7 (emissivity coefficient for Kovar based on the value for iron; this is considered to be constant over the temperature range)

K = 0.437 watts per sq in. per degree centigrade per in. (conductivity of Kovar[21] considered constant over the temperature range).

Let us assume a long Kovar cylinder having the dimensions and constants given above. We furthermore assume some reasonable temperature, say

* This method was suggested by Professor A. D. Moore of the U. of Michigan.

50°C, at one end of this cylinder and a temperature of 100°C at a plane one inch from this end. Referring to Fig. 4.1, the conduction-heat transfer between the plane x = 0 and x = 1 in. is therefore

$$q_c = K A_c \Delta t = 0.437 \times 4.6 \pi \times 10^{-3} \times 50 \text{ (watts)} . \quad (4.1)$$

The radiation loss for the section of cylinder between the planes x = 0 and x = 1 in. is given approximately by

$$q_r = \left(\frac{T_o + T_1}{2}\right)^4 \times 10^{-12} \times 36.9 \times e A_s = 0.54 \times 0.7 \times 1 \times 0.125 \pi \text{ (watts)}, \quad (4.2)$$

when there is no re-radiation back to the stem. Here T_o is the temperature at plane x = 0 and T_1 is the temperature at x = 1 in. The temperature is measured in degrees Kelvin.

Summing the radiation loss and conduction loss which must pass across the plane x = 1 in., we obtain the value of 0.466 watts. The latter is now considered as the conduction heat flow between plane x = 3 in. and x = 2 in., which in turn determines the temperature of 173.7°C at the x = 3 in. plane. The remainder of the calculations are simply a repetition of the first calculation extended to the required temperature of the emitting surface. Fig. 4.2 is a plot of the results of these calculations taken up to the activation temperature for oxide cathodes, i.e., approximately 1050°C.

An estimate of the power input into the emitting region of the cathode can now be made. The surface area of the oxide-coated nickel-based cathode is approximately 0.117 sq in. and the emissivity coefficient for oxide-coated nickel as given by Spangenberg[22] is 0.65 at 1000°C. The length

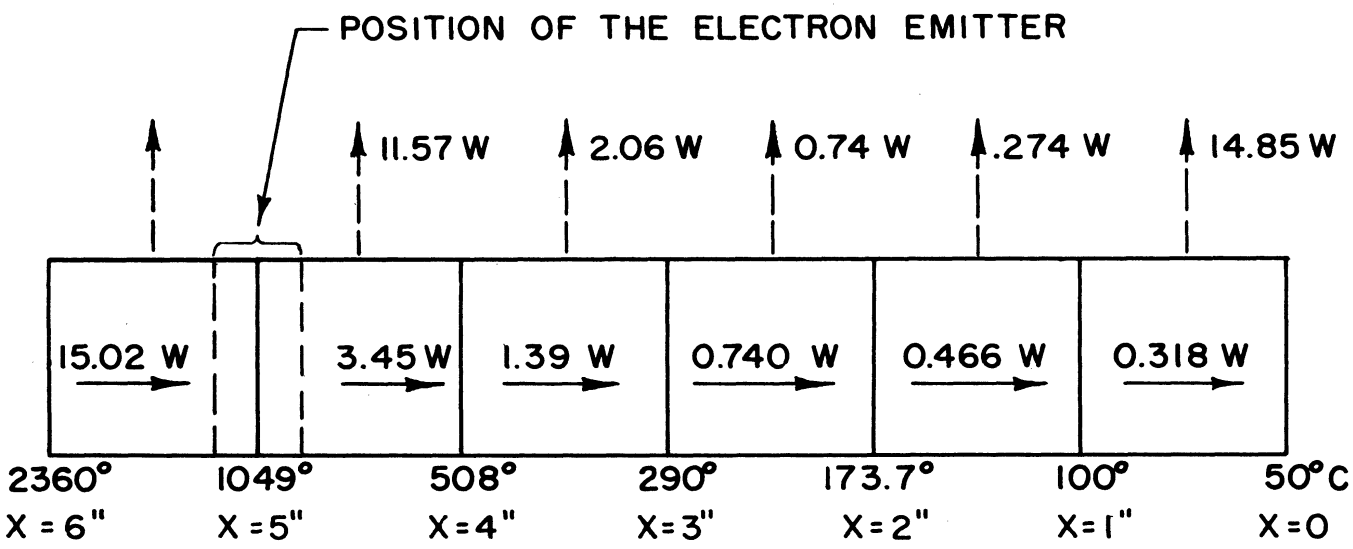

FIG. 4.1

CHART ILLUSTRATING THE METHOD OF CALCULATION OF THE TEMPERATURE ALONG THE CATHODE STEM

RADIATION (WATTS) — — — →

CONDUCTION (WATTS) ——→

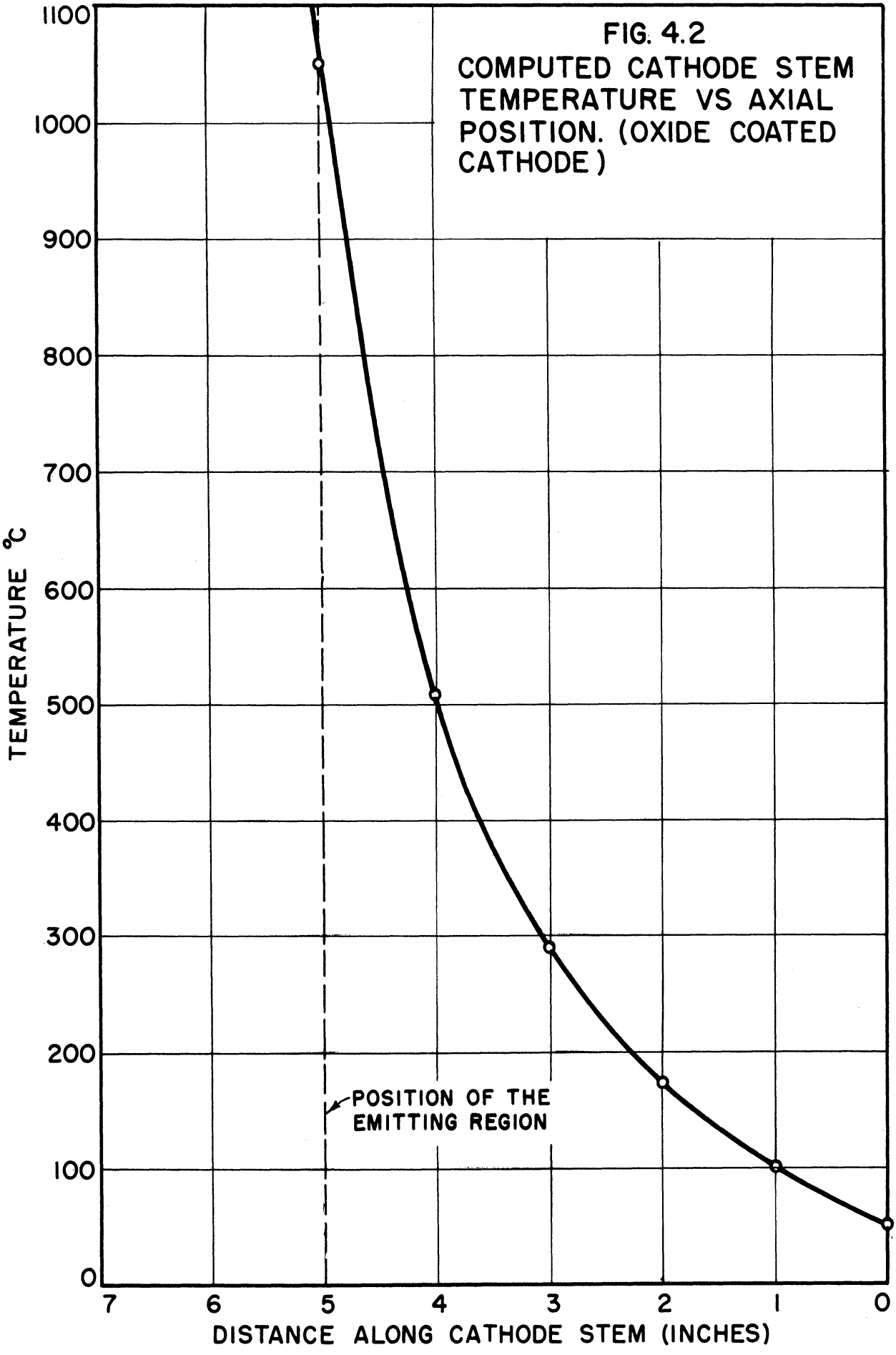
FIG. 4.2
COMPUTED CATHODE STEM TEMPERATURE VS AXIAL POSITION. (OXIDE COATED CATHODE)
TEMPERATURE °C
1100
1000
900
800
700
600
500
400
300
200
100
0
7
6
5
4
3
2
1
0
DISTANCE ALONG CATHODE STEM (INCHES)
POSITION OF THE EMITTING REGION

of nickel cylinder considered here is 0.240 in. Assuming a constant temperature of 1049°C over this length of nickel, the radiation loss is 13.2 watts. The maximum input at 1050°C is therefore given by the sum of this radiation loss and the conduction loss of 3.45 watts giving a total of 16.65 watts. Considering the assumptions made with regard to the constancy of the emissivity coefficient and conductivity with temperature, this is in good agreement with a measured value of 19.8 watts.

The temperature of the cathode stem at the position of the cathode seal is obtainable from the curve of Fig. 4.2. The cathode glass seal is 2.6 in. from the x = 5 in. plane, thus the computed temperature is 210°C. The actual temperature at this point must be lower since the conduction through the glass and the natural convection and conduction of heat from the external portion of the cathode stem must be considered. Thus the calculated value of 210°C is an indication of the maximum possible glass temperature. The critical temperature of the No. 707 glass used for this seal is 442°C. We therefore conclude that this glass seal will operate within safe temperature limits.

The step-by-step approach used above is also applicable to the solution for a cathode stem made up of a number of different materials joined together. Such a case arose in the design of the tungsten-helix cathode shown in Appendix D, Fig. D-5.

4.2. Calculation of the Temperature at the Position of the Glass Seal on the Bar-Anode Kovar Cylinder

The maximum possible temperature at the boundary of the inner Kovar cylinder (part 1 of Fig. 3.6) and the glass seal (part 8 of the same figure), may be estimated by means of a graphical computation. This

computation accounts for radiation and convection effects but neglects conduction. Thus the computed temperature is in error but corresponds to an upper temperature limit at the position of the glass seal and the inner Kovar cylinder.

From the previous calculations of temperature along the cathode stem we choose the temperature on the cathode stem corresponding to the position of the aforementioned glass seal. This position is approximately .375 in. from the cathode. Let the cathode have a temperature of 1050°C. From Fig. 4.2 we find the temperature at 0.375 in. from the cathode is 800°C.

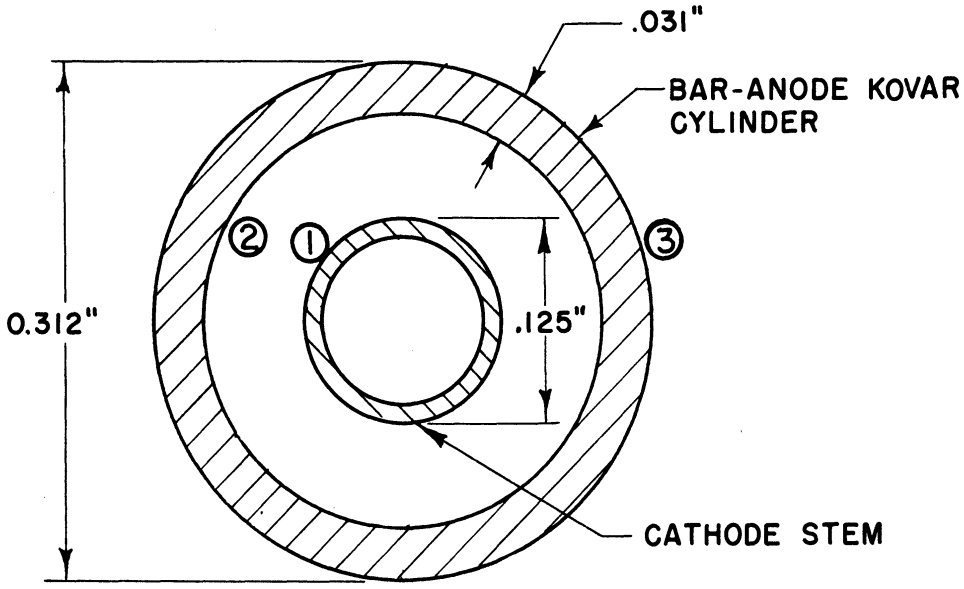

FIG. 4.3
SKETCH SHOWING THE DIMENSIONS USED IN THE HEAT PROBLEM

Fig. 4.3 is a sketch of the cross section of the cathode stem and the bar-anode Kovar cylinder. The radiation across the space from surface (1) to (2) in this figure depends upon the temperatures and the

radiation emissivity coefficients of both surfaces. Moore[23] has shown that the power, in watts, transferred per axial inch between two cylinders is

$$q_{12} = A_1 (E_1 - E_2) \frac{e_1 e_2}{e_1 (A_1/A_2) + e_2 - e_1 e_2 (A_1/A_2)} \frac{\text{watts}}{\text{axial in.}} . \quad (4.3)$$

Here

A_1 = 0.393 in.^{2} (surface area of the cathode stem per inch of length)

A_2 = 0.786 in.^{2} (inner surface area of Kovar cylinder per inch of length)

A_3 = 0.981 in.^{2} (outer surface area of Kovar cylinder per inch of length)

e_1 = 0.7 (emissivity coefficient of surface (1))

e_2 = 0.7 (emissivity coefficient of surface (2))

e_3 = 0.7 (emissivity coefficient of surface (3))

E_1 = 36.9 T_1^4 x 10^{-12} watts per sq in. (Stefan-Boltzmann radiation equation, T in degrees Kelvin) (4.4)

$$E_2 = 36.9\ T_2^4 \times 10^{-12} \text{ watts per sq in.} \quad (4.5)$$

Substitution of the constants listed above into Eq (4.3) gives

$$q_{12} = 0.239 (E_1 - E_2) \frac{\text{watts}}{\text{axial in.}} \quad (4.6)$$

If we assume that radiation and convection account for all losses, the heat-balance equation per unit length is

$$q_{12} = 0.239 (E_1 - E_2) = A_3 E_2 e_3 + h_c A_3 \Delta t . \quad (4.7)$$

Here h_c is a convection heat-transfer coefficient for a horizontal cylinder in air. The values for h_c have been computed for assumed temperature rises Δt above ambient (assume 25°C).[23] Temperature T_2' ($T_2 - 273 = T_2'$) is assumed and the total power in watts per axial inch radiated across surfaces (1) to (2) is then computed. The power, in watts, lost by radiation from the outer cylinder is also found using this value of assumed temperature. In Table 4.1 we show the calculations for assumed values of T_2' from 100°C through 500°C. The temperature, at the position of the glass seal, as found graphically in Fig. 4.4 is 400°C. Note that the convection loss is computed on the basis of temperature rise above ambient and is plotted against $(T_2' + 25)$°C.

From this graphical solution we conclude that, for normal operating conditions, this design is satisfactory. It should be understood that, because of the presence of conduction heat transfer, the actual temperature at the glass-to-metal boundary is significantly lower than 400°C.

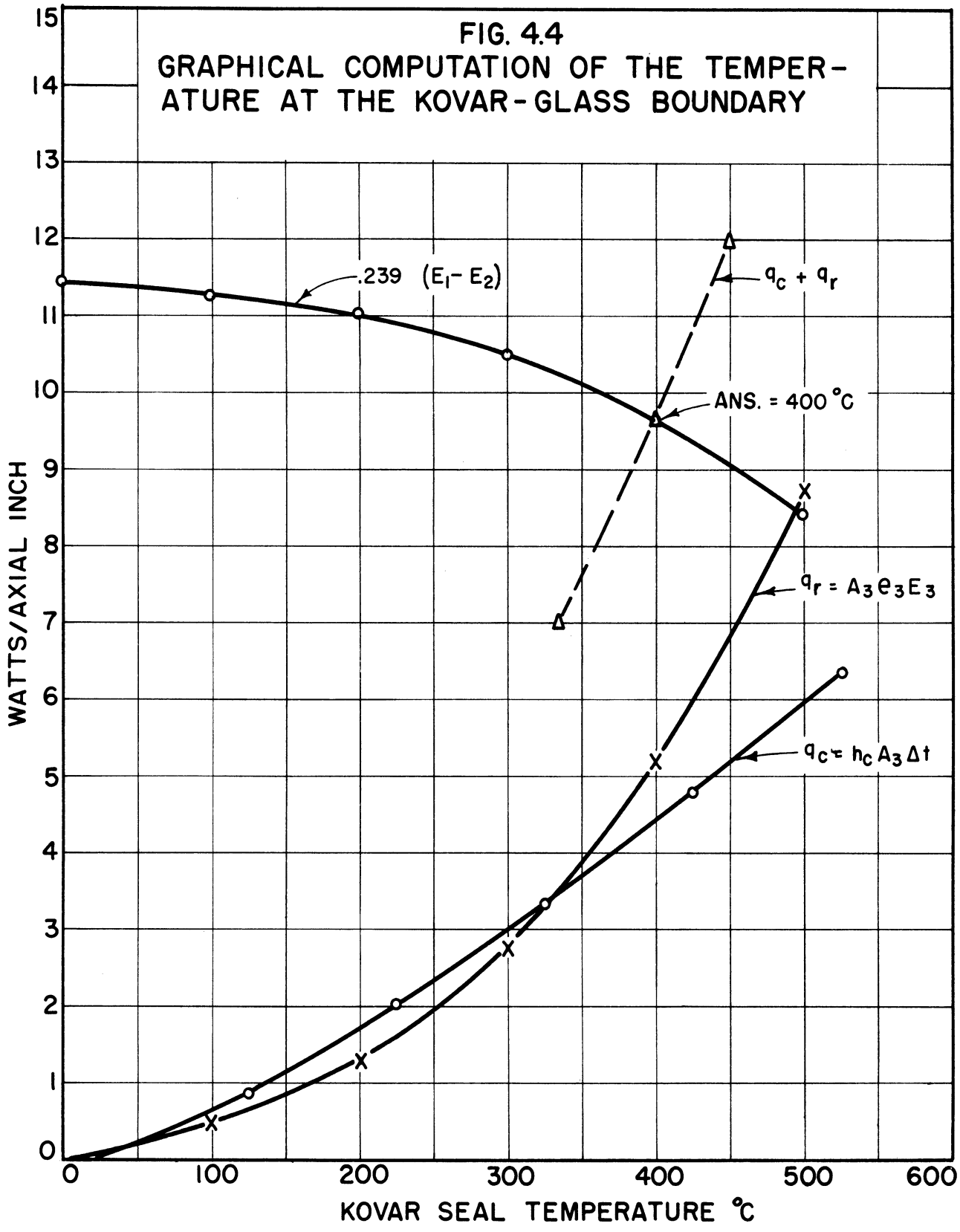
FIG. 4.4
GRAPHICAL COMPUTATION OF THE TEMPERATURE AT THE KOVAR-GLASS BOUNDARY
.239 (E1 - E2)
qc + qr
ANS. = 400 °C
qr = A3 e3 E3
qc = hc A3 Δt
WATTS/AXIAL INCH
KOVAR SEAL TEMPERATURE °C
0
1
2
3
4
5
6
7
8
9
10
11
12
13
14
15
0
100
200
300
400
500
600

TABLE 4.1

RADIATION

assumed* T_2' °C	$E_2 = E_3$	.239 E_2	.239(E_1 - E_2)	$A_3e_3E_3$
100	.72	.172	11.29	.495
200	1.85	.442	11.02	1.27
300	4.0	.956	10.5	2.75
400	7.5	1.795	9.66	5.15
500	12.7	3.04	8.42	8.72

*Note (T_2 - 273) = T_2'

CONVECTION

h_c	q_c	assumed Δt above 25°C
0.0086	0.844	100
0.0102	2.01	200
0.0113	3.32	300
0.0122	4.79	400
0.0129	6.33	500

CHAPTER V

THE COAXIAL-RESONATOR ANALYSIS

The resonators employed in conjunction with the Model 9 series of insertion magnetrons have been of the coaxial-line type in which the electrical length of the resonator, including the vanes and bars, may be one-half wavelength or an integral multiple of a half wavelength. The design parameters of the resonator structure for operation at a particular frequency are: (a) the capacitance between the magnetron vanes and bars, (b) the inductance of the vanes, (c) the length of the coaxial-line sections, and (d) the output-coupling system.

In the analysis presented below we consider the four quantities listed above with relation to the equations for: (a) the resonance frequency of the cavity inclusive of the vane-and-bar structure, (b) the external Q which is defined as 2π times the energy stored in the cavity divided by the energy lost in the load per cycle, and (c) the impedance between the vanes and bars as "seen" by the electrons "looking" radially out of the interaction space. The analysis is restricted to a lossless cavity in the absence of the cathode. A sketch, showing the geometry of the resonator and some of the associated notation, is shown in Fig. 5.1. In this analysis, we assume that the physical structure, which consists of the insertion magnetron and an external cavity, may be represented by the sketch indicated above. Effects due to glass seals are neglected, as are also the effects of spring-contact accessories. These practical aspects, although important, would, if considered, make it quite hopeless to attain analytical solutions.

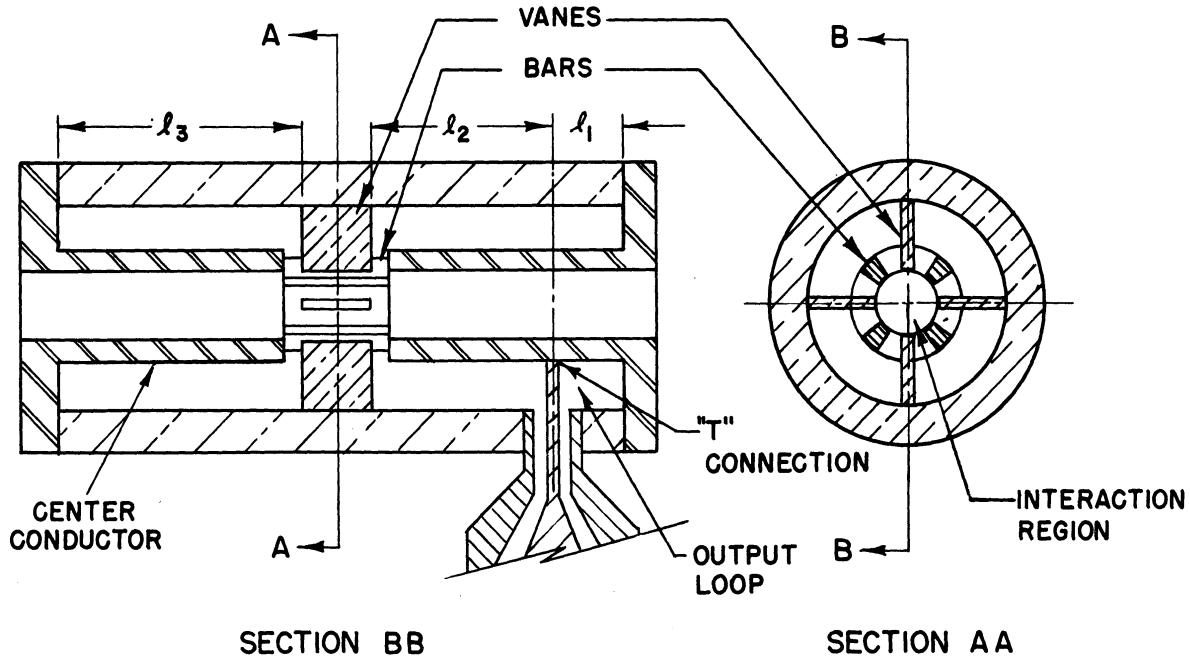

FIG. 5.1
SKETCH SHOWING THE GEOMETRY OF THE COAXIAL RESONATOR AND THE VANE-AND-BAR EXCITING STRUCTURE

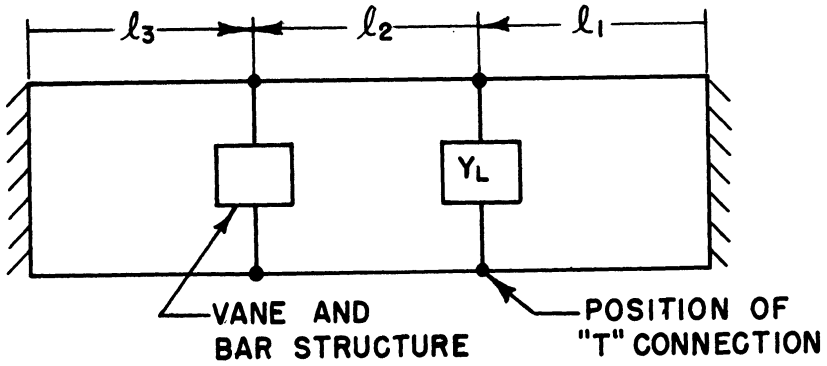

FIG. 5.2
TRANSMISSION LINE EQUIVALENT CIRCUIT

5.1 The General Case

We shall assume that the actual resonator system may be represented by a lossless transmission line with lumped-constant admittances as in Fig. 5.2, where $\ell_1 + \ell_2$ is not necessarily equal to ℓ_3. Here Y_L is the load admittance transferred into the coaxial cavity; ℓ_1, ℓ_2, and ℓ_3 are, respectively, the distance of the "T" coupling connection from one short-circuited end of the coaxial cavity, the distance measured from the "T" to the right edge of the vanes, and the distance from the remaining short-circuited end of the coaxial line to the left edge of the vanes.

For convenience in handling, the schematic circuit of Fig. 5.2 is divided into separate components as shown in Fig. 5.3. The admittances indicated on the diagrams define the notations used in the equations which follow.

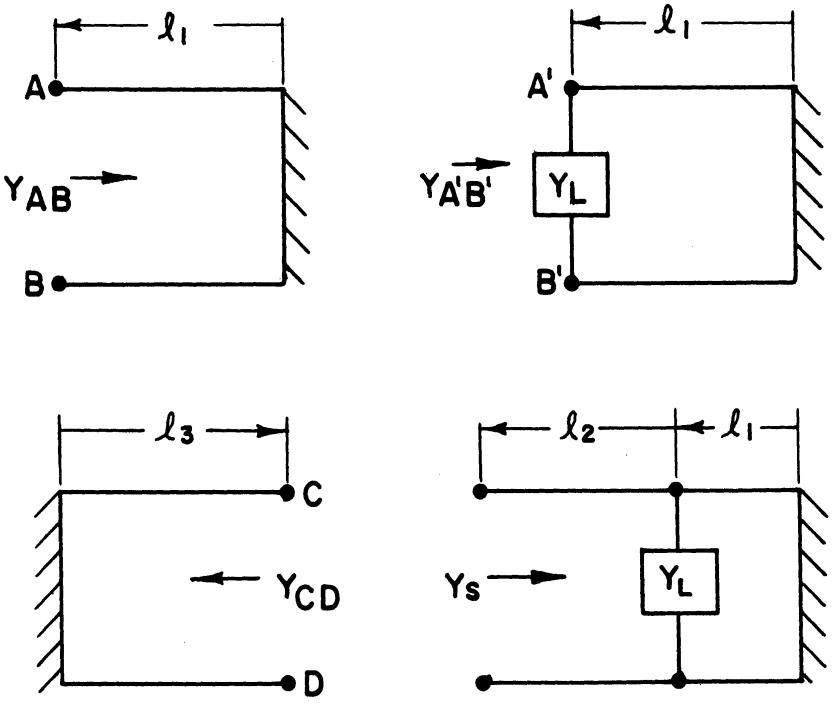

FIG. 5.3
COMPONENTS OF THE TRANSMISSION LINE EQUIVALENT CIRCUIT

Substituting into the equations for lossless transmission lines, we obtain

$$\frac{Y_S}{Y_0} = \frac{(Y_{AB} + Y_L) + j\, Y_0 \tan \beta \ell_2}{Y_0 + j(Y_{AB} + Y_L)\tan \beta \ell_2} \quad , \tag{5.1}$$

$$\frac{Y_{CD}}{Y_0} = - j \cot \frac{2\pi \ell_3}{\lambda} \quad , \quad Y_{AB} = - j\, Y_0 \cot \frac{2\pi\, \ell_1}{\lambda} \quad . \tag{5.2}$$

Let $Y' = Y_S + Y_{CD}$; then

$$\frac{Y'}{Y_0} = \frac{Y_L - j\, Y_0 \cot (2\pi \ell_1/\lambda) + j\, Y_0 \tan (2\pi \ell_2/\lambda)}{Y_0 + j \left[Y_L - j\, Y_0 \cot (2\pi \ell_1/\lambda)\right] \tan \beta \ell_2} - j \cot \frac{2\pi \ell_3}{\lambda} \quad . \tag{5.3}$$

Let

$$\theta_1 = \frac{2\pi\, \ell_1}{\lambda} \quad , \quad \theta_2 = \frac{2\pi\, \ell_2}{\lambda} \quad , \quad \theta_3 = \frac{2\pi\, \ell_3}{\lambda} \quad , \tag{5.4}$$

then —

$$\frac{\bar{Y'}}{Y_0} = \frac{Y_L + j\, Y_0 (\tan \theta_2 - 1/\tan \theta_1)}{Y_0 (1 + \tan \theta_2/\tan \theta_1) + j\, Y_L \tan \theta_2} - j \frac{1}{\tan \theta_3} \quad . \tag{5.5}$$

Eq (5.5) represents the normalized admittance of the equivalent circuit shown in Fig. 5.4, where Y' is the admittance of the coaxial cavity plus load at the position of the bar-and-vane structure.

We now consider the effects of the vane-and-bar geometry as employed in the Model-9 type magnetron. Fig. 5.5 defines the required notation which is used in the equations. Here L_V is the total inductance of all the vanes in parallel, and C_A is the total capacitance between the vanes and bars. The shunt admittance which is "seen" by the electrons is:

$$Y_{shunt} = \frac{Y'}{1 + j\omega Y' L_V} + j\, \omega C_A \quad . \tag{5.6}$$

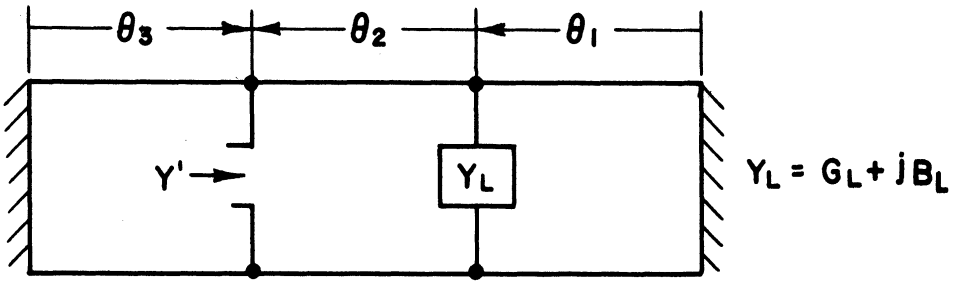

FIG. 5.4
EQUIVALENT CIRCUIT SHOWING THE ADMITTANCE OF THE COAXIAL LINE AT THE POSITION OF THE VANE-AND-BAR STRUCTURE.

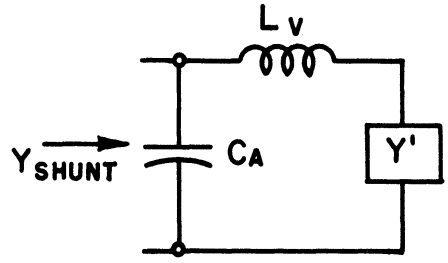

FIG. 5.5
EQUIVALENT CIRCUIT USED IN CALCULATION OF SHUNT ADMITTANCE BETWEEN ADJACENT ANODE SEGMENTS

Upon substitution of Eq (5.5) for Y' into Eq (5.6) and rationalizing, we obtain the expressions given by Eqs (5.7) and (5.8).

$$\frac{G_{shunt}}{G_L} = \frac{\csc^2 \theta_2}{\left[\frac{\omega L_V}{Z_0}\frac{\alpha}{b}\left(\frac{\beta}{\alpha}+\frac{B_L}{Y_0}\right) - \left(\frac{\gamma}{b}-\frac{B_L}{Y_0}\right)\right]^2 + \left[\omega L_V G_L \frac{\alpha}{b} - \frac{G_L}{Y_0}\right]^2}, \quad (5.7)$$

$$\frac{B_{shunt}}{Y_0} = \frac{\omega C_A}{Y_0} - \frac{\frac{\omega L_V}{Z_0}\left[\left(\frac{\beta}{b}+\frac{\alpha}{b}\frac{B_L}{Y_0}\right)^2+\left(\frac{\alpha}{b}\frac{G_L}{Y_0}\right)^2\right]-\left[\left(\frac{\gamma}{b}-\frac{B_L}{Y_0}\right)\left(\frac{\beta}{b}+\frac{\alpha}{b}\frac{B_L}{Y_0}\right)-\frac{\alpha}{b}\frac{G_L^2}{Y_0^2}\right]}{\left[\frac{L_V}{Z_0}\frac{\alpha}{b}\left(\frac{\beta}{\alpha}+\frac{B_L}{Y_0}\right)-\left(\frac{\gamma}{b}-\frac{B_L}{Y_0}\right)\right]^2+\left[\omega L_V G_L \frac{\alpha}{b}-\frac{G_L}{Y_0}\right]^2}. \quad (5.8)$$

Here

$$a = \tan\theta_1 \qquad \alpha = \left(1+\frac{b}{d}\right) \qquad \beta = \left(b-\frac{1}{a}-\frac{1}{d}-\frac{b}{ad}\right)$$

$$b = \tan\theta_2 \qquad \gamma = \left(1+\frac{b}{a}\right) \qquad Y_L = G_L + j\,B_L \,. \quad (5.9)$$

$$d = \tan\theta_3$$

5.2 The Symmetrical Case

Eqs (5.7) and (5.8) can be given a simpler approximate form by making use of the inequalities given below, which were determined from numerical computation. The resultant final approximate Eqs, (5.10) and (5.11), for shunt susceptance and shunt conductance have been checked numerically against the more exact Eqs, (5.7) and (5.8), and have been found to be correct to within three per cent for a self-contained magnetron[12] coupled to a matched load in the case of a symmetrically excited cavity, i.e., $\theta_1 + \theta_2 = \theta_3$.

Since the numerical computations indicate that:

$$\frac{B_L}{Y_0} \ll \frac{\beta}{\alpha} \quad ,$$

$$\frac{B_L}{Y_0} \ll \frac{\gamma}{b} \quad ,$$

and

$$\left[\omega L_V G_L \frac{\alpha}{b} - \frac{G_L}{Y_0}\right]^2 \ll \left[\frac{\omega L_V}{Z_0} \frac{\alpha}{b} \left(\frac{\beta}{\alpha} + \frac{B_L}{Y_0}\right) - \left(\frac{\gamma}{b} - \frac{B_L}{Y_0}\right)\right]^2 ,$$

then

$$\frac{G_{shunt}}{G_L} \cong \frac{(\alpha\gamma + b\beta)}{\left[\omega L_V Y_0 \beta - \gamma\right]^2} \quad , \tag{5.10}$$

also, since

$$\left(\frac{\alpha}{b} \frac{G_L}{Y_0}\right)^2 \ll \left(\frac{\beta}{b} + \frac{\alpha}{b} \frac{B_L}{Y_0}\right)^2 \quad ,$$

and

$$\frac{\alpha}{b} \frac{G_L^2}{Y_0^2} \ll \left(\frac{\gamma}{b} - \frac{B_L}{Y_0}\right) \left(\frac{\beta}{b} + \frac{\alpha}{b} \frac{B_L}{Y_0}\right) ,$$

then

$$\frac{B_{shunt}}{Y_0} \cong \frac{\omega C_A}{Y_0} - \frac{\beta}{(\omega L_V Y_0 \beta - \gamma)} \quad . \tag{5.11}$$

After substituting for the values of α, β, and γ in Eqs (5.10) and (5.11), and including the relation $(\theta_1 + \theta_2) = \theta_3$, we obtain

$$G_{sh} \cong G_L Z_0^2 \frac{\sin^2 \theta_1}{4 \cos^2 \theta_3} \frac{1}{\left[\omega L_V + (Z_0/2) \tan \theta_3\right]^2} \quad , \tag{5.12}$$

$$B_{sh} \cong \omega C_A - \frac{1}{\omega L_V + (Z_0/2) \tan \theta_3} \quad . \tag{5.13}$$

Eq (5.13), when set equal to zero, gives the condition for cold resonance, i.e., cold resonance of the cavity in the absence of the cathode.

To obtain an expression for Q_{ext} for symmetrical geometry, we assume B_{shunt} varies linearly with wavelength in the region $\omega = \omega_0$. Then:

$$\left(\frac{d\ B_{sh}}{d\omega}\right)_{\omega = \omega_0} x \quad (\omega_1 - \omega_0) \quad = \quad G_{shunt}\ , \tag{5.14}$$

or

$$\frac{1}{G_{sh}} \left(\frac{d\ B_{sh}}{d\omega}\right)_{\omega = \omega_0} \quad = \quad \frac{1}{\omega_1 - \omega_0} \tag{5.15}$$

Here ω_0 corresponds to the cold-resonance frequency and ω_1 corresponds to the half-power frequency. Multiplying both sides of Eq (5.15) by $\omega_0/2$ we obtain

$$\frac{\omega_0}{2\ G_{sh}} \left(\frac{d\ B_{sh}}{d\omega}\right)_{\omega = \omega_0} \quad = \quad \frac{\omega_0}{2(\omega_1 - \omega_0)} \quad = \quad Q_{ext}. \tag{5.16}$$

Upon carrying out the indicated differentiation, we obtain

$$Q_{ext} \quad = \quad \left\{ C_A + \frac{L_V + (\theta_3\ Z_0/2\omega_0)\ \sec^2 \theta_3}{\left[\omega_0 L_V + (Z_0/2) \tan \theta_3\right]^2} \right\} \frac{\omega_0}{2\ G_{shunt}} \ . \tag{5.17}$$

In the case of a "T" coupling to the output line, calculations have shown that the load admittance is transferred into the cavity at the position of the "T" with very nearly a one-to-one transformation ratio. The deviation from a one-to-one transformation ratio depends on the load susceptance. For the case of the "T" coupling, Eq (5.17), after substituting for G_{shunt}, becomes

$$Q_{ext} = \frac{1}{G_L \sin^2 \theta_1} \left[\frac{2\omega_0 L_V \cos^2 \theta_3}{Z_0^2} + \frac{\omega_0 C_A \sin^2 \theta_3}{2} \right. \tag{5.18}$$

$$\left. + \frac{\theta_3}{Z_0} + \frac{2\omega_0 C_A \omega_0 L_V \sin \theta_3 \cos \theta_3}{Z_0} \right] .$$

If we substitute the resonance condition

$$\omega_0 C_A = \frac{1}{\omega L_V + (Z_0/2) \tan \theta_3} \tag{5.19}$$

into Eq (5.17) and then let $\omega_0 L_V$ go to zero, we obtain

$$Q_{ext} = \frac{\omega_0 C_A}{G_{sh}} \left[\frac{1}{2} + \frac{1}{2} \frac{2\theta_3}{\sin 2\theta_3} \right] . \tag{5.20}$$

Eq (5.20) indicates the division of energy storage between the lumped capacitance and the line for a symmetrical structure. Letting θ_3 go to zero in Eq (5.20) results in the relation for Q_{ext} for a lumped-constant circuit, i.e.,

$$Q_{ext} = \frac{\omega_0 C_A}{G_{shunt}} . \tag{5.21}$$

The significant results of the analysis presented in this chapter are summarized below.

The General Case $\theta_1 + \theta_2 \neq \theta_3$

The important results are the following:

Eq (5.7)(for the shunt conductance between anode segments "seen" by the electrons "looking" radially outward from the interaction space).

Eq (5.8)(for the shunt susceptance between anode segments "seen" by the electrons "looking" radially outward from the interaction space).

This equation (when B_{shunt} is set equal to zero) can be used to determine the cold-resonance frequency of the resonator in the absence of the cathode.

The Symmetrical Case ($\theta_1 + \theta_2 = \theta_3$)

Eq (5.12) (for the shunt conductance between anode segments).

Eq (5.13) (for the shunt susceptance between anode segments). This equation (when B_{shunt} is set equal to zero) can be used to determine the cold-resonance frequency of the resonator in the absence of the cathode.

Eqs (5.17), (5.18), and (5.20) (for the external Q of the circuit in the absence of the cathode). These equations clearly indicate the relationships between the design parameters. Here we see the significance of the quantity C_A when low-Q operation is desired. Since C_A depends, in part, on interaction space design the lowest attainable external Q depends on the compromise made between interaction space design and circuit design.

CHAPTER VI

PRESENTATION AND INTERPRETATION OF EXPERIMENTAL RESULTS

The presentation of the experimental results is divided into three parts; namely, high-Q, intermediate-Q, and low-Q operation. The Q referred to here is the external Q which is defined as follows:

$$Q_{ext} = 2\pi \frac{\text{energy stored in circuit}}{\text{energy dissipated in the load per cycle}} . \qquad (6.1)$$

In practice it is found that an order of magnitude relation between the space-charge effects on the frequency of oscillation is given by

$$\frac{\omega - \omega_o}{\omega_o} \cong \frac{1}{2Q_L} , \qquad (6.2)$$

where Q_L is the loaded Q of the circuit. Q_L is defined by the relation

$$Q_L = 2\pi \frac{\text{energy stored in circuit}}{\text{energy dissipated in the load and cavity per cycle}} . \qquad (6.3)$$

The relation between the external Q and the loaded Q is given by

$$\frac{1}{Q_{ext}} = \frac{1}{Q_L} - \frac{1}{Q_o} , \qquad (6.4)$$

where Q_o is the internal Q defined as follows:

$$Q_o = 2\pi \frac{\text{energy stored in circuit}}{\text{energy dissipated in the cavity per cycle}} . \qquad (6.5)$$

In the material which follows we have made the tacit assumption that

$$Q_o \gg Q_L \text{ and } Q_{ext} \cong Q_L , \tag{6.6}$$

for both the high and intermediate-Q regions of operation. The error arising from this assumption is not serious since Eq (6.2) is an order of magnitude relation.

We can now state the three ranges of external-Q in terms of the space-charge effects on frequency as follows:

High Q_{ext} — less than 1/2% frequency pushing

Intermediate Q_{ext} — between 1/2% and 5% frequency pushing

Low Q_{ext} — greater than 5% frequency pushing.

The terms high-Q and intermediate-Q operation, as employed here, imply that the frequency of magnetron operation is determined primarily by the properties of the circuit. The term low-Q operation, on the other hand, implies that the frequency of magnetron operation is substantially independent of the circuit and depends primarily on the anode potential and magnetic field. These two types of magnetron operation appear to overlap at values of loaded Q of the order of 5 to 10.

The experimental work was carried out with two primary objectives in mind. These were:

(a) To determine the feasibility of operating the insertion tube as a mechanically tunable magnetron over a wide range of wavelengths.

(b) To find out whether or not wide-range electronic tuning could be attained with this tube and its associated circuitry, and

to determine the limiting factors in this type of operation.

There were, in addition, other important objectives in the experimental program as follows:

(c) To determine the effect of loading on upper-mode-boundary current and on frequency pushing.

(d) To obtain design experience for the construction of higher-power and higher-frequency ceramic-seal tubes of similar geometry.

Before presenting the experimental data for the insertion tube operating as a magnetron, one point with regard to the d-c diode characteristics of the tube (no magnetic field) should be indicated. Fig. 6.1 shows the d-c emission characteristics for the Model 9A, No. 39 tube which were obtained within a short time after its oxide-coated cathode had been activated. It is interesting to note that the anode current is not equally divided between the bar and the vane anodes when both sets of anodes are at the same potential relative to the cathode. The reason for this unequal division of total current is explainable in terms of the intercepting cross sections presented to radial electron flow by the bar anodes and vane anodes, respectively. The intercepting cross section of the vane anodes is larger than that of the bar anodes since electrons which traverse slots between anode segments are eventually captured by the vane anodes. The division of total current is not significantly unequal when the tube operates with a magnetic field.

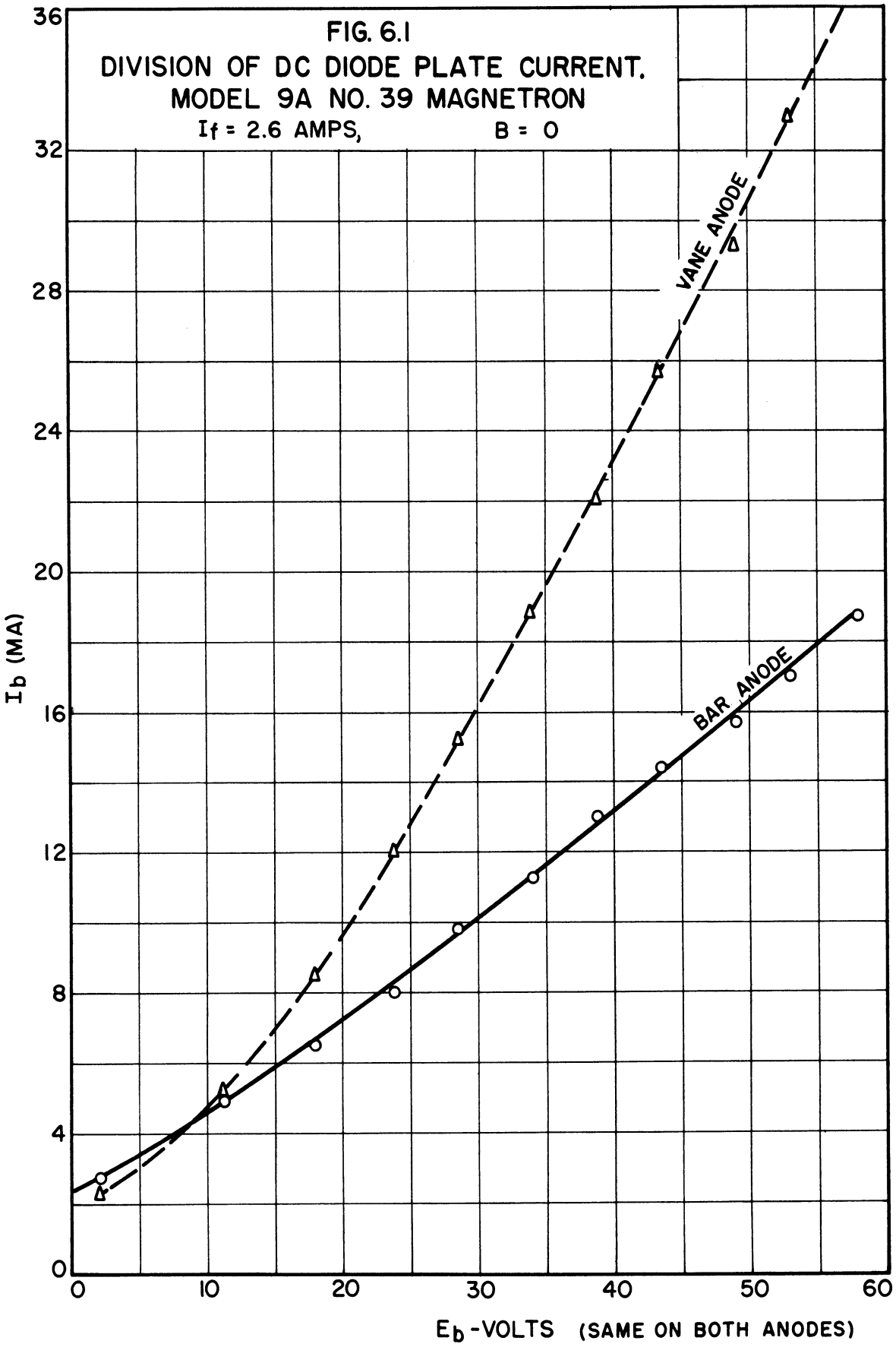
FIG. 6.1
DIVISION OF DC DIODE PLATE CURRENT.
MODEL 9A NO. 39 MAGNETRON
If = 2.6 AMPS, B = 0
VANE ANODE
BAR ANODE
Ib (MA)
Eb -VOLTS (SAME ON BOTH ANODES)
0
4
8
12
16
20
24
28
32
36
0
10
20
30
40
50
60

6.1. High-Q Magnetron Operation

The coaxial cavities employed for high-Q operation of the insertion magnetron have been designated No. 1 and No. 3, and are depicted in Figs. 6.2 and 6.3, respectively. Cavity No. 1 was subsequently modified to provide movable shorting slugs for tuning. In addition, a series of tapped holes were provided for facilitating changes in the coupling probe position in the cavity. A photograph of the modified version of cavity No. 1 and its electromagnet is given in Fig. 6.4.

The first operating test on the insertion magnetron was made using tube No. 39 in cavity No. 1, which was non-tunable at the time of this test. The tube was operated with a 15 microsecond pulse having a repetition rate of 60 pulses per second. Oscillation was observed at 10.7 cm, which corresponds to the 3/2-wavelength TEM coaxial-cavity mode. Oscillation was also observed at approximately 30 cm corresponding to the 1/2-wavelength coaxial mode. The anode segments for both of the above cavity modes operate in the π-mode. Typical pulsed-performance oscillograms showing the 10.7-cm mode of operation are shown in Fig. 6.5. Note that the slope of the vertical portion of the volt-ampere characteristic in Fig. 6.5(b) is significantly less than that in Fig. 6.5(a). The larger leakage current indicated by the lower slope is attributed to the increased cathode end-shield emission caused by the elevated cathode temperature.

The anode potential corresponding to the 10.7-cm mode was approximately 900 volts with a magnetic-flux density of 1280 gauss.

An experiment was performed to determine the minimum wavelength attainable as well as a tuning curve for the tunable version of cavity No. 1.

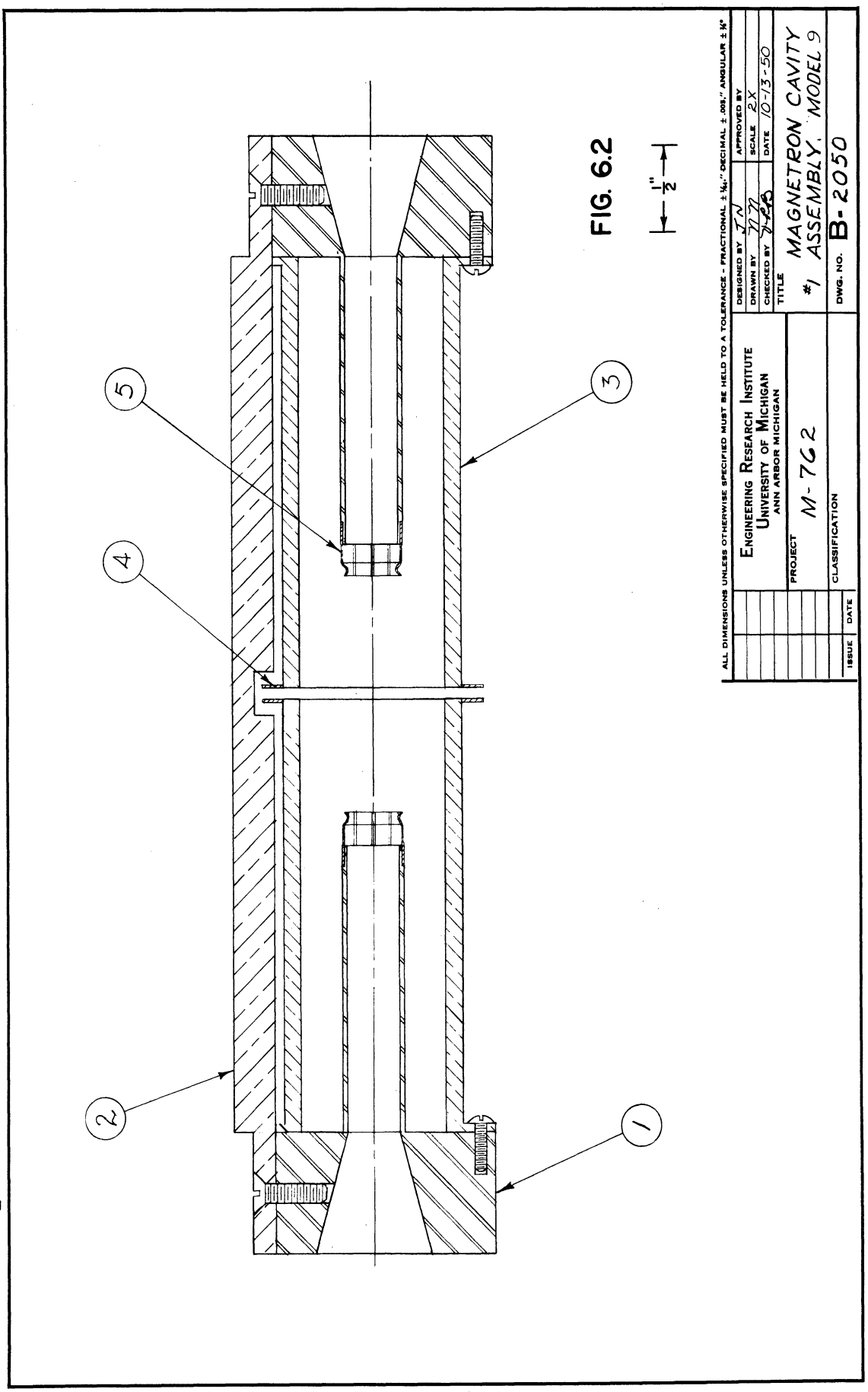
5
4
3
2
1
1/2"
ALL DIMENSIONS UNLESS OTHERWISE SPECIFIED MUST BE HELD TO A TOLERANCE - FRACTIONAL ± 1/64" DECIMAL ± .005" ANGULAR ± 1/2°
ENGINEERING RESEARCH INSTITUTE
UNIVERSITY OF MICHIGAN
ANN ARBOR MICHIGAN
DESIGNED BY TN
DRAWN BY TT
CHECKED BY
APPROVED BY
SCALE 2X
DATE 10-13-50
PROJECT M-762
TITLE #1 MAGNETRON CAVITY ASSEMBLY, MODEL 9
CLASSIFICATION
DWG. NO. B-2050
ISSUE
DATE
DWG. NO. B

FIG. 6.2

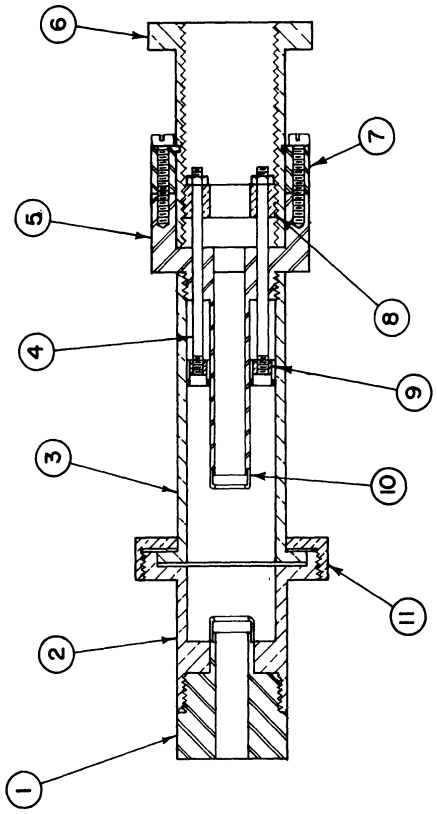

FIG. 6.3

1"

ALL DIMENSIONS UNLESS OTHERWISE SPECIFIED MUST BE HELD TO A TOLERANCE - FRACTIONAL ± 1/64," DECIMAL ± .005," ANGULAR ± 1/2°

ENGINEERING RESEARCH INSTITUTE UNIVERSITY OF MICHIGAN ANN ARBOR MICHIGAN	DESIGNED BY J. S. N.	APPROVED BY	
	DRAWN BY [illegible]	SCALE FULL	
	CHECKED BY J. S. N.	DATE 6-7-51	
PROJECT M-921	TITLE CAVITY NO. 3 MOD. 9 MAG.		
CLASSIFICATION	DWG. NO. B-2053		

ISSUE	DATE

DWG. NO. B

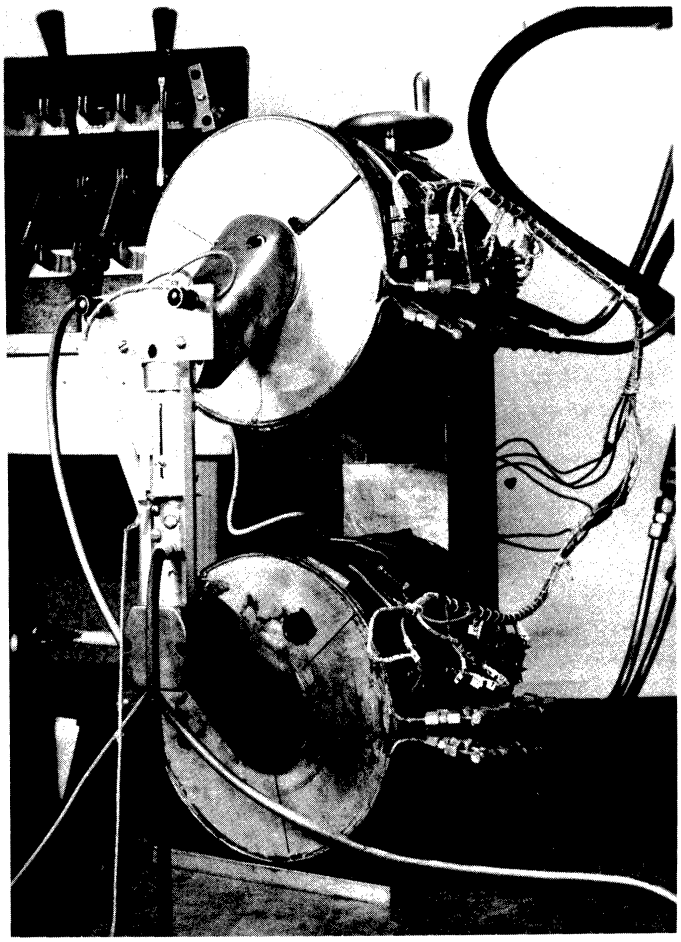

FIG. 6.4

PHOTOGRAPH OF CAVITY
NO. 1 IN ELECTROMAGNET

B = 1280 GAUSS
I_{fil} = 2.0 AMP

(a)

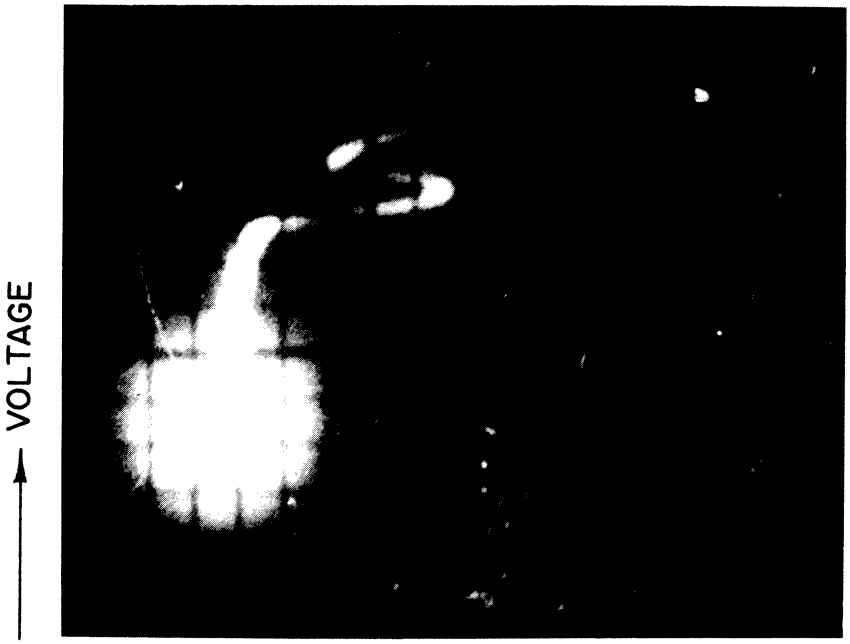

B = 1280 GAUSS
I_{fil} = 2.5 AMP

(b)

FIG. 6.5 PULSED PERFORMANCE OSCILLOGRAMS
MODEL 9A MAGNETRON

CURRENT CALIBRATION = 25 MA. PER DIV.
VOLTAGE CALIBRATION ≅ 192 V. PER DIV.

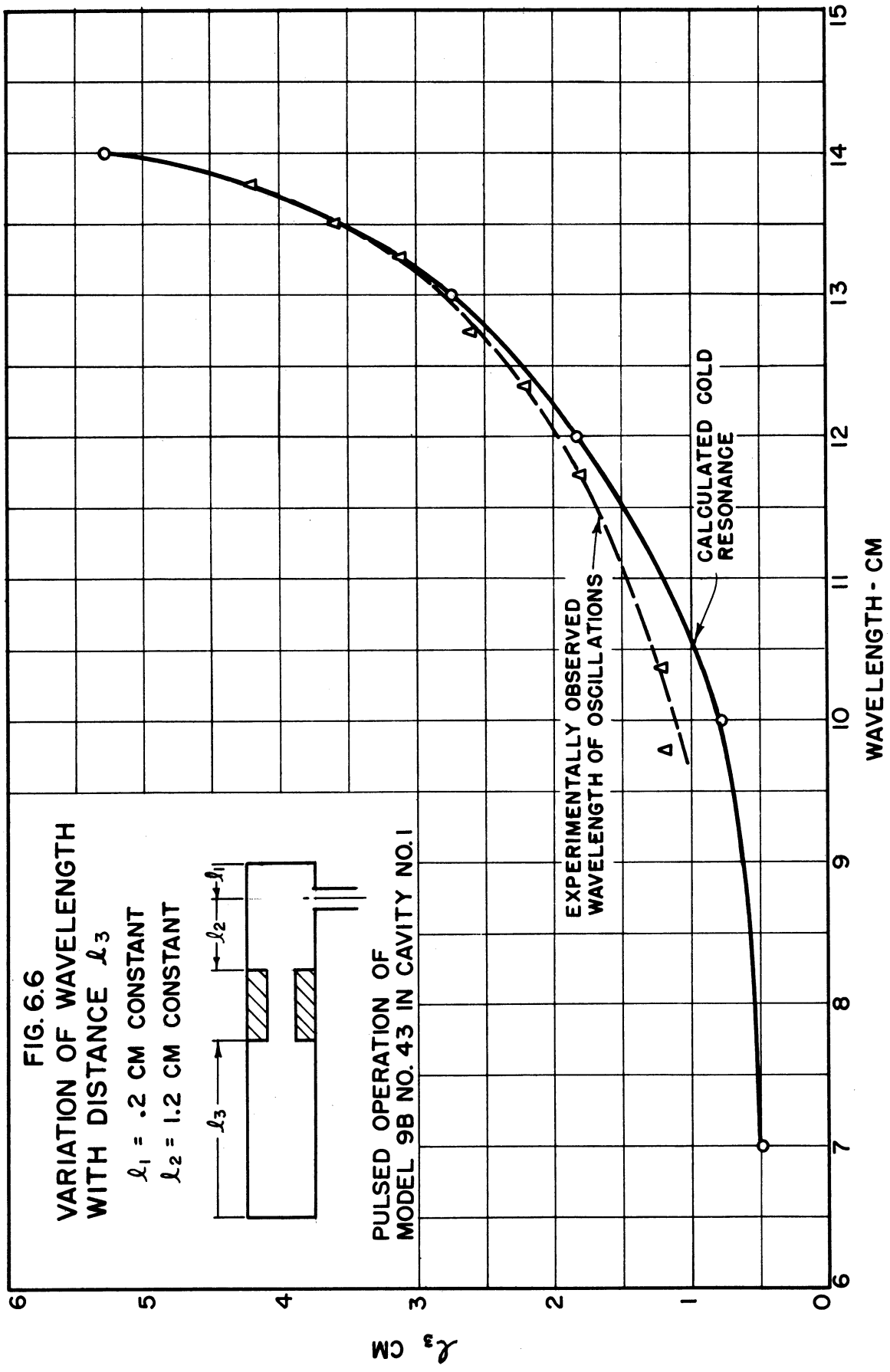
FIG. 6.6
VARIATION OF WAVELENGTH WITH DISTANCE ℓ_3
ℓ_1 = .2 CM CONSTANT
ℓ_2 = 1.2 CM CONSTANT
ℓ_3
ℓ_2
ℓ_1
PULSED OPERATION OF MODEL 9B NO. 43 IN CAVITY NO. 1
EXPERIMENTALLY OBSERVED WAVELENGTH OF OSCILLATIONS
CALCULATED COLD RESONANCE
λ_3 CM
WAVELENGTH - CM
0
1
2
3
4
5
6
7
8
9
10
11
12
13
14
15

In this experiment the Model 9B, No. 43 (oxide-coated cathode) was operated under pulsed conditions. The conditions for this experiment are listed below.

I_{fil} = 2.25 amperes

B = 1200 gauss

ℓ_1 = 0.2 cm (distance of output probe from one tuner slug)

ℓ_2 = 1.2 cm (distance from right edge of vanes to output probe)

ℓ_3 = (variable distance from movable tuner slug face to left edge of vanes).*

The results of this experiment are given in Fig. 6.6 together with a theoretical tuning curve which has been computed using Eq (5.8) and the tube constants calculated in Appendix B. The agreement between the calculated and experimental plots should not necessarily be considered as a verification of the theory, since the computations do not include the effects of the cathode circuit or the glass seals. However, it is reasonable to conclude that the general shape of the experimental tuning curve is predictable from the theory for this unsymmetrical case.

Cavity No. 3, shown in Fig. 6.3, was constructed in order to obtain further information regarding the mechanical tunability of the insertion magnetron. One of the important aspects of wide-range tuning is the degree of variation of upper-mode-boundary current** with frequency. Figs. 6.7 and 6.8 give the results of two experiments which were conducted to

---

* The cathode bypass No. 1 shown in Appendix D, Drawing D-2, was employed in this experiment.

** See Section 1.4 for a definition of upper-mode-boundary current.

determine the upper-mode-boundary current as a function of oscillator wavelength as well as wavelength as a function of tuner position. The conditions for this experiment using the same "ℓ" notations as in the previous case were:

Pulsed operation of Model 9B, No. 43

ℓ_1 = 0.318 cm

ℓ_2 = 1.082 cm

ℓ_3 = variable

I_{fil} = 2.0 amps.

B = 1650 gauss

The external cathode bypass referred to in Figs. 6.7 and 6.8 is given in Appendix D, Drawing D-1.

The significant results of this experiment are apparent from Figs. 6.7 and 6.8. Here we observe that when the cathode bypass causes an increase in operating wavelength, the upper-mode-boundary current is reduced, whereas, if this shift is toward lower wavelengths, the upper-mode-boundary current is increased with respect to that obtained in the absence of the cathode bypass. It is important to realize that the cathode circuit consists of a section of coaxial transmission line inside the evacuated envelope in addition to any external circuit components. The foregoing results demonstrate the feasibility of operating the insertion magnetron in a mechanically tunable cavity over a wide wavelength range with a reasonable upper-mode-boundary current. The conditions in this experiment were not necessarily those which would result in optimum upper-mode-boundary current for a given bandwidth. It should therefore be possible

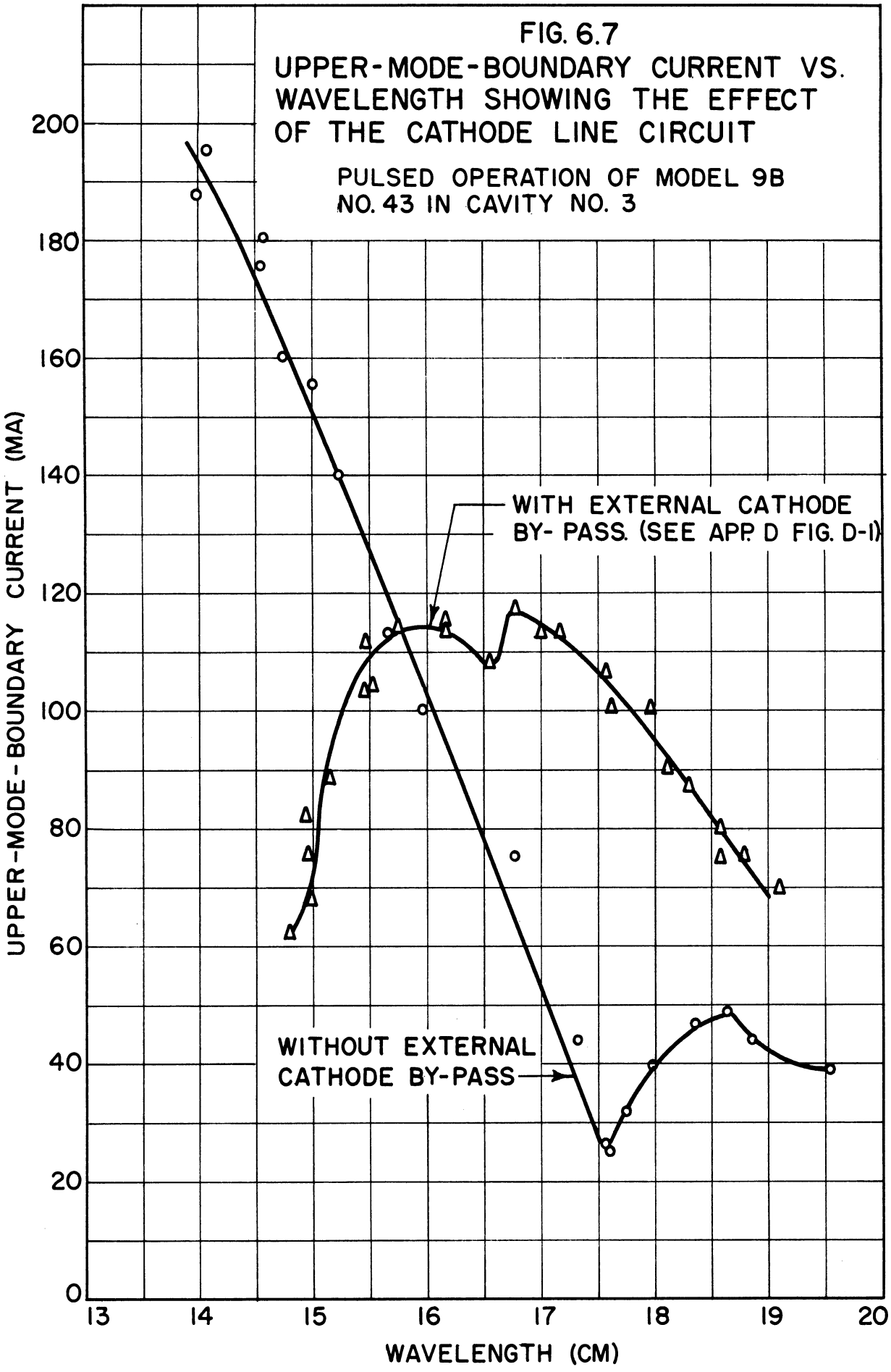
FIG. 6.7
UPPER-MODE-BOUNDARY CURRENT VS. WAVELENGTH SHOWING THE EFFECT OF THE CATHODE LINE CIRCUIT
PULSED OPERATION OF MODEL 9B NO. 43 IN CAVITY NO. 3
WITH EXTERNAL CATHODE BY-PASS. (SEE APP. D FIG. D-1)
WITHOUT EXTERNAL CATHODE BY-PASS
UPPER-MODE-BOUNDARY CURRENT (MA)
WAVELENGTH (CM)
0
20
40
60
80
100
120
140
160
180
200
13
14
15
16
17
18
19
20

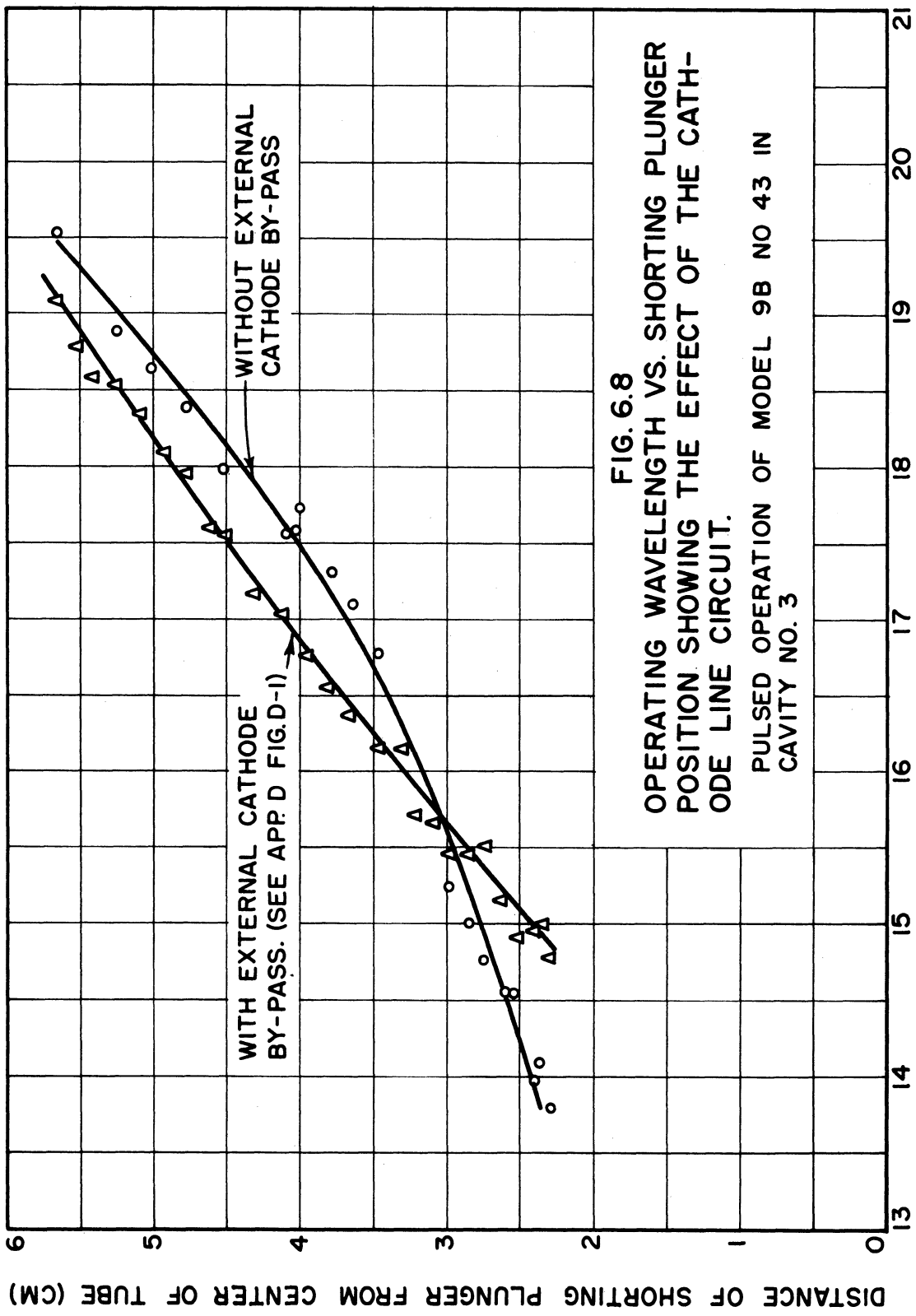
WITHOUT EXTERNAL CATHODE BY-PASS
WITH EXTERNAL CATHODE BY-PASS. (SEE APP. D FIG. D-1)
FIG. 6.8
OPERATING WAVELENGTH VS. SHORTING PLUNGER POSITION SHOWING THE EFFECT OF THE CATHODE LINE CIRCUIT.
PULSED OPERATION OF MODEL 9B NO 43 IN CAVITY NO. 3
DISTANCE OF SHORTING PLUNGER FROM CENTER OF TUBE (CM)
WAVELENGTH (CM) MEASURED AT THE LOWER MODE BOUNDARY
0
1
2
3
4
5
6
13
14
15
16
17
18
19
20
21

to improve the mode boundary versus bandwidth characteristics by further study of cathode-circuit effects.

The c-w power output available from the insertion structure has been as high as three watts with high-Q operation. The following data are typical for high-Q, c-w performance.

E_b (volts)	I_b (ma.)	I_{fil} (amps.)	B (gauss)	λ (cm)	P_o (watts)
800	20	2.0	1770	20.090	3.0

This information was obtained using the Model 9A, No. 39 tube with the arrangement of apparatus shown in Fig. 6.10. The shorted-stub tuner was adjusted to obtain maximum power output. Observation of the signal on a spectrum analyzer indicated a noise level approximately 20 db below the signal level.

Model 9C, No. 48 was pulse-tested in cavity No. 3. This tube employs an oxide-coated cathode and may be used with an external cathode bypass. All attempts to obtain tunable output with this tube and cavity failed. Very low power was detected at a wavelength near 7 cm irrespective of the position of the movable short. This is indicative of resonance in the vane-mode of oscillation. The term "vane mode" signifies a mode of oscillation characteristic of the vane-type magnetron and is encountered with the vane-and-bar geometry when the phase difference between r-f potentials of adjacent vane-anode segments is π radians. This is not the only phase difference which is associated with the vane magnetron type of operation, but it is the most common one. Within the limits imposed by this tube structure, changing the vane-mode resonance wavelength can be accomplished

by changing the radial length of the vanes or the angular displacement between vanes.[12]

6.2. Intermediate-Q Operation

An external circuit was designed for low-Q operation, but was modified to perform the following experiment, in which the external Q varies from approximately 10 to 100. An assembly drawing of cavity No. 2 is given in Fig. 6.9.

A sketch showing the modified version of cavity No. 2, employed in the following experiment, is shown in Fig. 6.10. Listed below are the conditions of the experiment.

Model 9A, No. 39 Tube

Pulsed operation.

Wavelength measured at both the high and low-current ends of the volt-ampere characteristic for each position "d" of the tunable shorting stub.

Upper-mode-boundary current measured for each position "d" of the tunable shorting stub.

I_{fil} = 2.15 amperes — constant.

B = 1850 gauss — constant.

Note: This insertion tube uses an oxide-coated cathode. A cathode-line choke and bypass is contained inside the vacuum envelope.

Fig. 6.11 shows the results of this experiment. It is interesting to observe that the pushing (increase of frequency with increase in plate current), is positive for "d" less than 0.9 cm, negative at 0.9 cm, positive from "d" = 0.9 cm to 1.5 cm, and zero for "d" = 1.5 to 1.6 cm.

DWG. NO. B

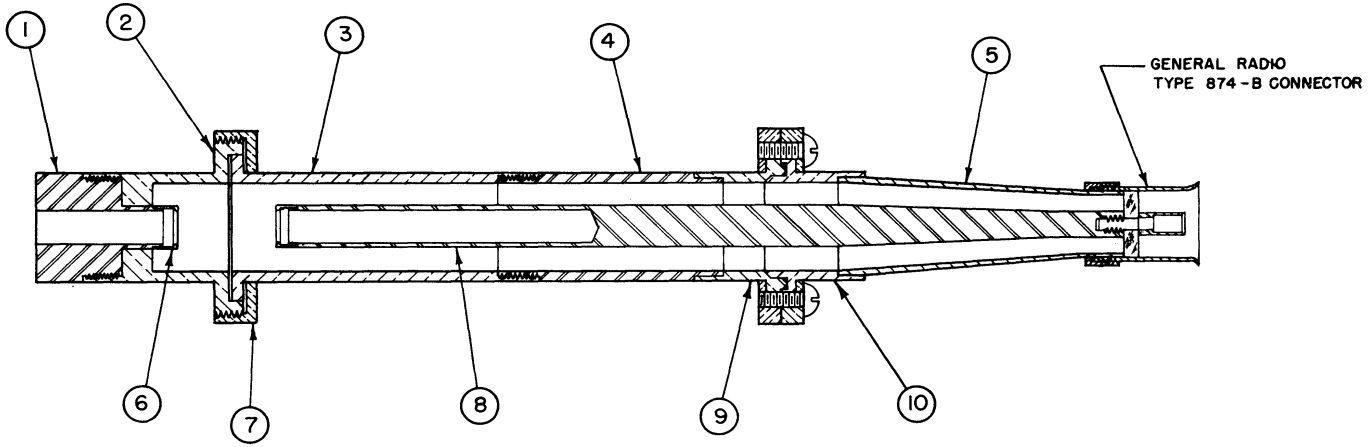

FIG. 6.9

1"

ALL DIMENSIONS UNLESS OTHERWISE SPECIFIED MUST BE HELD TO A TOLERANCE - FRACTIONAL ± 1/64" DECIMAL ± .005" ANGULAR ± 1/2°

ISSUE	DATE	ENGINEERING RESEARCH INSTITUTE UNIVERSITY OF MICHIGAN ANN ARBOR MICHIGAN	DESIGNED BY J. S. N.	APPROVED BY
			DRAWN BY W W	SCALE FULL
			CHECKED BY W R B.	DATE 3-16-51
		PROJECT M-921	TITLE CAVITY NO. 2, MOD. 9 MAG.	
		CLASSIFICATION	DWG. NO. B- 2052	

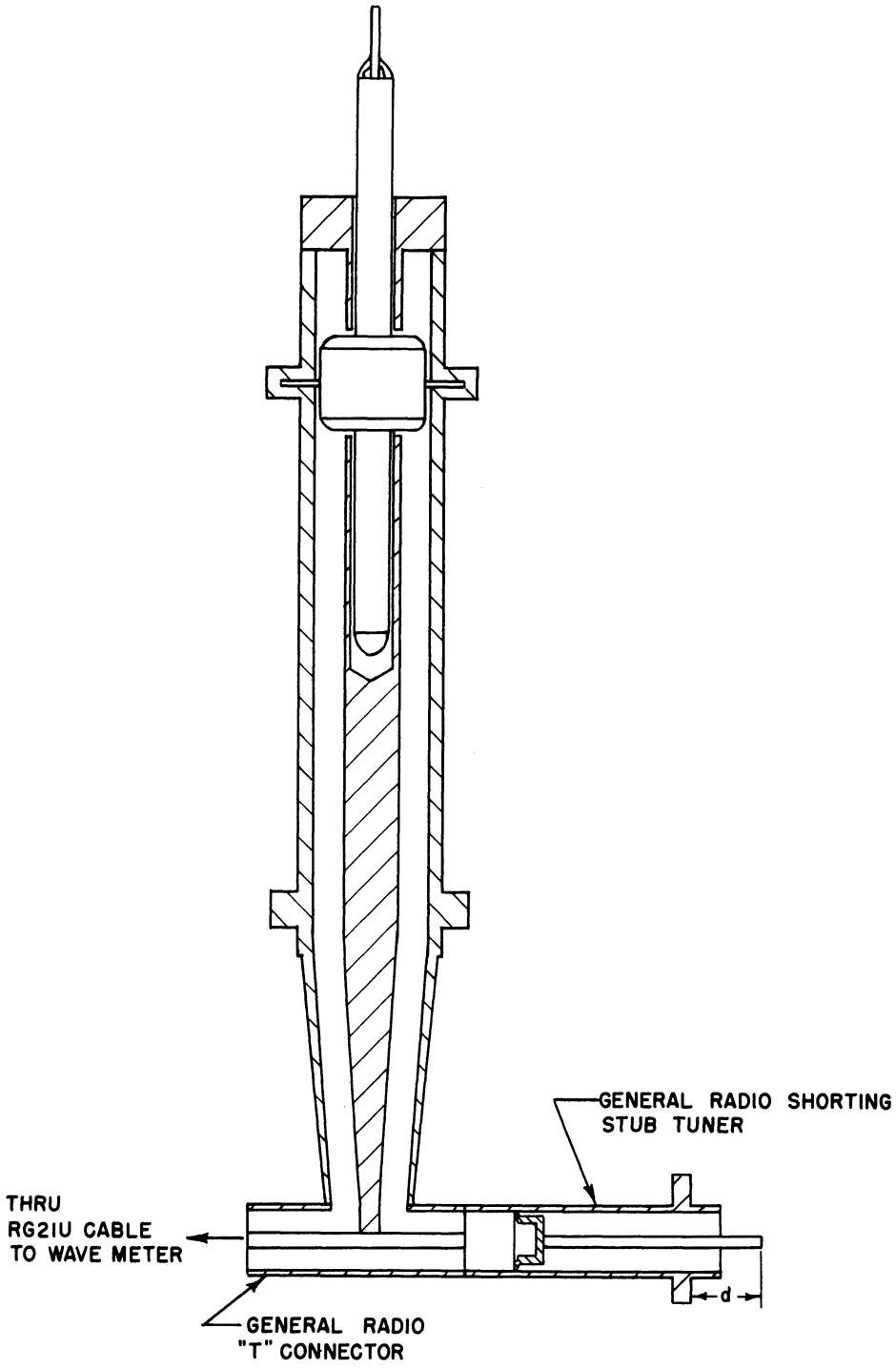

FIG. 6.10
ARRANGEMENT USED TO STUDY THE EFFECT OF THE LOAD ON UPPER-MODE-BOUNDARY CURRENT AND FREQUENCY PUSHING.

FIG. 6.11

EFFECT OF LOAD ON UPPER-MODE-BOUNDARY CURRENT AND FREQUENCY PUSHING.

EXPERIMENTAL SET-UP AS IN FIG. 6.10
(INTERMEDIATE-Q, PULSED OPERATION)
MODEL 9A NO. 39 MAGNETRON

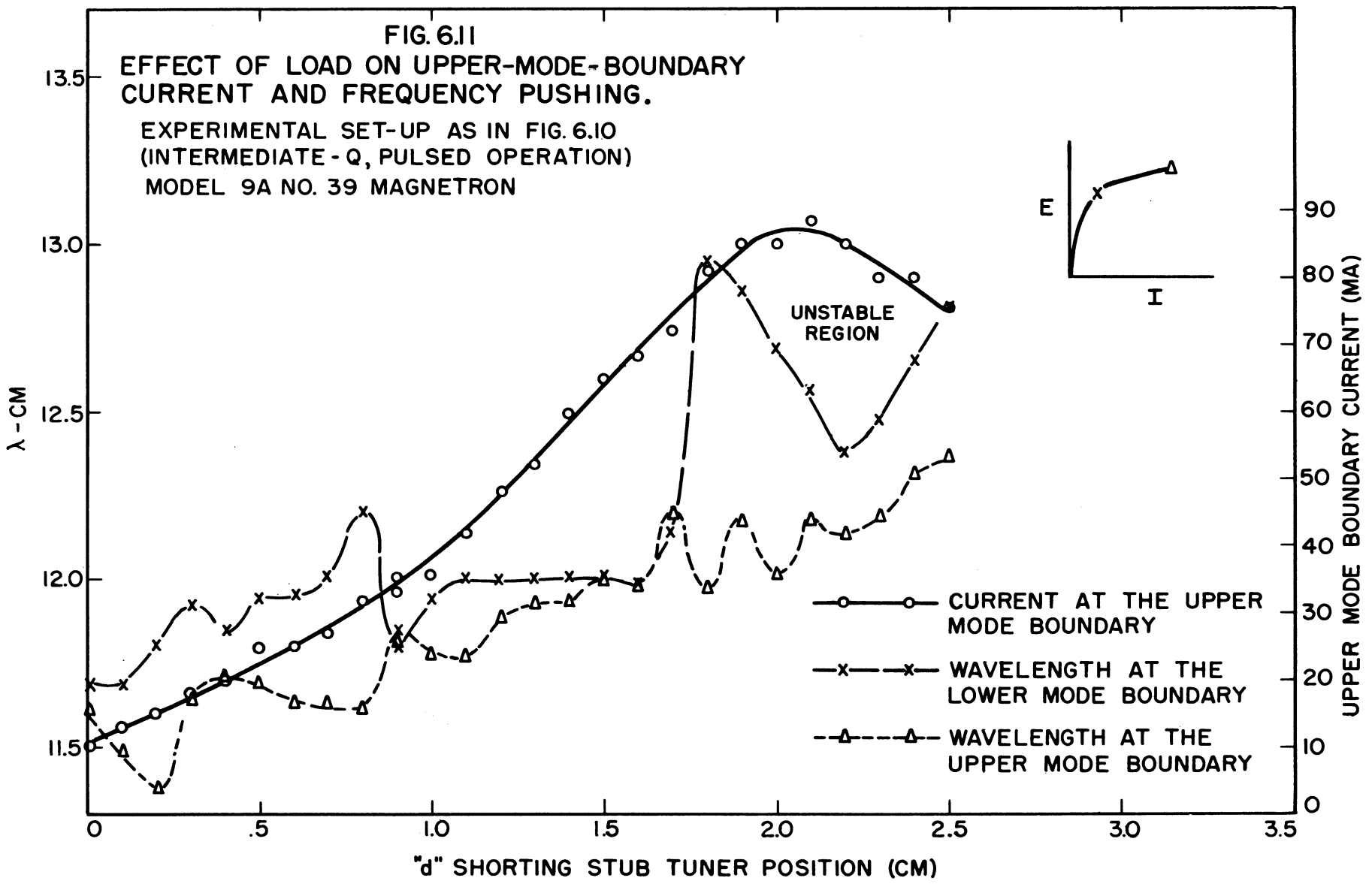

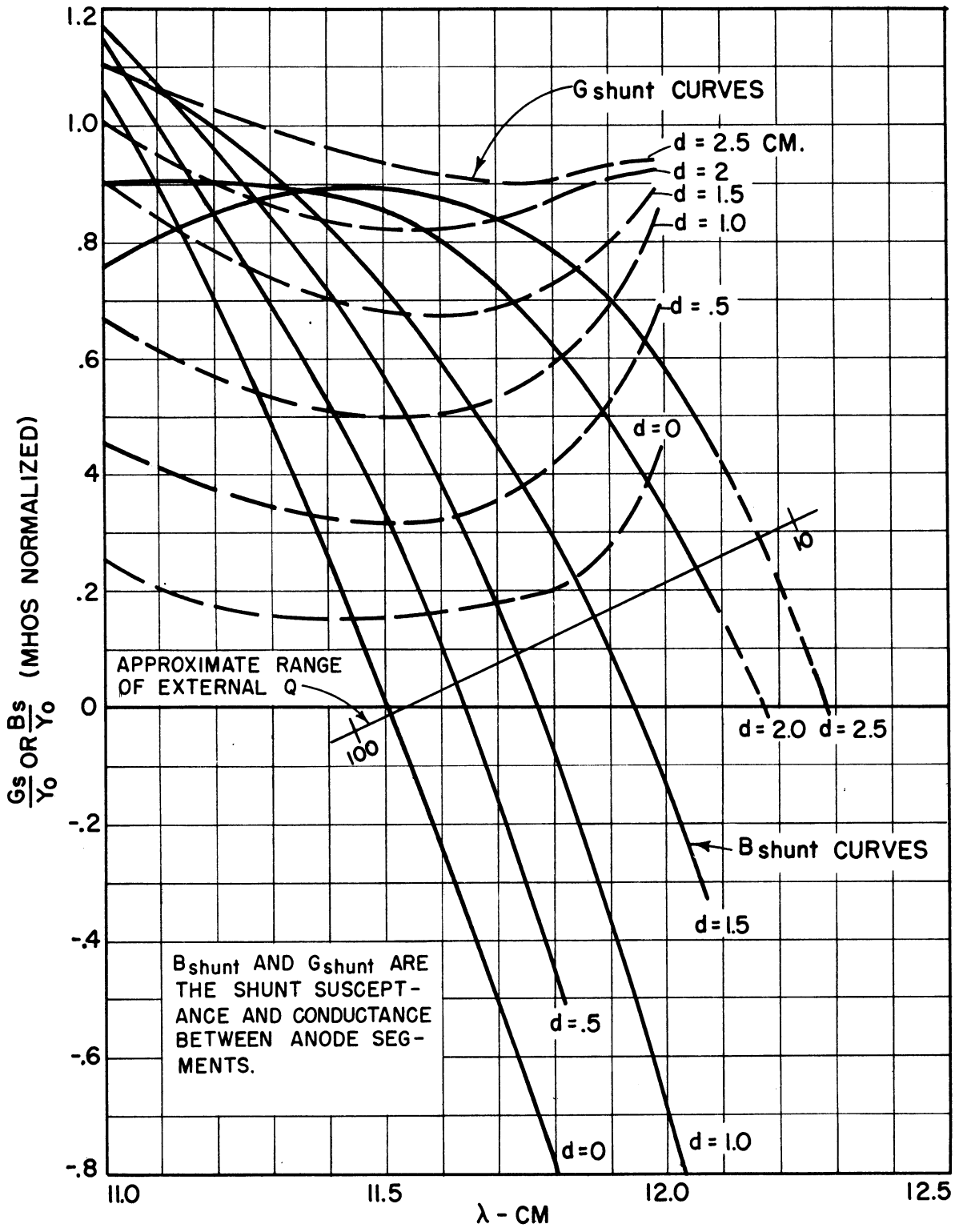

FIG. 6.12

NORMALIZED G_{shunt} AND B_{shunt} VS. WAVELENGTH WITH "d" AS A PARAMETER FOR CAVITY NO. 2 WITH REACTANCE TUNER. $Y_0 = .02$ MHOS

Calculations of the shunt susceptance and shunt conductance between adjacent anode segments as a function of wavelength were made for some of the values of "d" used in the experiment above. These calculations are based on the assumption of a lossless cavity and do not take cathode-line effects into account. The output circuit is assumed to be terminated in its characteristic impedance, i.e., 50 ohms. Values used for the vane-to-bar capacitance, and vane inductance were 2.0 $\mu\mu$f and 100 $\mu\mu$h, respectively. The results of the calculations are shown graphically in Fig. 6.12. If the wavelengths corresponding to the computed values of zero shunt susceptance are plotted against the distance "d", one obtains the solid curve shown in Fig. 6.13(a). It is interesting to note that the computed curve is in close agreement with the average of the curve for wavelength versus "d" for the maximum current readings. The variations present in the experimental curve could easily be the result of an improperly matched, long output line. Assuming this to be true, we observe upon study of both the computed shunt susceptance curves in Fig. 6.12 and the experimental results in Fig. 6.11, that the tube reaches the wavelength corresponding to the maximum current when the circuit susceptance tends to become capacitive. Furthermore, if the magnetron is oscillating at some wavelength, say 11.8 cm, corresponding to the region of negative pushing, a small increase in "d" tends to make the circuit capacitive for this wavelength. This can be seen with the aid of Fig. 6.12. It appears, from these observations, that the magnetron "prefers" to operate with the circuit inductive and therefore changes to a longer wavelength at which the inductive susceptance predominates. It is perhaps premature to conclude that the above speculation is correct without further

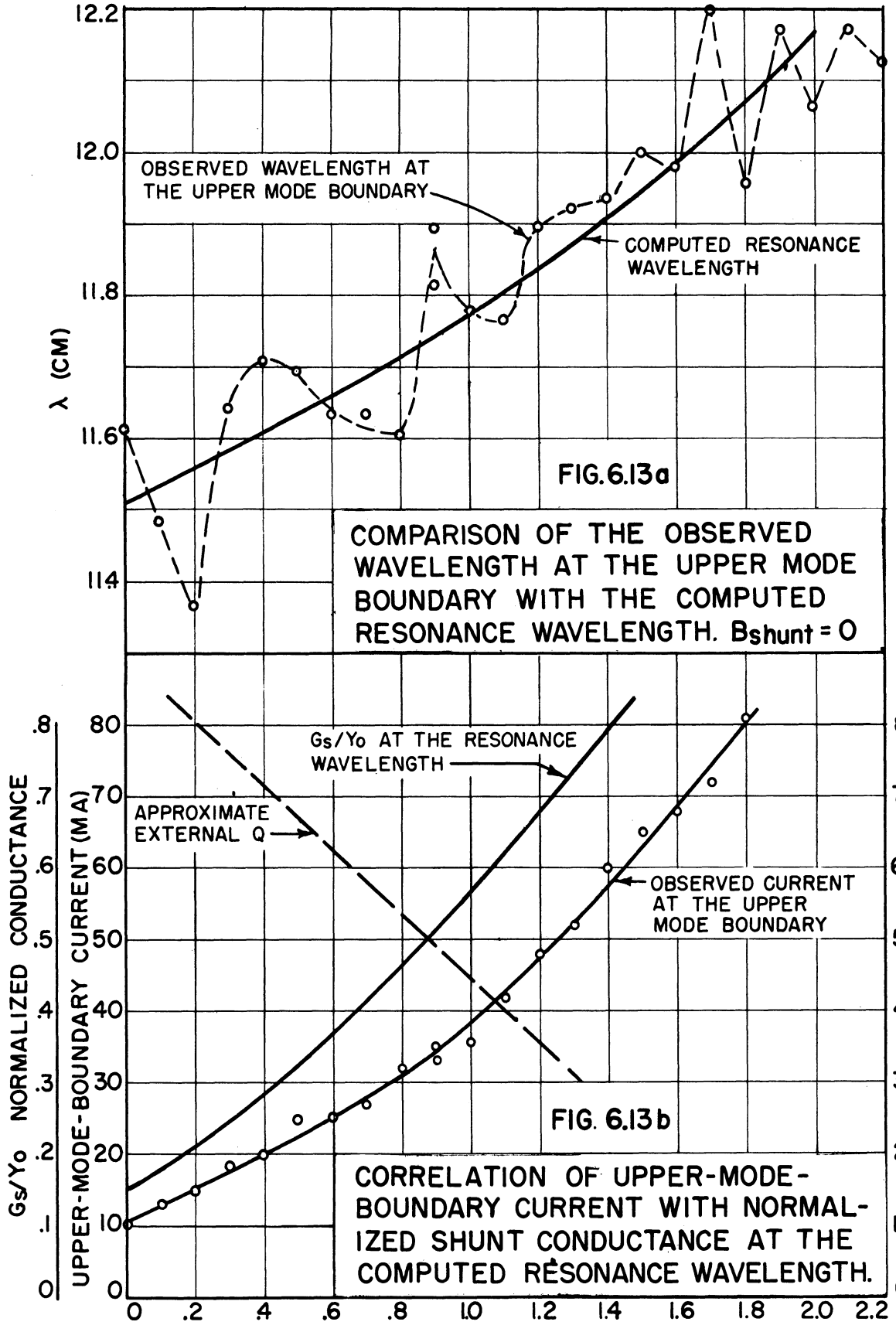

FIG. 6.13a

COMPARISON OF THE OBSERVED WAVELENGTH AT THE UPPER MODE BOUNDARY WITH THE COMPUTED RESONANCE WAVELENGTH. $B_{shunt} = 0$

FIG. 6.13b

CORRELATION OF UPPER-MODE-BOUNDARY CURRENT WITH NORMALIZED SHUNT CONDUCTANCE AT THE COMPUTED RESONANCE WAVELENGTH.

experimental and theoretical study. The qualitative picture does however agree with one of the reasons given in the literature[24] for the existence of an upper-mode boundary.

One further point should be mentioned with regard to the experimental data presented above. If one plots the computed circuit conductance for the wavelengths and "d" positions corresponding to the point of upper-mode-boundary current the results indicate a direct correlation between this current and the computed shunt conductance. This is readily apparent from Fig. 6.13(b). This correlation is in contradiction to that which is generally observed for magnetron oscillators having Q's of the order of 10 or larger. One possible explanation of the correlation found here may be inferred from the computed curves given in Fig. 6.11. A study of the manner in which the conductance varies with wavelength along a constant "d" line shows that the magnitude of the conductance decreases as the wavelength of operation decreases toward the upper-mode-boundary wavelength. This differs from the more generally observed cases in which the conductance is relatively constant over the range of frequency pushing. Hence if one considers the magnetron as a constant-current generator operating into a constant conductance, the r-f voltage across the tank and the r-f power output would increase rapidly as the resonance frequency of the tank circuit is approached. If, however, the circuit conductance decreases with an increase in frequency, the power output would tend to rise more slowly than it would for the constant-conductance load. This would take place in spite of a rapid rise in r-f voltage which would in turn result in stronger (radial field) phase-focusing action. Under these conditions, the radial

r-f field phase-focussing action may be sufficient to prevent loss of synchronism (between the space-charge spokes and the r-f potential travelling wave) until the region is reached in which the conductance no longer decreases with increasing frequency.

6.3. Low-Q Magnetron Operation

The first steps taken in attempting to attain low-Q voltage-tunable operation were directed toward the reduction of the Q of the circuits by means of lossy materials. Uskon cloth,* steel wool, and a sand-and-carbon mixture were some of the materials used in the initial phases of the investigation. All of these lossy materials were successful insofar as it was possible to attain a voltage-tunable signal from the insertion structure by using them. A typical arrangement employing a sand-and-carbon mixture as an absorption medium is shown in Fig. 6.14. With this arrangement it was possible to obtain c-w output from 11.8 to 20.3 cm for the Model 9B, No. 43 magnetron. The magnetic field used was 1200 gauss and the filament current was 1.67 amperes. Anode voltages were in the neighborhood of 1000 volts with plate currents reaching a maximum of 6 ma. at the low wavelength end of the voltage-tunable range. No extensive data were taken with this apparatus primarily because the output as viewed on a spectrum analyzer indicated a tunable, broad, noisy signal with a bandwidth greater than the maximum bandwidth of the analyzer, which in this case was 40 megacycles. The power output of the broad noise signal varied considerably over the tuning range, and was estimated to be of the order of 100 milliwatts at most.

---

* This is a cloth impregnated with carbon.

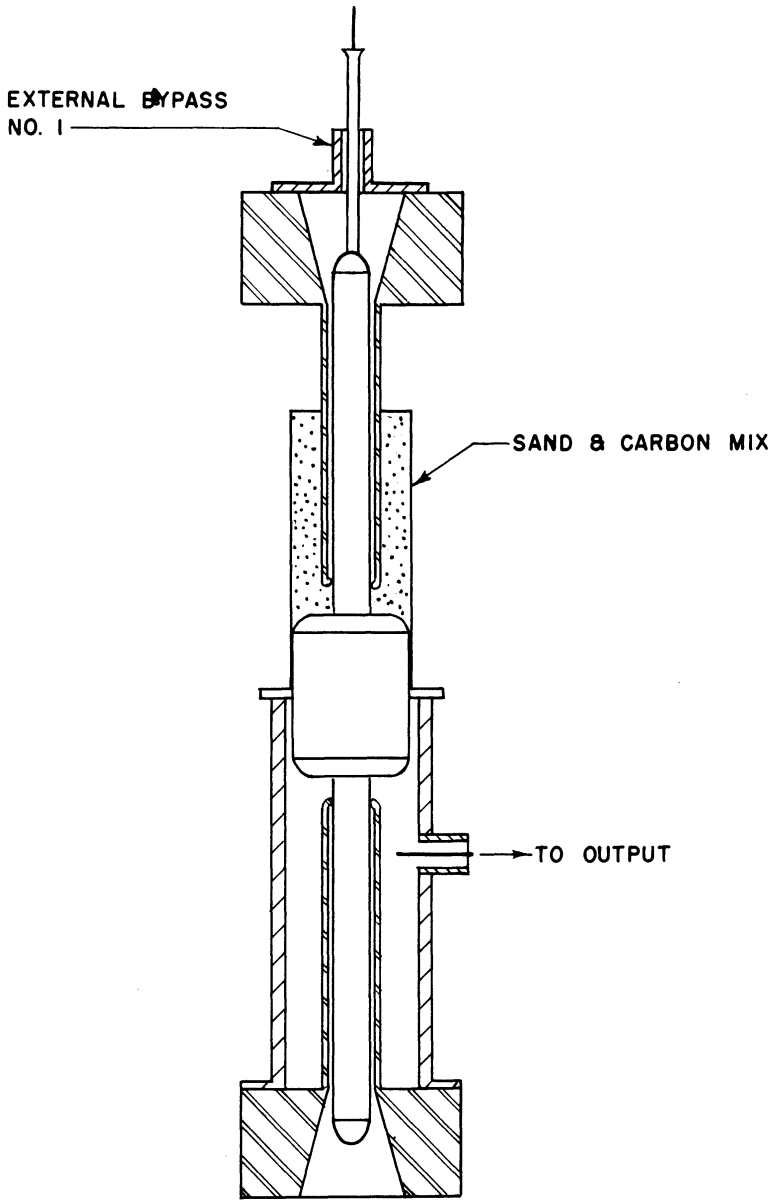

FIG. 6.14

SKETCH OF EXPERIMENTAL SET UP FOR LOW Q OPERATION USING CAVITY NO. 1

MODEL 9B NO.43 MAGNETRON

Cavity No. 2 (see Fig. 6.9) was designed to permit low-Q operation with a minimum of unusable absorbed power. The output from this coaxial circuit was initially terminated in its characteristic impedance of 50 ohms. Under this condition the external Q of the system, which is given approximately by $\omega_0 C_A/G_{sh}$,* is of the order of one or two. Although low-Q operation was attained with this direct termination into 50 ohms, the power output was too small to be measured accurately on a power bridge. It was possible, however, to measure relative output and wavelength by using a high-gain amplifier to amplify the output from a crystal detector.

The modifications made on cavity No. 2 to increase the power output are shown in Fig. 6.15. The purpose of the carbon iris was to increase the resistive component of the impedance "seen" by the electrons. This was only partially accomplished, since the effect of the iris was also reactive. The aquadag coating indicated inside the upper portion of the coaxial structure was employed to decrease the Q of this section of the line. Calculations assuming a short circuit at the upper face of the carbon iris gave a cavity resonance wavelength of 13.5 cm. The arrangement shown in Fig. 6.15 was employed in order to obtain the volt-ampere characteristics and power output for two different filament temperatures. The experimental results are given in Fig. 6.16 for the Model 9A, No. 39 magnetron. Here the magnetic-flux density was 1760 gauss for both sets of curves. The signal output as viewed on a spectrum analyzer was still broad and noisy, so that frequency measurements were meaningless. However, it is interesting to note that the frequency of the broad noise signal decreased with increasing cathode temperature. The sharp peak in power

---

* See Eq (5.21)

output is directly related to the resonant properties of the coaxial circuit employed here.

A volt-ampere characteristic for the Model 9B, No. 43 insertion tube is shown in Fig. 6.17. The external circuit employed to obtain this curve was the same as indicated in Fig. 6.15 except for the absence of the aquadag coating, and the presence of an external cathode bypass.* The magnetic field was 1550 gauss and the filament current 2.0 amperes. The wavelengths and power outputs indicated on the volt-ampere characteristic represent measured values for a broad noisy signal except near the high-Q resonance region of 14 cm. We observe here a significant wavelength shift from 17.0 cm to 13.21 cm with a small increase in output power. The wavelengths corresponding to the two lowest voltage points on the volt-ampere characteristic were not measurable with the arrangement of apparatus employed to obtain these data. No reasonable explanation can be presented, at this time, to account for the positive and negative frequency pushing indicated along the upper horizontal portion of the volt-ampere characteristic.

In the voltage-tunable operation attained by Wilbur and his group at the General Electric Company below 1000 megacycles, the relation between frequency and operating voltage was found to coincide with the Hartree relation. This group also found that a clean signal could be generated only by using a temperature-limited emitter. Either pure tungsten or specially designed oxide-coated cathodes were found satisfactory. Conventional oxide cathodes resulted in unstable or noisy operation. This

---

* See Appendix D, Fig. D-1.

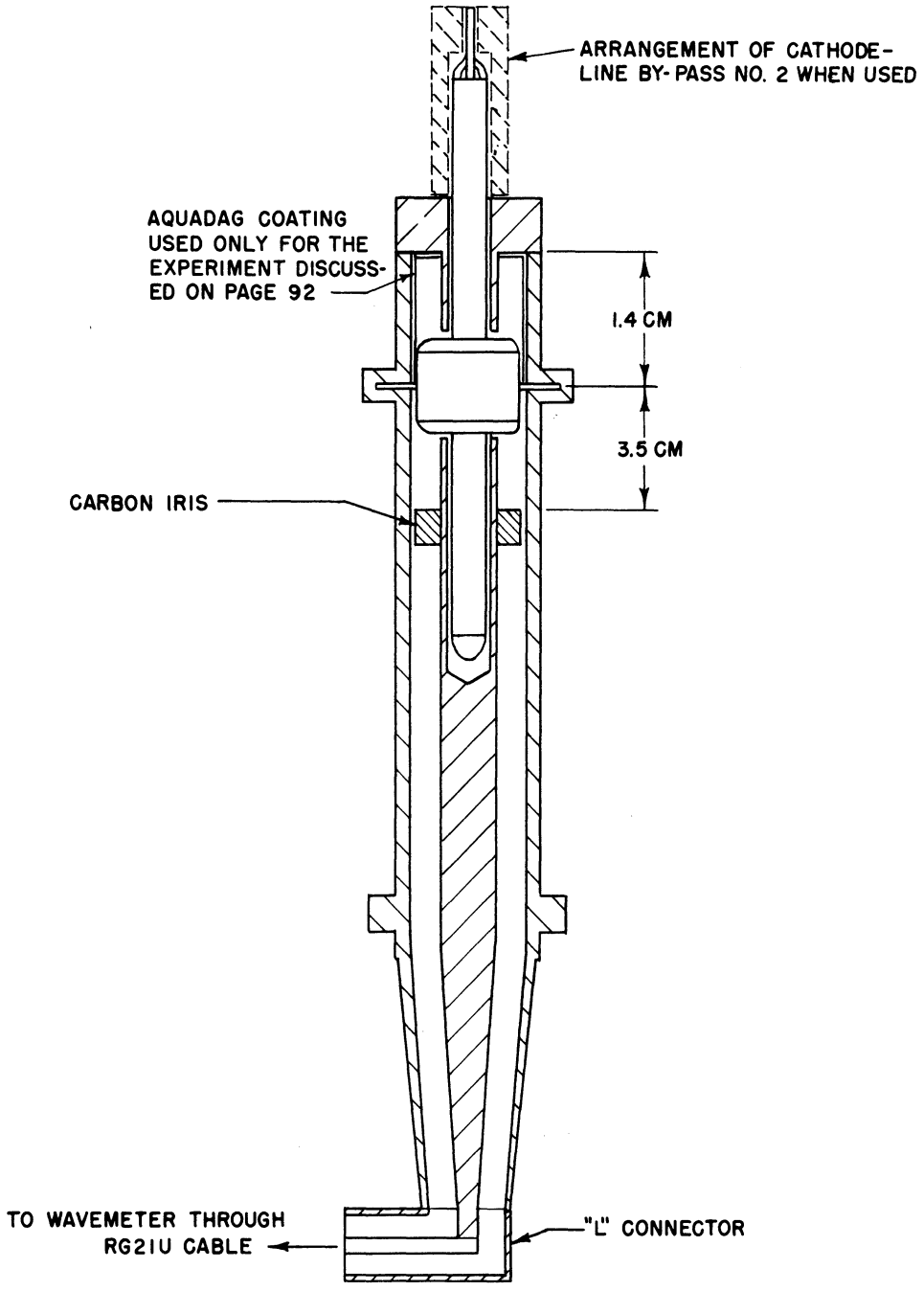

FIG. 6.15
SKETCH OF EXPERIMENTAL SET UP FOR LOW Q
OPERATION IN CAVITY NO. 2

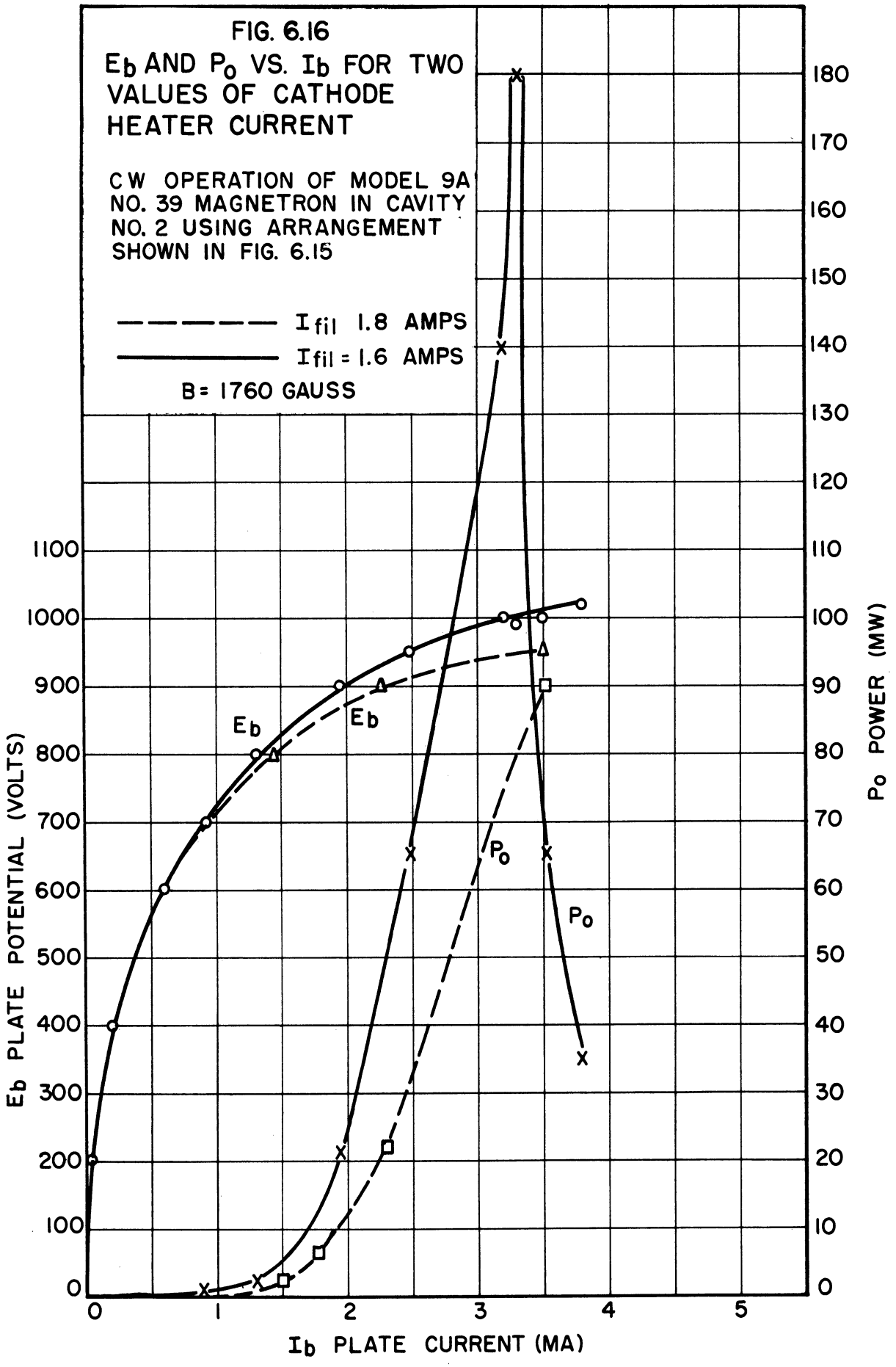
FIG. 6.16
Eb AND Po VS. Ib FOR TWO VALUES OF CATHODE HEATER CURRENT
CW OPERATION OF MODEL 9A NO. 39 MAGNETRON IN CAVITY NO. 2 USING ARRANGEMENT SHOWN IN FIG. 6.15
Ifil 1.8 AMPS
Ifil = 1.6 AMPS
B = 1760 GAUSS
Eb
Eb
Po
Po
Eb PLATE POTENTIAL (VOLTS)
Po POWER (MW)
Ib PLATE CURRENT (MA)
0
100
200
300
400
500
600
700
800
900
1000
1100
0
10
20
30
40
50
60
70
80
90
100
110
120
130
140
150
160
170
180
0
1
2
3
4
5

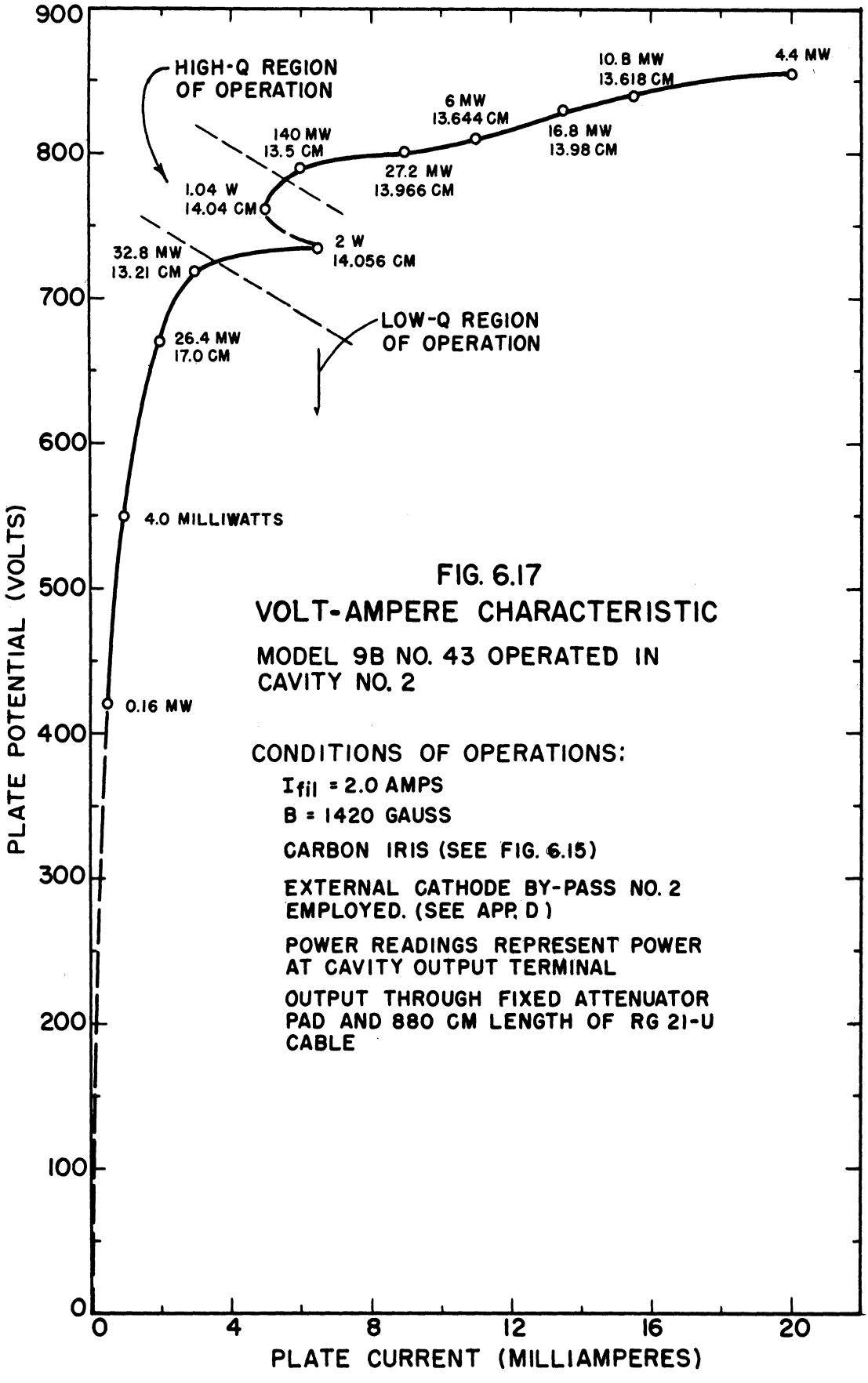

FIG. 6.17

VOLT-AMPERE CHARACTERISTIC

MODEL 9B NO. 43 OPERATED IN CAVITY NO. 2

CONDITIONS OF OPERATIONS:

I_{fil} = 2.0 AMPS

B = 1420 GAUSS

CARBON IRIS (SEE FIG. 6.15)

EXTERNAL CATHODE BY-PASS NO. 2 EMPLOYED. (SEE APP. D)

POWER READINGS REPRESENT POWER AT CAVITY OUTPUT TERMINAL

OUTPUT THROUGH FIXED ATTENUATOR PAD AND 880 CM LENGTH OF RG 21-U CABLE

also turned out to be the case in the microwave range using the insertion tube described here.

An experiment employing the Model 9B, No. 49 insertion tube was conducted to investigate the effect of a tungsten cathode on voltage-tunable output. Model 9B, No. 49 employs a pure tungsten helical cathode and was provided with an external bypass in the cathode line for this experiment. An assembly drawing for the cathode is shown in Appendix D, Fig. D-5. The cathode supply consisted of storage batteries and the anode potential was obtained from a series of minimax batteries. Fig. 6.9 shows the external circuit* employed to obtain the voltage-tuning data given in Table 6.1 below.

TABLE 6.1

E_b (volts)	I_b (microamps)	I_{fil} (amps)	λ (cm)	B (gauss)
740	80	6.76	18.210	1520
850	80	6.8	14.628	1520
940	160	7.0	12.492	1520
1080	500	7.1	11.34	1520

In this experiment it was found necessary to adjust the cathode current for each anode voltage in order to obtain a clean signal. The frequency was sensitive to cathode current, decreasing with increasing current. Fig. 6.18 shows a plot of the frequency versus anode potential

* The external cathode-line bypass (No. 2) was used in this experiment.

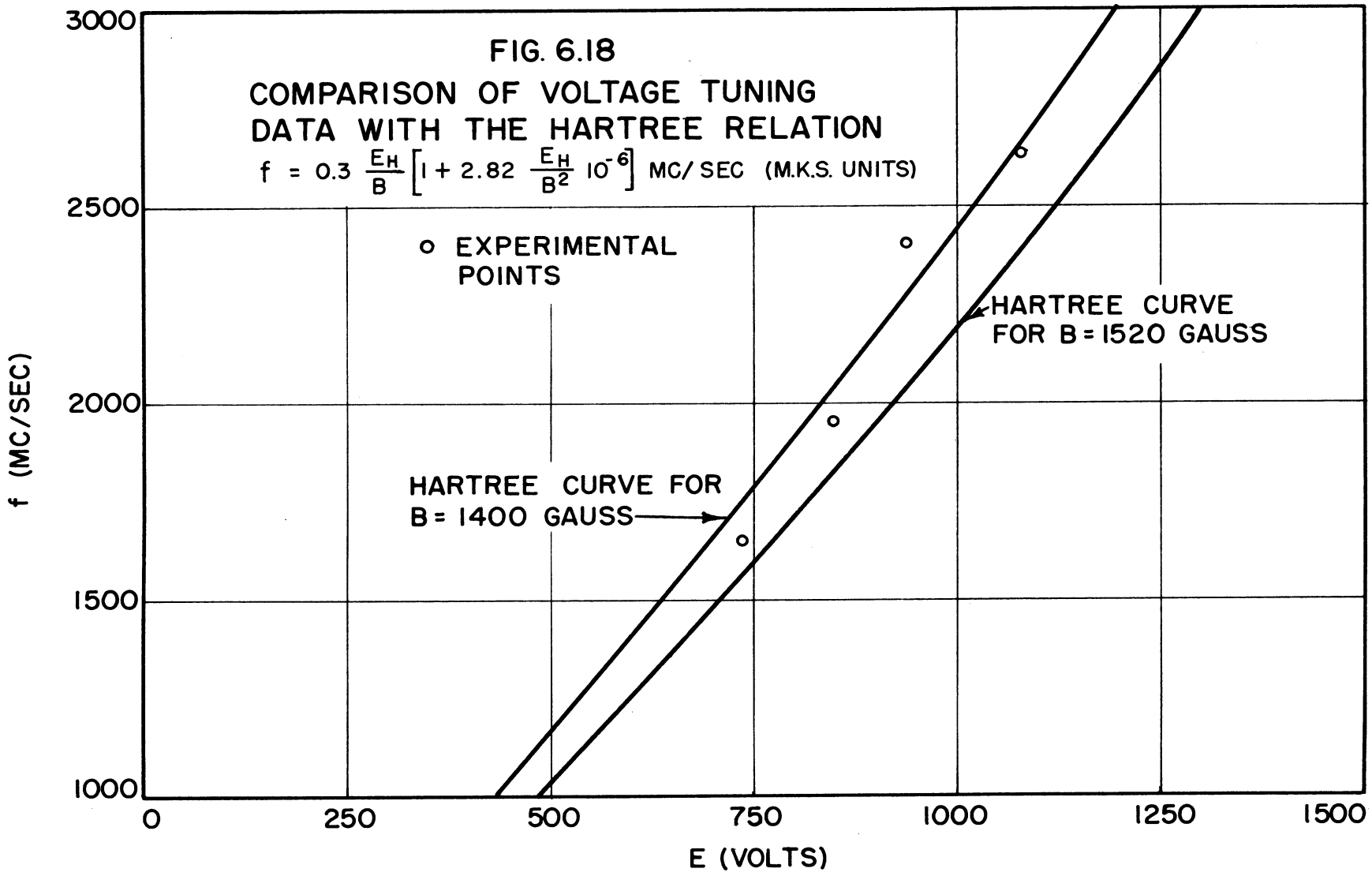
FIG. 6.18
COMPARISON OF VOLTAGE TUNING DATA WITH THE HARTREE RELATION
f = 0.3 $\frac{E_H}{B}\left[1 + 2.82 \frac{E_H}{B^2} 10^{-6}\right]$ MC/SEC (M.K.S. UNITS)
o EXPERIMENTAL POINTS
HARTREE CURVE FOR B = 1520 GAUSS
HARTREE CURVE FOR B = 1400 GAUSS
f (MC/SEC)
E (VOLTS)
3000
2500
2000
1500
1000
0
250
500
750
1000
1250
1500

from Table 6.1. Note the close correspondence between the experimental data and the curve computed from the Hartree equation for a magnetic field of 1400 gauss. It should be pointed out that the measured flux density (1520 gauss) given in Table 6.1 is considered to be somewhat in error. This error in measured flux density came about because the outer Kovar cylinder of the insertion structure could not be simulated when the $B - I_{field}$ curve was obtained. The output available in the form of a clean voltage-tunable signal varied between 10 and 30 microwatts over the measured frequency range.

A different approach to the study of voltage-tunable operation made use of the arrangement shown in Fig. 6.19. The block diagram shown in this figure illustrates how the insertion-tube magnetron was used as a local oscillator for an s-band spectrum analyzer. The frequency of the insertion magnetron is swept at a 60-cycle rate with a sine-wave source in series with the anode d-c supply. Since the horizontal sweep of the cathode-ray oscillograph is obtained with the same 60-cycle supply, the frequency of the voltage-tunable insertion tube is proportional to the horizontal deflection on the CRO. Z-axis blanking was employed to remove the signal output from the screen during the return trace of the 60-cycle sweep. With this arrangement it was possible to measure the total width of the frequency-modulated magnetron output by mechanically tuning a reflex klystron signal generator through the frequency range. Frequency measurements were obtained from the klystron signal source for different settings of the mechanically-tunable klystron cavity. Fig. 6.20(a) shows the results of one of the tests made with the apparatus described above. In this figure two separate oscillograph traces are presented, each of which

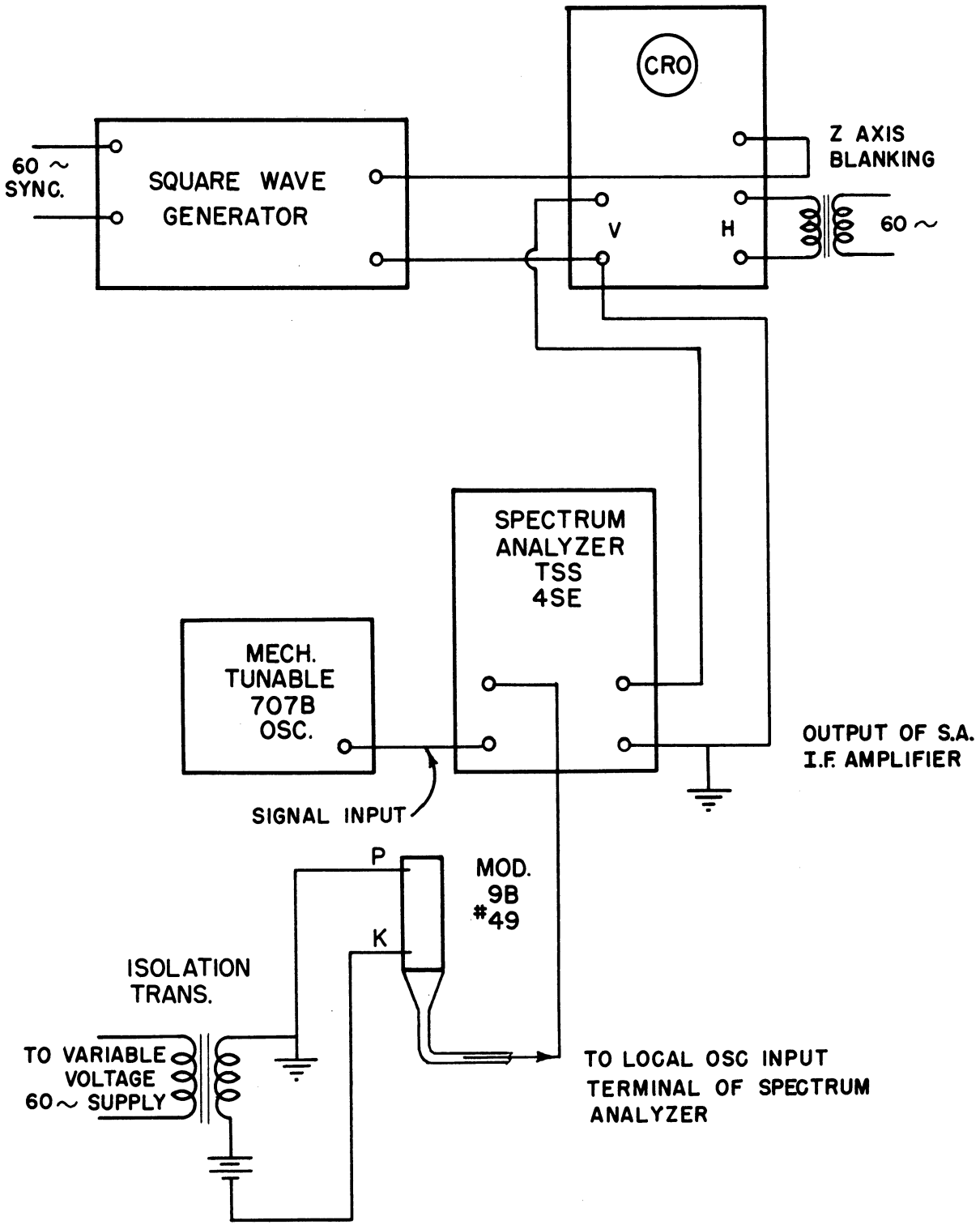

FIG. 6.19

EXPERIMENTAL SET UP USING INSERTION TUBE AS LOCAL OSCILLATOR FOR SPECTRUM ANALYZER.

shows the amplitude of the intermediate-frequency amplifier output as a function of local-oscillator sweep voltage (or frequency). The upper trace was photographed with a 2042 mc/sec klystron signal-generator frequency. The lower trace shows the results with a 1690 mc/sec external-signal input. The above frequencies correspond to the positions lying midway between the vertical pips shown in the upper and lower traces, respectively. The frequency difference between two adjacent vertical pips corresponds to 40 mc, which is twice the intermediate frequency of the spectrum analyzer. The total voltage-tuned frequency difference obtained from the local oscillator for this particular test was therefore 2062-1670 or 392 mc/sec.

The conditions under which the magnetron was operated are listed below.

Model 9B, No. 49 Tube

This tube uses a pure tungsten helix cathode.

Cathode bypass used is shown in Appendix D, Dwg. D-1.

Cavity No. 2 through GR "L" connector and one 37-in. section of RG-21U GR cable to spectrum analyzer.

E_b = 860 volts.

E_{ac} = 226 volts peak to peak (60-cycle modulating voltage).

A polystyrene disk partially coated with aquadag was placed inside the cavity 3 inches below the center of the tube.

I_b = 75 μ amps.(average)

I_{fil} = 6.7 amps.

B = 1580 gauss

Fig. 6.20(b) depicts the output of the voltage-tunable local oscillator versus frequency in the uppermost trace. The frequencies corresponding to the two tall pips in the center trace are 1680 $\pm$ 20 mc/sec. The conditions used to obtain this picture are the same as given immediately above except for the following:

E_b = 845 volts

E_{ac} = 390 volts (peak to peak)

I_b = 10 μ amps. (average)

I_{fil} = 6.3 volts

B = 1695 gauss

Note: The output from the magnetron was taken through a GR "L" connector and one 37-in. section of GR RG-21U cable to a crystal detector. The output of the crystal detector is displayed in the top trace.

The oscillogram given in Fig. 6.20(c) was obtained with the same circuit conditions as for the preceding test except that here the cathode bypass was not employed. The voltages, currents and magnetic field for this case were:

E_b = 860 volts

E_{ac} = 226 volts (peak to peak)

I_b = 75 μ amps. (average)

B = 1580 gauss

I_{fil} = 6.7 amps. (top trace)

I_{fil} = 6.8 amps. (bottom trace)

These oscillograms portray the effect of a long line on the power output versus frequency of a tunable magnetron. The top trace is essentially

the impedance of a transmission line as a function of frequency when the line is many wavelengths long.[25] The lower trace shows the effect of a slight increase in the temperature of the cathode. We observe that in the lower trace, the output versus frequency no longer resembles the response expected with a constant-current generator. Here we find a clue to the properties of voltage-tunable operation in magnetrons. Since the anode voltage determines the frequency of the r-f output, and if the top oscillogram in Fig. 6.20(c) represents the output obtained with an r-f constant-current generator, then it is reasonable to ascribe the r-f constant-current properties of the magnetron mainly to the temperature-limited operation of the cathode.

An attempt to determine the effect of magnetic-field distribution in the interaction space on the noise output of the insertion tube, resulted in the oscillogram shown in Fig. 6.20(d). The traces represent the output through a crystal detector versus frequency for two magnetic-field conditions. Listed below are the conditions of the experiment.

Model 9B, No. 49 Tube

Cavity No. 2 — with a carbon iris 3.5 cm from the nearest vane edge. The carbon iris O.D. was 0.600-in. wide and .250-in. long.

Output — Through GR "L" connector and a 10DB GR fixed attenuator pad to crystal rectifier and then to the oscillograph.

Magnetic field —
Top trace — Normal operation.
Bottom trace — Magnetic-field distribution changed with an external iron bar.

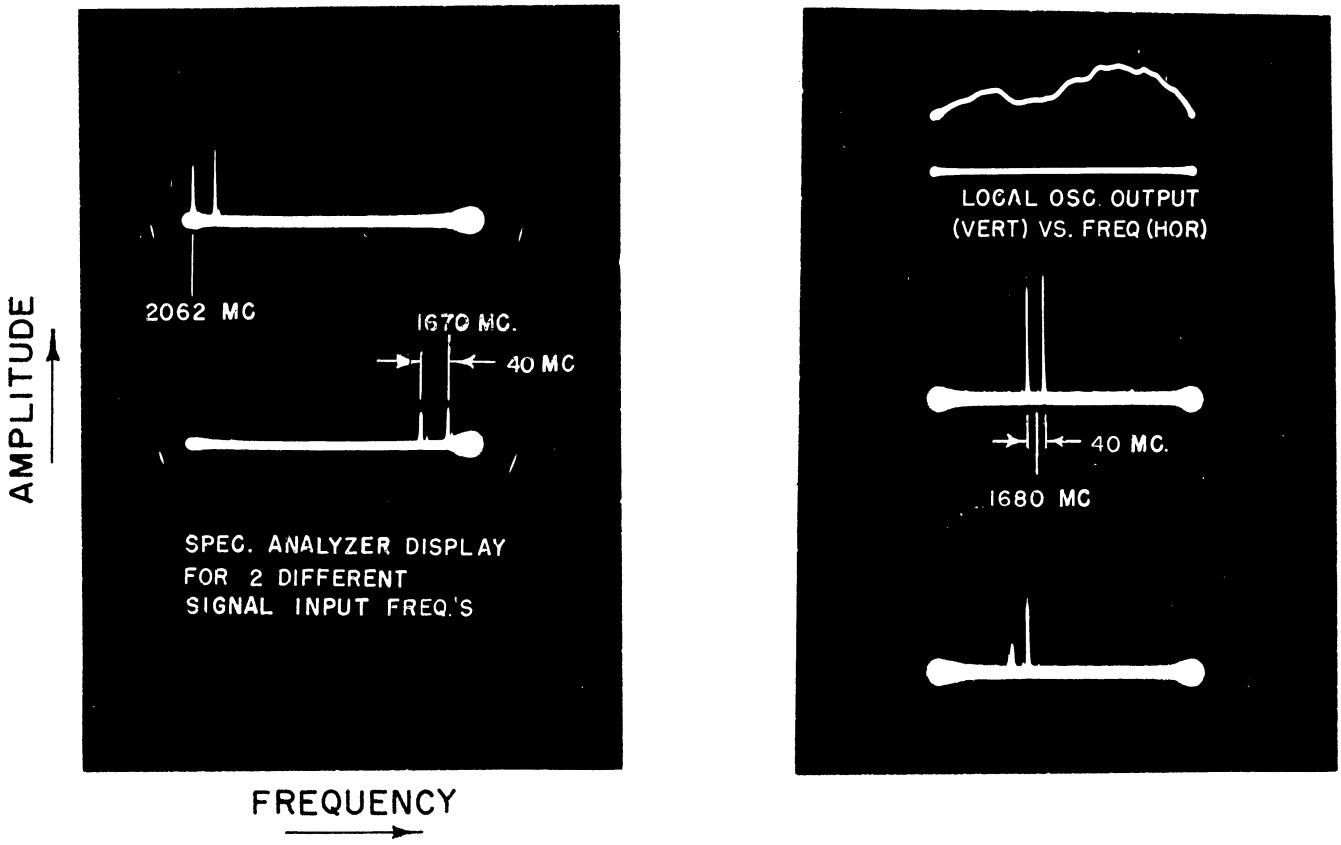

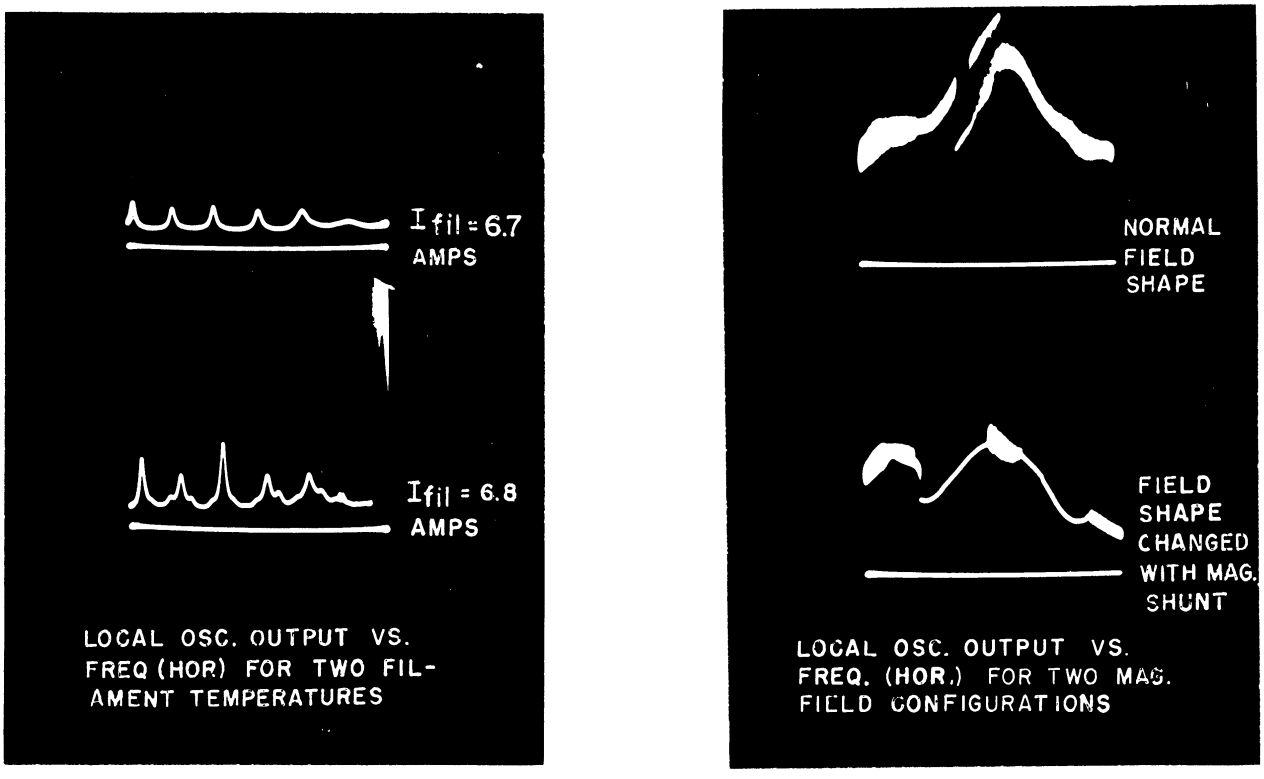

FIG. 6.20

OSCILLOGRAPH TRACES OBTAINED WITH THE EXPERIMENTAL ARRANGEMENT SHOWN IN FIG. 6.19

E_b = 700 volts

E_{ac} = 382 volts (peak to peak) 60-cycle modulation

I_b = 450 μ amps. (average)

I_{fil} = 7.1 amps.

B = 1420 gauss

Although the exact magnetic-field distributions are not known for this experiment, the field distribution which gave the results shown in the bottom trace of Fig. 6.20(d) is presumed to be asymmetric with respect to the anode axis. The study of the field distributions is complicated by the presence of the vane-anode Kovar cylinder which forms a magnetic shunt.

6.4. Qualitative Theory of Low-Q Magnetron Operation

In this section we shall present those factors which, in view of experimental results, are considered pertinent to the establishment of any complete theory of low-Q operation. For completeness, a summary of the theory of low-Q operation as proposed by Welch[26] will also be presented. The important experimental results are:

1. In clean-signal voltage-tunable operation the frequency is proportional to the anode voltage and the constant of proportionality is given by the Hartree relation.

2. The frequency range of operation is of the order of two to one.

3. The external Q is low, therefore the shunt susceptance varies slowly with frequency.

4. The interaction space appears to have the properties of a constant-current generator when the load is frequency sensitive.

5. The efficiency is low; of the order of 1 per cent.

6. The temperature of the cathode is lower than for normal magnetron operation and is critical for clean-signal output. (Applies to both tungsten and oxide-coated cathodes.)

7. The frequency decreases with increasing cathode temperature.

8. When the conditions of operation result in a noise band, the bandwidth of the noise is roughly 5 per cent of the average operating frequency and the noise band is voltage-tunable.

9. The constant-current generator characteristics of the magnetron are modified when the cathode temperature is raised above a critical level.

10. Stable operation could not be maintained with an oxide-coated cathode.

11. Noise can be reduced over a frequency range by adjustment of the shape of the magnetic field.

A theory proposed by Welch explains voltage tuning in terms of the induced current resulting from rotating space-charge spokes. The effects of conduction current are considered secondary since d-c current is small for this type of operation. According to this theory the space-charge spoke width and the electrical space phase angle between the spoke and the fundamental component of the r-f potential traveling wave must satisfy the following conditions:

(a) The electrical space phase angle between the space-charge spoke and the fundamental component of the r-f potential traveling wave must be equal to the circuit phase angle.

(b) The power produced in the load must be consistent with the magnitude of the induced current.

Items (a) and (b) together are equivalent to requiring that both the total shunt susceptance (circuit plus electronic) and total shunt conductance be zero for stable oscillation.

(c) The magnitude of the induced current depends on the width and density of the space-charge spoke.

(d) The width of the space-charge spoke is a function of the r-f amplitude and the difference between the operating and Hartree potentials. This width corresponds to the leading half (in space) of the region over which the instantaneous total potential is greater than the Hartree level.

After applying the foregoing requirements to frequency pushing in high-Q magnetron operation, Welch reaches the following conclusions:

(a) As the anode potential is raised above the starting potential for a given mode of operation the spoke width increases and the space phase angle between the spokes and the r-f potential traveling wave decreases.

(b) The Hartree level remains substantially constant since the frequency does not vary rapidly and, the difference between the operating anode potential and the Hartree level increases.

(c) The circuit phase angle changes rapidly with frequency as the separation between the Hartree level and anode potential increases.

For low-Q operation the theory assumes the existence of a highly inductive non-resonant circuit and a temperature-limited emitter. The conclusions reached under these conditions are:

(a) The width of the spoke cannot change very much since the current is limited.

(b) The Hartree level and anode potential rise together as the frequency increases.

(c) The circuit phase angle and the difference between the Hartree level and the operating potential change slowly with frequency to produce the required slowly varying phase angle.

This proposed theory is substantiated by items 1, 2, 3, 4, and 6 of the experimental results listed at the beginning of this section. All of the other observations except items 5 and 7 are related to noise and will probably require an extension of the theory based on statistical methods. One plausible explanation for the frequency decrease with increasing cathode temperature is available at this time. When the cathode temperature is raised, an expanding subsynchronous space-charge hub forms, causing the effective capacitance between anode segments to increase. This increase in effective circuit capacitance would result in a decrease in frequency. It is quite possible that this is only a second-order effect since the phase of the space-charge spoke would also be affected by the increase in emission from the cathode according to the foregoing theory

proposed by Welch. The very low efficiencies encountered with low-Q operation are in part explainable in terms of the small phase-focusing action available from the low r-f fields. In addition the leakage current is a large fraction of the total current. Thus there are at least two factors which contribute to low "effective electronic efficiency" and therefore to low overall efficiency. These factors are also present in normal magnetron operation in the low-current region[27] but do not present any serious obstacles since higher efficiency operation can be attained by operating at higher anode currents and r-f voltages.

CHAPTER VII

CONCLUSIONS

It has been shown possible to achieve either mechanical or electronic tuning in the microwave region. In this respect this investigation has achieved the primary objectives. The problems which have arisen although formidable are not considered insurmountable.

As a result of this study it has become apparent that the future success of microwave magnetron electronic tuning will, to a great extent, rest upon a satisfactory solution of a microwave circuit problem. The voltage-tunable power output limitation experienced in this investigation is attributed primarily to the characteristics of the circuits employed. Briefly stated, the circuit characteristics desirable for voltage tuning are low conductance as well as an inductive susceptance which varies slowly with frequency. If these circuit characteristics are "seen" by the electrons in the interaction space the generation of significant microwave power is assured. Attempts to obtain the required circuit characteristics will involve a reduction of the anode vane-to-bar capacitance which in turn will be restricted by interaction space design.

The problem of noise reduction and the extension of the low-noise band of operation with a particular cathode temperature is a serious one but it will, in the opinion of the author, be solved more easily than the circuit problem. It has been shown that a pure tungsten cathode is more satisfactory than an oxide-coated cathode for clean-signal operation. The G. E. group has shown that oxide-coated cathodes with certain geometric properties can also

be made to operate in a satisfactory manner. There are many possible variations both in cathode geometry and cathode materials which must be investigated before any general conclusions can be reached with regard to optimum clean-signal operation.

The potentialities of the insertion magnetron as a tool for the study of mode-boundary and pushing have been demonstrated by the results obtained in this investigation. The effects of the cathode circuit on upper-mode-boundary current are of particular significance for high-Q tunable operation and the results obtained are very encouraging.

Experience gained in the design, construction, and operation of this tube will be extremely valuable for the development of higher-power, higher-frequency ceramic-seal tubes. It appears feasible at this time to extend the upper frequency of this structure to approximately 6000 megacycles per second with high-Q operation.

The potentialities of the insertion magnetron are yet to be realized. It is our belief that this structure can be developed into a commercially valuable microwave generator in the foreseeable future.

APPENDIX A

THE MAGNETRON EQUATIONS

APPENDIX A

THE MAGNETRON EQUATIONS*

In this section we shall derive those relations which are of particular significance in the operation of a traveling-wave magnetron. The results will provide a valuable physical picture of the potential distributions and critical anode potentials which are characteristic of this type of magnetron. We shall have need of certain equations which are derived below for the non-oscillating smooth-bore magnetron.

A.1. The Non-Oscillating Smooth-Bore Magnetron

One of the equations of motion for this case is obtained by equating the moment of force tending to rotate an electron about the axis of the interaction space to the rate of change of angular momentum about this same axis. The moment of force is the product of the azimuthal force on an electron and the radial distance from the axis. The angular momentum is the product of the moment of inertia $m_e r^2$ and the angular velocity $d\theta/dt$. Thus we have:

$$r\left(Be\,\frac{dr}{dt}\right) = \frac{d}{dt}\left(mr^2\,\frac{d\theta}{dt}\right). \qquad \text{(A1-1)}$$

This equation can be written as follows:

$$\frac{Be}{2m}\,\frac{dr^2}{dt} - \omega\,\frac{dr^2}{dt} = r^2\,\frac{d\omega}{dt}, \qquad \text{(A1-2)}$$

---

* The procedure used here follows that presented by Prof. W. G. Dow in his course in Microwave Electron Tubes at the University of Michigan.

where

$$\omega = \frac{d\theta}{dt} . \tag{A1-3}$$

If we let $\omega_L = Be/2m$ the equation becomes, after separation of variables,

$$\frac{dr^2}{r^2} = - \frac{d\omega}{\omega - \omega_L} . \tag{A1-4}$$

Integration results in

$$\ell n\ r^2 = - \ell n\ (\omega - \omega_L) + \ell n\ C , \tag{A1-5}$$

or

$$r^2 = \frac{C}{\omega - \omega_L} . \tag{A1-6}$$

To obtain the constant of integration let $\omega = 0$ at the cathode where $r = r_c$ with the result

$$C = - \omega_L\ r_c^2 , \tag{A1-7}$$

and

$$\omega = \omega_L \left(1 - \frac{r_c^2}{r^2} \right) . \tag{A1-8}$$

The equation for the angular velocity of an electron at radius r, given above, assumes no energy exchange between the electron and its surroundings. No restrictions have been placed on the radial velocity. The angular velocity of any electron at radius r must therefore be that given by Eq (A1-8) regardless of electron orbit. The energy, in electron volts, corresponding to the value of ω given in Eq (A1-8) is labeled "the tangential energy curve" in Fig. A1-1.

The potential distribution for the static cylindrical magnetron may be obtained by writing a second equation of motion for an electron in the crossed electric and magnetic fields.

$$m \frac{d^2r}{dt^2} = - Ber\omega + mr\omega^2 + e \frac{dE}{dr} . \qquad (A1\text{-}9)$$

To solve this equation for E we employ the relation for the conservation of energy

$$\frac{1}{2} m\omega^2 r^2 = Ee , \qquad (A1\text{-}10)$$

after assuming that all the energy is tangential energy. Then also, the radial acceleration d^2r/dt^2 is zero. Eq(A1-9), after substitution for ω from Eq (A1-10), is after rearrangement:

$$\frac{r}{\sqrt{E}} \frac{dE}{dr} + 2 \sqrt{E} = rB \sqrt{\frac{2e}{m}} . \qquad (A1\text{-}11)$$

This can be written as follows:

$$2 \frac{d}{dr} \left(\sqrt{E}\, r \right) = rB \sqrt{\frac{2e}{m}} . \qquad (A1\text{-}12)$$

Upon integration we obtain

$$2 \sqrt{E}\, r = \sqrt{\frac{2e}{m}}\ B \frac{r^2}{2} + C . \qquad (A1\text{-}13)$$

The constant may be evaluated by letting E = 0 at $r = r_c$. The equation for the potential distribution in the static magnetron is thus given by

$$E = \frac{e}{8m} B^2 r^2 \left(1 - \frac{r_c^2}{r^2}\right)^2 . \qquad \text{(A1-14)}$$

This equation gives the potential distribution within the space charge of a smooth-bore diode magnetron if all the electrons travel in circular orbits around the cathode. A sketch of the potential distribution given by Eq (A1-14) is shown in Fig. A1-1. If r is set equal to the anode radius r_a, the corresponding anode potential is that for which electrons just graze the anode;

$$E_U = \frac{e}{8m} B^2 r_a^2 \left(1 - \frac{r_c^2}{r_a^2}\right)^2 . \qquad \text{(A1-15)}$$

The potential E_U is commonly known as the Hull cutoff potential.

A.2. The Non-Oscillating Magnetron with an Applied R-F Voltage

In order to find the potential distribution in a magnetron having an externally-applied r-f field, a quantity corresponding to the energy per radian given up to an applied r-f field is added to Eq (A1-1). The resulting relation is

$$Ber \frac{dr}{dt} = e \frac{dE_{rf}}{d\theta} + \frac{d}{dt}\left(mr^2 \frac{d\theta}{dt}\right) . \qquad \text{(A2-1)}$$

Expansion of the last term on the right and rearrangement of the left member gives

$$\frac{1}{2} Be \frac{dr^2}{dt} = e \frac{dE_{rf}}{d\theta} + m \frac{d\theta}{dt} \frac{dr^2}{dt} + mr^2 \frac{d}{dt}\left(\frac{d\theta}{dt}\right) . \qquad \text{(A2-2)}$$

The last term is zero if the angular velocity is independent of time. We shall assume that all the electrons are traveling with an angular

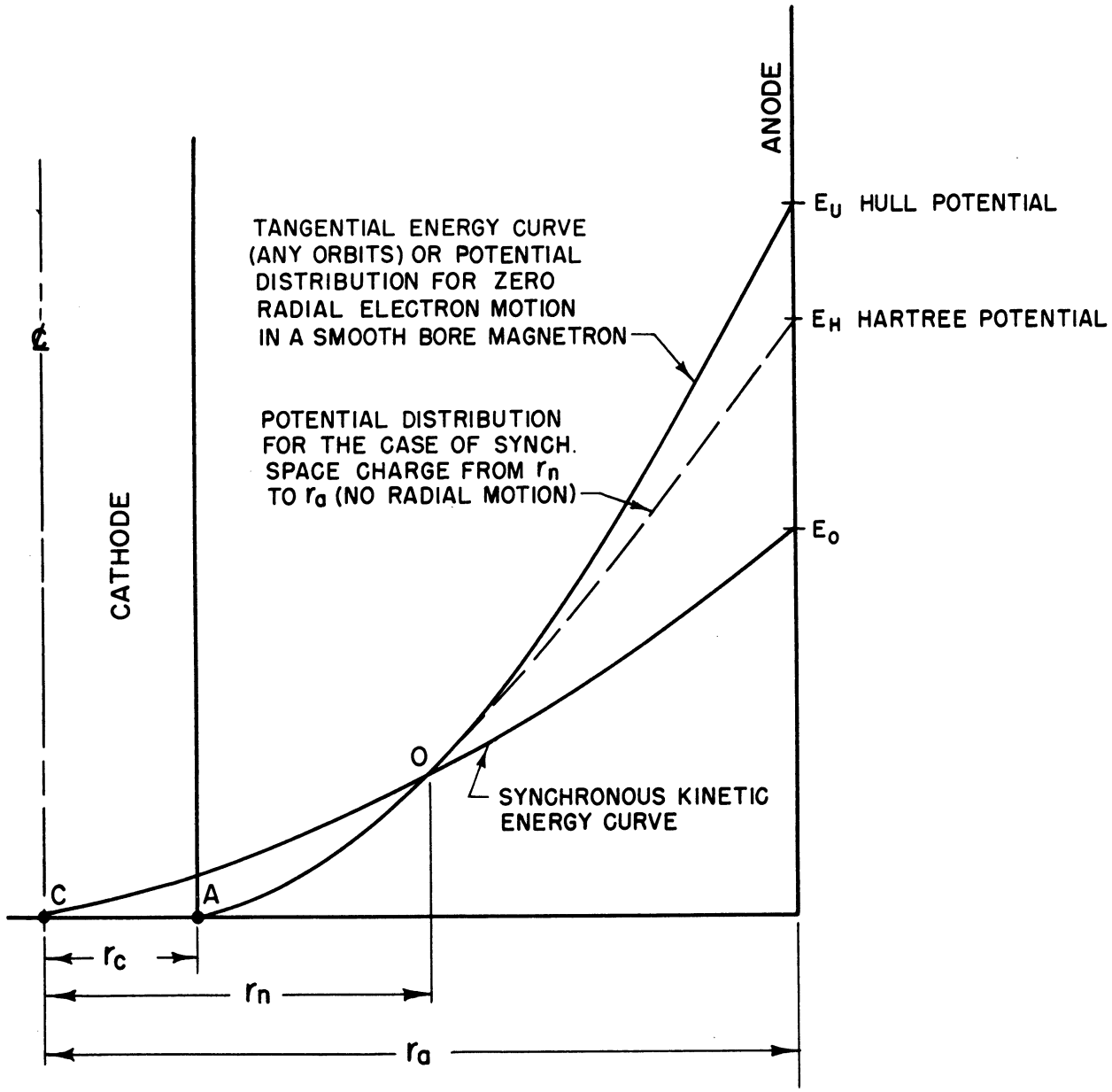

FIG. A1-1
SKETCH SHOWING THE ENERGY CURVES AND POTENTIAL DISTRIBUTIONS DISCUSSED IN THE TEXT.

velocity corresponding to the velocity of one of the r-f field traveling-wave components. For instance, in the π mode, we have

$$\frac{d\theta}{dt} = \omega_n = \frac{2\pi f}{N/2} . \qquad \text{(A2-3)}$$

Here N is the number of anode segments. Substitution of ω_n for $d\theta/dt$ gives:

$$e\, d\, E_{rf} = \frac{1}{2} Be\, \omega_n\, dr^2 - m\, \omega_n^2\, dr^2 . \qquad \text{(A2-4)}$$

Upon integration, the equation for $e\, E_{rf}$ becomes:

$$e\, E_{rf} = \left[\frac{1}{2} Be\, \omega_n - m\, \omega_n^2\right] r^2 + \text{const} . \qquad \text{(A2-5)}$$

In order to determine the constant, we need first to define a radius r_n below which the electrons are traveling at less than synchronous velocity. The energy equation given by

$$e\, E_r = \frac{1}{2} m\, \omega_n^2\, r^2 , \qquad \text{(A2-6)}$$

defines the kinetic energy in electron volts which an electron has if rotating at an angular velocity ω_n at any radius r. In particular, the kinetic energy in electron volts of a synchronous electron at anode radius r_a is

$$E_o = \frac{1}{2} \frac{m}{e} \omega_n^2\, r_a^2 . \qquad \text{(A2-7)}$$

A sketch of the synchronous kinetic energy curve for the electron is given in Fig. A1-1 as curve C-O-E_o . Further reference to Fig. A1-1 indicates

that from the origin C to the radius r_n, electrons will be below synchronism because the energy available from the d-c field is inadequate. From radius r_n to the anode the electrons are assumed to be rotating synchronously with the r-f field and giving up energy to it. The constant in Eq (A2-5) is now easily determined by letting e E_{rf} equal zero at radius r_n. The result after making the substitution

$$\omega_L = \frac{Be}{2m} , \tag{A2-8}$$

and rearrangement is:

$$e\,E_{rf} = 2\left(\frac{\omega_L}{\omega_n} - 1\right)\left(\frac{m\,\omega_n^2\,r^2}{2} - \frac{m\,\omega_n^2\,r_n^2}{2}\right). \tag{A2-9}$$

The use of Eq (A1-14) gives:

$$E_n = \frac{e}{8m} B^2\, r_n^2 \left[1 - \frac{r_c^2}{r_n^2}\right]^2 , \tag{A2-10}$$

and

$$E_o = \frac{e}{8m} B_o^2\, r_a^2 \left[1 - \frac{r_c^2}{r_a^2}\right]^2 . \tag{A2-11}$$

Here E_n is the potential at the edge (at $r = r_n$) of the sub-synchronous space-charge swarm when the magnetic field is B webers per square meter. E_o is defined in Eq (A2-7) and B_o is defined below in Eq (A2-15).

From Eqs A2-10 and A2-11, we obtain

$$\frac{E_n}{E_o} = \frac{B^2}{B_o^2}\,\frac{r_n^2}{r_a^2}\,\frac{\left[1 - \frac{r_c^2}{r_n^2}\right]^2}{\left[1 - \frac{r_c^2}{r_a^2}\right]^2} . \tag{A2-12}$$

From Eqs (A2-6) and (A2-7), we obtain

$$\frac{E_n}{E_o} = \frac{r_n^2}{r_a^2} . \tag{A2-13}$$

Substitution of Eq (A2-13) into Eq (A2-12) gives:

$$\frac{B}{B_o} = \frac{1 - \left(\frac{r_c}{r_a}\right)^2}{1 - \left(\frac{r_c}{r_n}\right)^2} . \tag{A2-14}$$

B_o is defined as the magnetic field required to allow synchronous electrons to exist at the anode and is easily obtained from Eq (A1-8) by letting $\omega = \omega_n$ when $r = r_a$. The result is

$$B_o = \frac{2m}{e} \omega_n \frac{1}{\left[1 - \frac{r_c^2}{r_a^2}\right]} . \tag{A2-15}$$

From this equation, we can find

$$\frac{B}{B_o} = \frac{Be}{2m} \frac{1}{\omega_n} \left[1 - \frac{r_c^2}{r_a^2}\right] , \tag{A2-16}$$

or

$$\frac{B}{B_o} = \frac{\omega_L}{\omega_n} \left(1 - \frac{r_c^2}{r_a^2}\right) . \tag{A2-17}$$

Upon setting Eq (A2-17) equal to Eq (A2-14), we find

$$r_n^2 = \frac{\frac{\omega_L}{\omega_n} r_c^2}{\frac{\omega_L}{\omega_n} - 1} . \tag{A2-18}$$

Substitution of the relation for r_n^2 into Eq (A2-9) results in

$$e E_{rf} = m \omega_L \omega_n (r^2 - r_c^2) - m \omega_n^2 r^2 . \qquad \text{(A2-19)}$$

If we assume that all the electrons move in circular synchronous orbits, conservation of energy requires that the potential energy of an electron at radius r be given by

$$e E = e E_{rf} + \frac{1}{2} m \omega_n^2 r^2 . \qquad \text{(A2-20)}$$

The equation for the potential distribution in a non-oscillating magnetron which gives energy to a tangential r-f field is therefore

$$E = \frac{m}{e} \omega_L \omega_n (r^2 - r_c^2) - \frac{1}{2} \frac{m}{e} \omega_n^2 r^2 . \qquad \text{(A2-21)}$$

The potential on the anode E_H obtained by letting $r = r_a$ is commonly known as the Hartree voltage. This voltage is the theoretical starting or threshold voltage for an oscillating magnetron. A sketch of the potential distribution corresponding to the Hartree relation is given in Fig. A1-1 as curve A-O-E_H. The Hartree relation is often written in the more convenient dimensionless form

$$\frac{E_H}{E_o} = 2 \frac{B}{B_o} - 1 . \qquad \text{(A2-22)}$$

A.3. Magnetron Scaling and Magnetron Design

There are at least two avenues of approach in the design of a magnetron. One is to base a new design upon the characteristics of a known operating magnetron through the "scaling rules"; the other is to use the

Hartree relation given by Eq (A2-22), in addition to the equation for electronic efficiency given by

$$\eta_e = 1 - \frac{E_o}{E_a} , \qquad \text{(A3-1)}$$

and imposing the requirements for power output, cathode emission and heat dissipation.[19] The quantity E_o has been defined as the kinetic energy of a synchronous electron at the anode radius. The efficiency relation (A3-1) is therefore the fraction of the d-c energy converted to r-f energy, where E_a represents the d-c energy input.

We shall consider the scaling relations to a limited extent in order to relate the performance of an ideal magnetron with measurable parameters. The scaling relations are based on dimensional analysis applied to Maxwell's equations for the r-f fields and to the equations of motion of the electrons.[9b,8b] There are three equations which are of particular significance in dealing with scaling; these are essentially normalization factors which permit one to design a new magnetron on the basis of a known operable magnetron. These equations are:

$$E_o = \frac{1}{2}\frac{m}{e}\left(\frac{2\pi c}{n\lambda}\right)^2 r_a^2 , \qquad \text{(A3-2)}$$

$$B_o = 2\frac{m}{e}\left(\frac{2\pi c}{n\lambda}\right)\frac{1}{\left[1 - \left(\frac{r_c}{r_a}\right)^2\right]} , \qquad \text{(A3-3)}$$

$$I_o = \frac{2\pi\, a_1}{\left[1 - \left(\frac{r_c}{r_a}\right)^2\right]^2 \left[\frac{r_a}{r_c} + 1\right]} \frac{m}{e}\left(\frac{2\pi c}{n\lambda}\right)^3 r_a^2\, \epsilon_o\, L \qquad \text{(A3-4)}$$

Here

$$\epsilon_o = \frac{10^{-9}}{36\pi} \text{ farads/meter}$$

$$c = 3 \times 10^8 \text{ meters/sec.}$$

$a_1 \cong 1$ for ordinary values of r_c/r_a

L = cathode-emitting length (meters).

The equations for E_o and B_o may be considered as relations giving the values of E and B at the point of tangency of the cutoff curve, Eq (A1-15), and the Hartree curve, Eq (A2-22), or may be given a more physical interpretation as follows. E_o is the energy in electron volts for a synchronous electron at the anode radius. B_o is the magnetic field required to produce this synchronous velocity when a potential E_o is applied to the anode of a non-oscillating magnetron. I_o is the current that just begins to flow when the magnetic field is B_o and the anode voltage reaches E_o with zero r-f voltage. If one knows the quantities

$$\frac{E_a}{E_o} , \frac{B}{B_o} , \frac{I}{I_o} , \tag{A3-5}$$

for an operable magnetron, then if a new magnetron is designed so that the ratios given above are equal to those for the prototype, the new magnetron will in general given equivalent performance insofar as the interaction space is concerned. In addition to the agreement between these respective normalized factors one must have a "workable r-f circuit", sufficient cathode emission, and adequate heat dissipation.

Curves for E_o versus anode radius r_a (in centimeters) with $n\lambda$ as a parameter are given in Fig. A3-1. Fig. A3-2 gives B_o as a function of cathode-anode radius ratios and $n\lambda$.

The Hull and Hartree equations when normalized reduce to

$$\frac{E_U}{E_o} = \left(\frac{B}{B_o}\right)^2 , \qquad \text{Hull} \tag{A3-6}$$

and

$$\frac{E_H}{E_o} = \frac{2B}{B_o} - 1 , \qquad \text{Hartree} \tag{A3-7}$$

Experimentally, the maximum current at which pulsed magnetrons stop oscillating is given approximately by

$$\frac{I_{A/2}}{I_o} = \frac{1}{2}\left(\frac{E_U}{E_o}\right)^{3/2} = \frac{1}{2}\left(\frac{B}{B_o}\right)^3 . \tag{A3-8}$$

$I_{A/2}$ is called the one-half Allis current. This value of current is approximately one-third of the Langmuir non-magnetic diode current which is

$$I_L = \epsilon_o L \frac{8\sqrt{2}}{9\beta^2}\sqrt{\frac{e}{m}}\frac{E_a^{3/2}}{r_a} \text{ (amperes)} , \tag{A3-9}$$

where β^2 is a dimensionless function of r_a/r_c.[28]

Normalization of the Langmuir diode current gives

$$\frac{I_L}{I_o} = \frac{a_2}{a_1}\left(\frac{E}{E_o}\right)^{3/2} , \tag{A3-10}$$

where a_2/a_1 is a function of r_a/r_c and has a value of approximately four-thirds for a range of r_a/r_c from 1 to 3.[9a]

Slater[8b] suggests a method for roughly approximating the lines of constant B (on a performance chart), representing magnetron performance in the oscillatory region. These lines correspond to zero current at the

Hartree voltage and to the one-half Allis current at the Hull voltage. The equation for these lines is

$$\frac{E}{E_o} = 2\frac{B}{B_o} - 1 + \frac{2\left[\frac{B}{B_o} - 1\right]^2}{\left(\frac{B}{B_o}\right)^3}\frac{I}{I_o} . \qquad \text{(A3-11)}$$

Fig. A3-3 indicates the respective locations of the curves for some of the important relations presented above as they appear on a magnetron performance chart. Although the foregoing relations are essentially independent of the resonant circuit employed, a resonant circuit is required for the existence of operating curves at constant magnetic field as indicated by the operating line of Fig. A3-3.

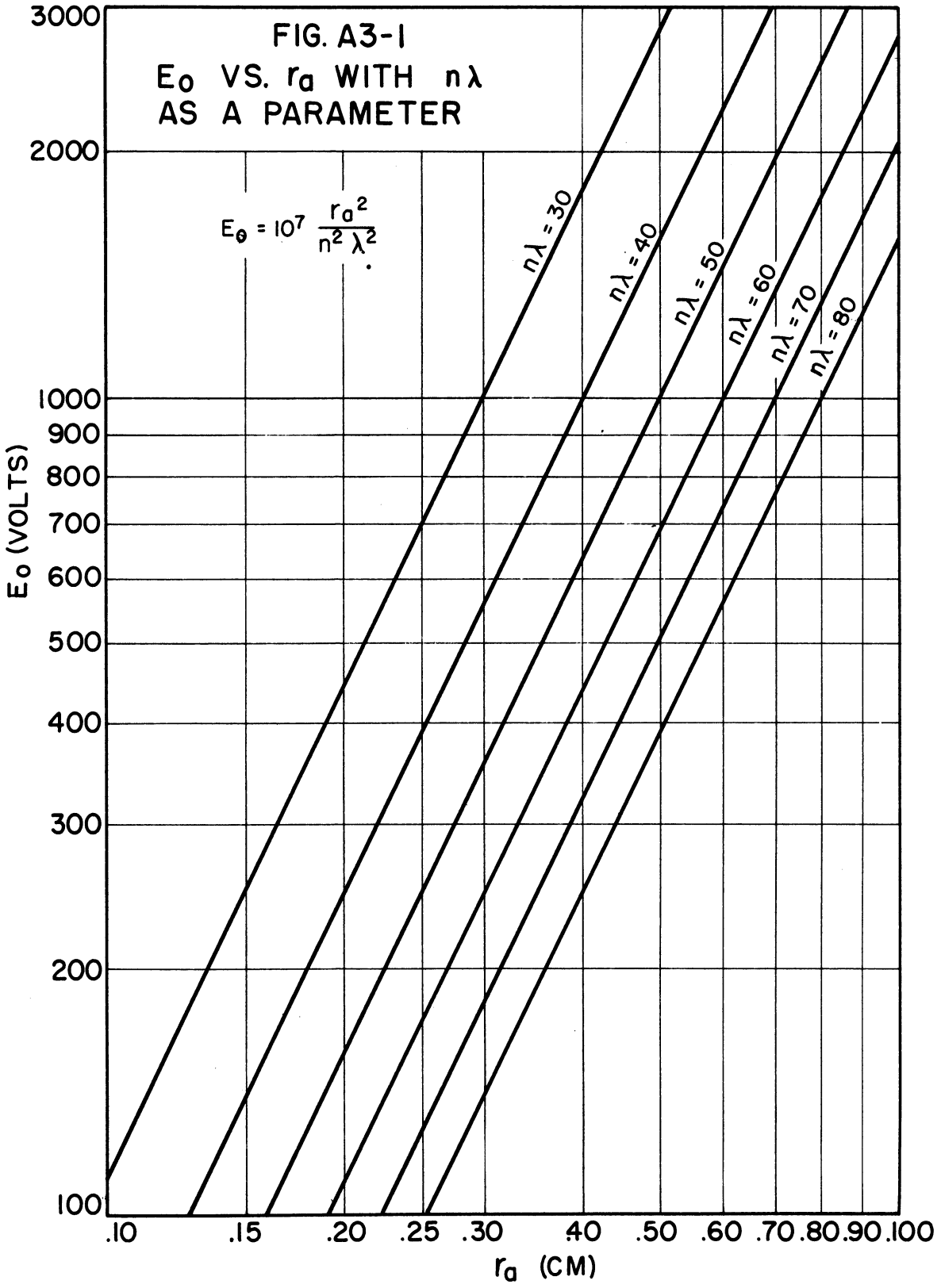
FIG. A3-1
E0 VS. ra WITH nλ
AS A PARAMETER
$E_0 = 10^7 \frac{r_a^2}{n^2 \lambda^2}$
nλ = 30
nλ = 40
nλ = 50
nλ = 60
nλ = 70
nλ = 80
E0 (VOLTS)
3000
2000
1000
900
800
700
600
500
400
300
200
100
.10
.15
.20
.25
.30
.40
.50
.60
.70
.80
.90
.100
ra (CM)

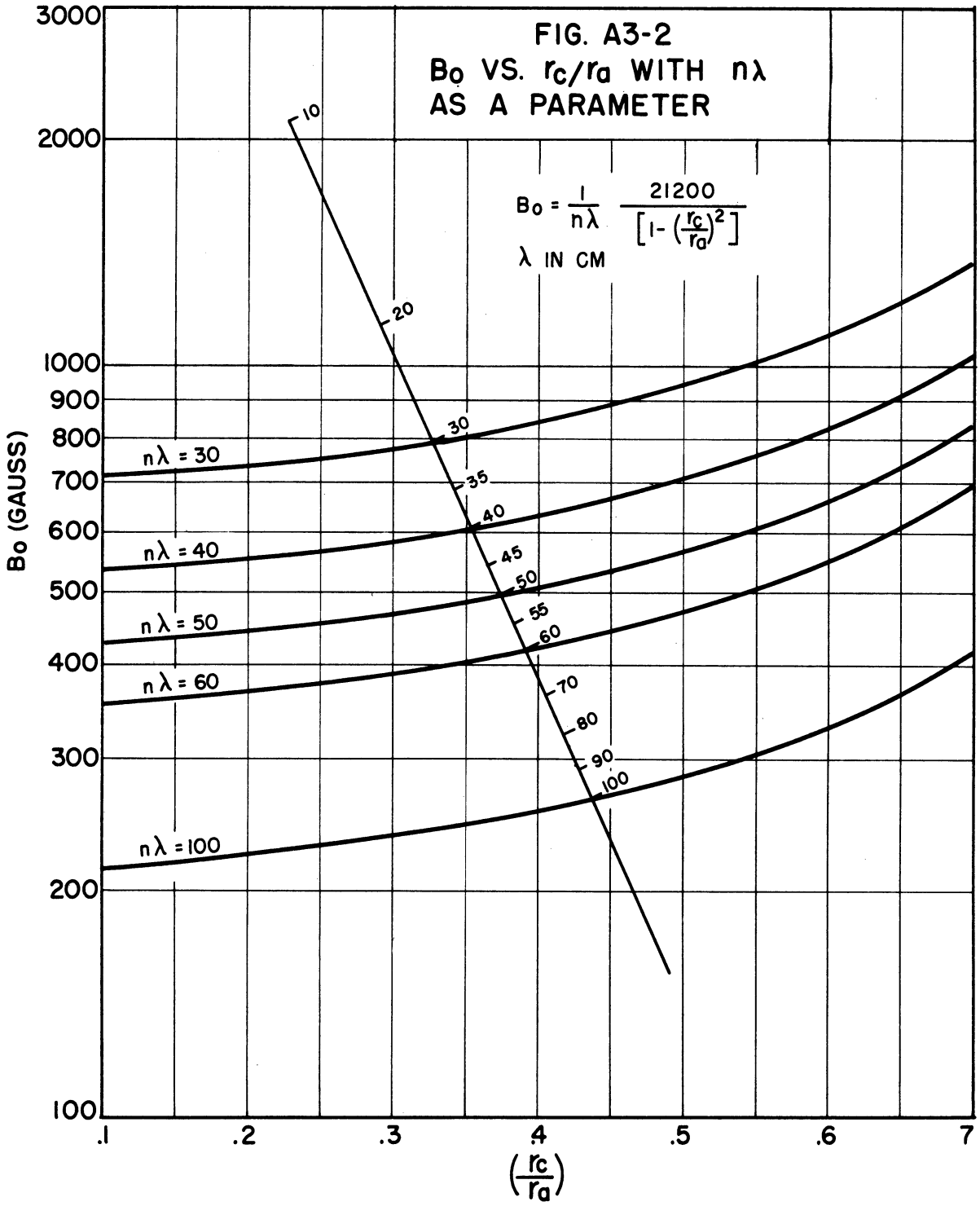
FIG. A3-2
Bo VS. rc/ra WITH nλ
AS A PARAMETER
Bo = 1/nλ · 21200/[1-(rc/ra)²]
λ IN CM
Bo (GAUSS)
3000
2000
1000
900
800
700
600
500
400
300
200
100
nλ = 30
nλ = 40
nλ = 50
nλ = 60
nλ = 100
10
20
30
35
40
45
50
55
60
70
80
90
100
.1
.2
.3
.4
.5
.6
7
(rc/ra)

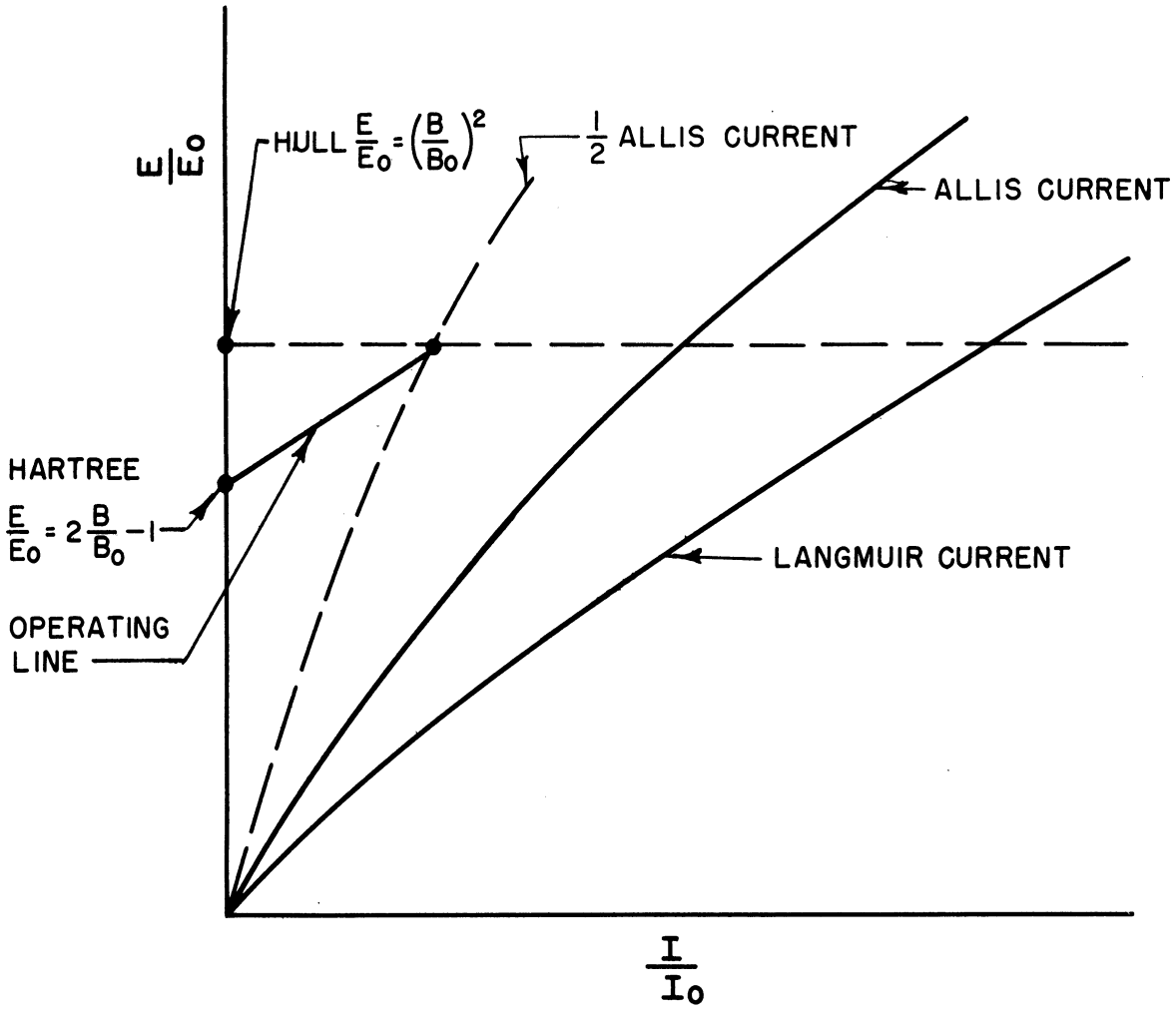

FIG. A3-3
SKETCH SHOWING SOME OF THE IMPORTANT MAGNETRON RELATIONS IN GRAPHICAL DIMENSIONLESS FORM.

APPENDIX B

CALCULATION OF C_A AND L_V

APPENDIX B

CALCULATION OF C_A AND L_V

The use of field maps for calculations of bar-to-vane capacitance and of vane inductance is considered to be justified, since the dimensions of the vanes and bars are small relative to the free-space wavelength.* The error incurred by considering the field distributions in two dimensions rather than in three dimensions is assumed to be greater than any field-mapping inaccuracies. The calculated bar-to-vane capacitance is probably correct to within ten per cent. This is a rough estimate because the answer is obtained on the basis of two-dimensional maps.[29] Calculations of vane inductance are based on the assumption of a uniformly distributed current density over the surface of the vane. This is, of course, only a very rough first approximation, since the edges of the vanes facing longitudinally into the coaxial-line segments are essentially integral parts of the line terminations. The current density in the vanes should therefore be greater at these edges than anywhere else on the surface of the vanes. Although the distribution of current density is not directly available, we can obtain at least an order of magnitude of the inductance by the approach used herein.

The capacitance is obtained from the two-dimensional maps by using the relation:

$$C = \epsilon_o \frac{\text{Number of squares along an equipotential}}{\text{Number of squares along a flux line}}$$

---

* See Reference 9b, pp. 228-231 for a complete discussion.

(Capacitance is then in farads per meter measured perpendicularly into the paper.) The inductance is obtained by using the relation:

$$L = \mu_o \frac{\text{Number of squares along a magnetic equipotential line}}{\text{Number of squares along a magnetic flux line}} .$$

(Inductance is then in henries per meter measured perpendicularly into the paper.

Computations

Vane-to-Bar Capacitance: From the map of Fig. B-1 we have:

$$C_o \cong \epsilon_o \frac{10 \text{ squares}}{4 \text{ squares}} \text{ (farads per meter of map depth into the paper)} .$$

The map depth into the paper is equal to the vane height, which is 0.250 inch or 6.35×10^{-3} meters. Then:

$$C_1 = \epsilon_o \frac{10}{4} \times 6.35 \times 10^{-3} \text{ (farads for one 30-degree section of the full twelve-anode picture)} .$$

We now consider the top and bottom edge capacitance from the map of Fig. B-2.

$$C_{edge_o} = \epsilon_o \frac{8.5}{2} \text{ (farads per meter of vane thickness)} .$$

Taking half the vane thickness as the dimension required in the 30-degree section in the map of Fig. B-1, and considering both the top and bottom edges of the vanes, we get:

$$C_{edge_1} \cong \epsilon_o \frac{8.5}{2} \times 0.83 \times 10^{-3} \text{ (farads per 30-degree section)} .$$

The total capacitance per 30-degree section is:

$$C/\text{section} = C_1 + C_{edge_1} = 0.172 \mu\mu f .$$

Since there are twelve of these 30-degree sections in parallel for the complete system, we obtain;

$$C_A = 12 (C_1 + C_{edge_1}) = 2.06 \mu\mu f .$$

Vane Inductance:* From the map of Fig. B-3, we obtain:

$$L_o \cong \mu_o \frac{4 \text{ squares}}{7.3 \text{ squares}} \text{ henries per meter of map depth (for 1/4 of the vane periphery).}$$

Taking the entire periphery into account, we obtain:

$$L_1 = \frac{L_o}{4} \text{ (henries per meter of vane depth into the paper) .}$$

Since the vane depth into the paper is approximately 0.158 inch or 4.0×10^{-3} meters, the inductance for one vane is

$$L_{v_1} = 4.0 \times 10^{-3} L_1 = 6.87 \times 10^{-10} \text{ henries .}$$

The total inductance for six vanes in parallel is

$$L_V = \frac{L_{v_1}}{6} = 115 \mu\mu\text{henries .}$$

---

* The distance between adjacent vanes has been taken as the average for for the map of Fig. B-3.

FIG. B-1
ONE SECTION OF THE MODEL 9A VANE
AND BAR EXCITING STRUCTURE

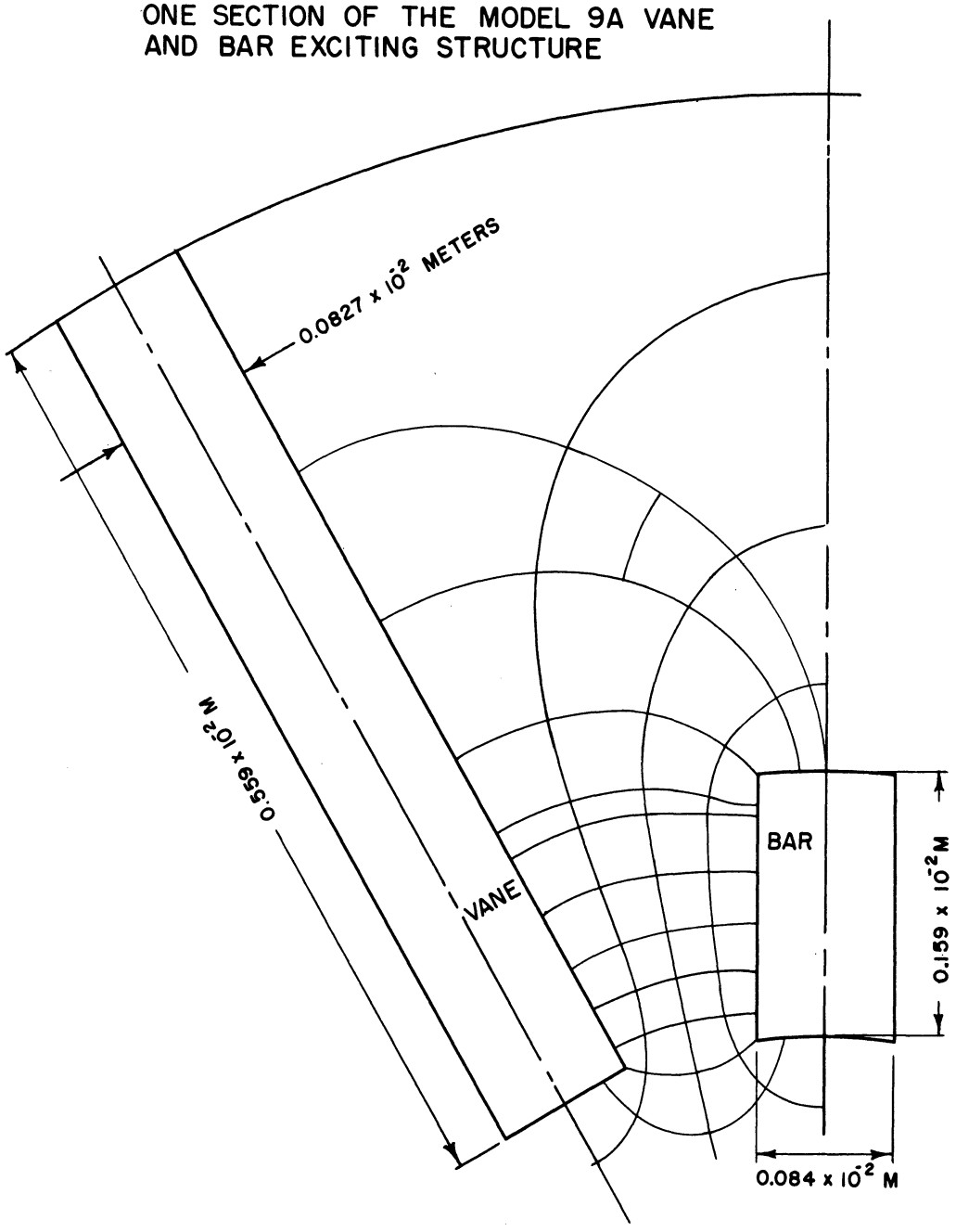

FIG. B-2
FLUX PLOT FOR THE COMPUTATION OF END CAPACITANCE BETWEEN VANES AND BARS

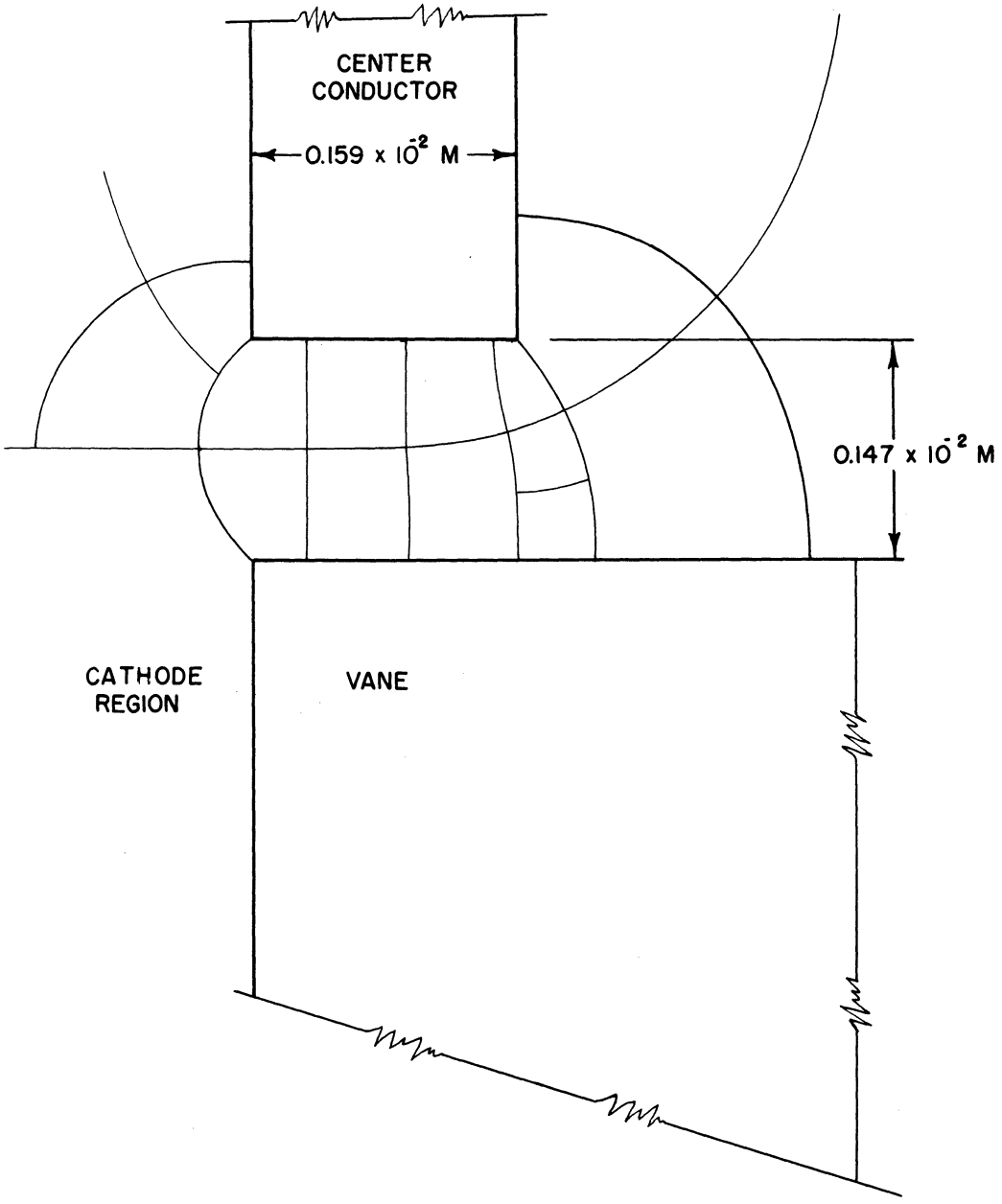

FIG. B-3; FLUX PLOT FOR THE CALCULATION OF VANE INDUCTANCE

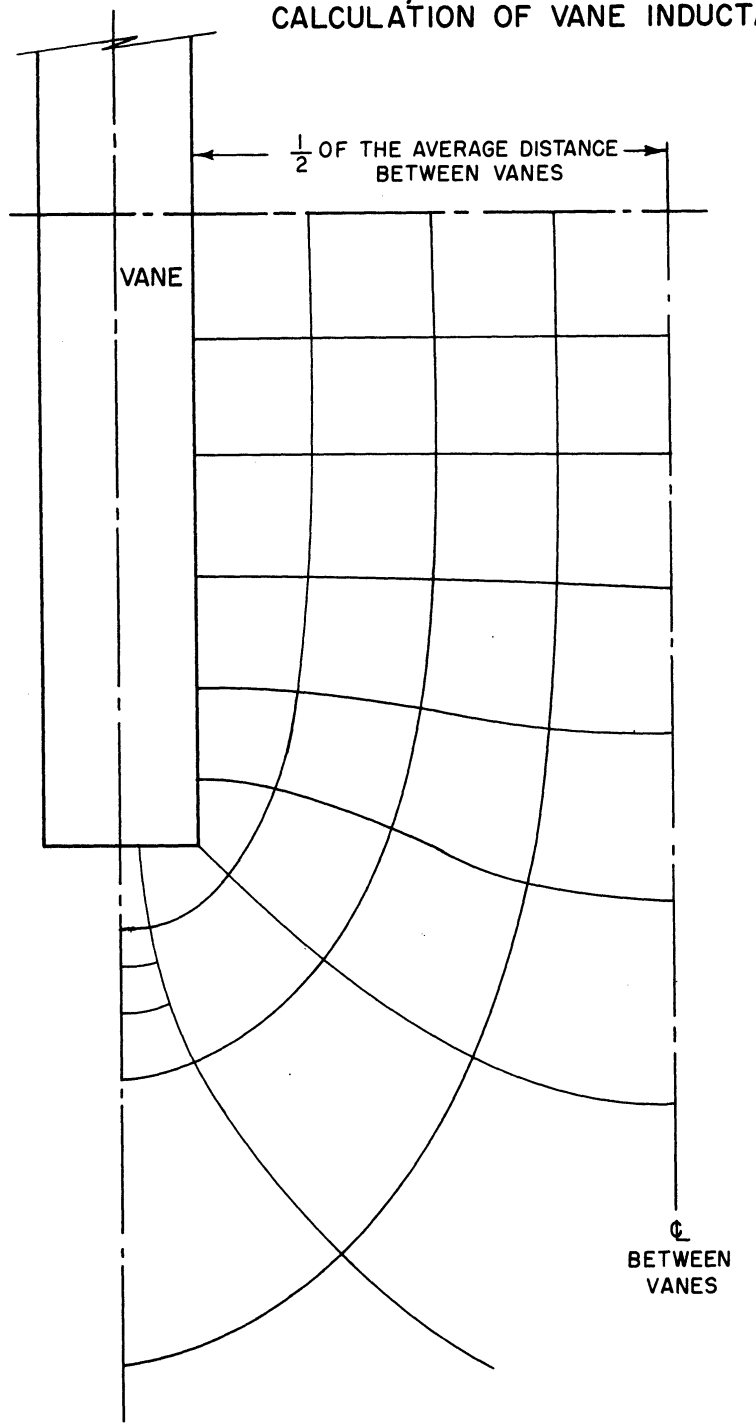

APPENDIX C

MODEL 9B DETAIL DRAWINGS

SYM	CHANGES
A	WAS .381
B	WAS .125
C	WAS .125
D	WAS .242
E	WAS 22½°
	EQUAL SPACING

DWG. NO. A

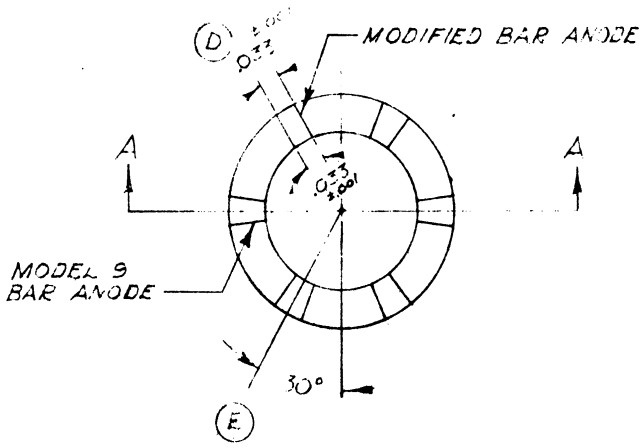

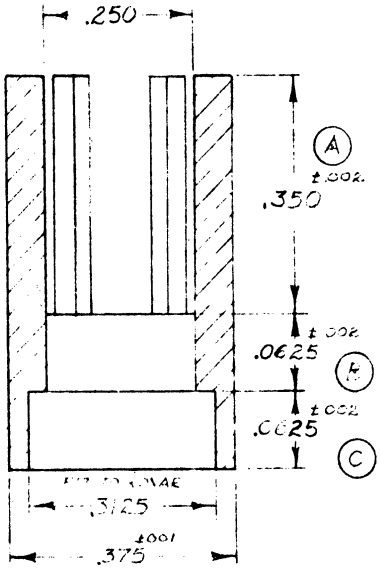

SECTION A A

OFHC COPPER 1 REQ'D

ALL DIMENSIONS UNLESS OTHERWISE SPECIFIED MUST BE HELD TO A TOLERANCE - FRACTIONAL ± 1/64," DECIMAL ± .005," ANGULAR ± ½°

		ENGINEERING RESEARCH INSTITUTE UNIVERSITY OF MICHIGAN ANN ARBOR MICHIGAN	DESIGNED BY J.A. DRAWN BY N.T. CHECKED BY [illegible]	APPROVED BY SCALE 4X DATE 7-25-50
		PROJECT M-762	TITLE ANODE FINGERS (BAR ANODES)	
2	[illegible]	CLASSIFICATION	DWG. NO. A- 5021	
ISSUE	DATE			

SYM	CHANGES
A	WAS .125
B	WAS .250

DWG. NO. A

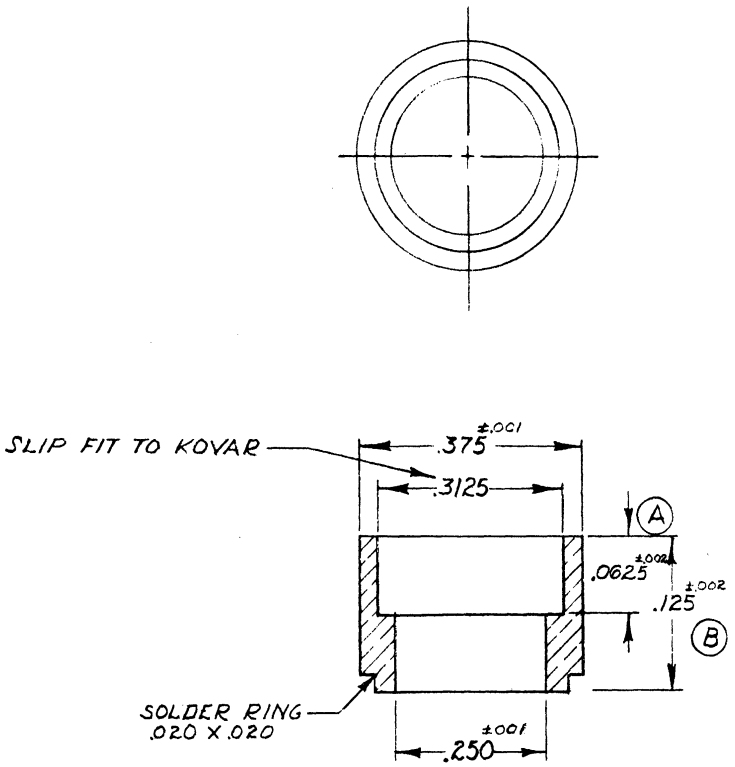

OFHC COPPER 1 REQD

ALL DIMENSIONS UNLESS OTHERWISE SPECIFIED MUST BE HELD TO A TOLERANCE - FRACTIONAL ± 1/64," DECIMAL ± .005," ANGULAR ± ½°

		ENGINEERING RESEARCH INSTITUTE UNIVERSITY OF MICHIGAN ANN ARBOR MICHIGAN	DESIGNED BY JN	APPROVED BY
			DRAWN BY MM	SCALE 4X
			CHECKED BY JRG	DATE 7-26-50
		PROJECT M-762	TITLE ANODE CAP	
2 ISSUE	10-21-50 DATE	CLASSIFICATION	DWG. NO. A- 5022	

SYM	CHANGES
A	WAS .1875

DWG. NO. A

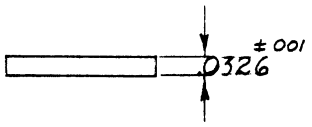

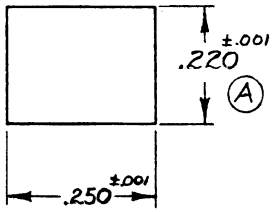

OFHC COPPER 6 REQ'D

ALL DIMENSIONS UNLESS OTHERWISE SPECIFIED MUST BE HELD TO A TOLERANCE - FRACTIONAL ± 1/64," DECIMAL ± .005," ANGULAR ± ½°

		ENGINEERING RESEARCH INSTITUTE UNIVERSITY OF MICHIGAN ANN ARBOR MICHIGAN	DESIGNED BY JN DRAWN BY MM CHECKED BY [illegible]	APPROVED BY SCALE 4X DATE 7-26-50
		PROJECT M-762	TITLE ANODE VANE	
2 ISSUE	10-21-50 DATE	CLASSIFICATION	DWG. NO. A-5023	

DWG. NO. A

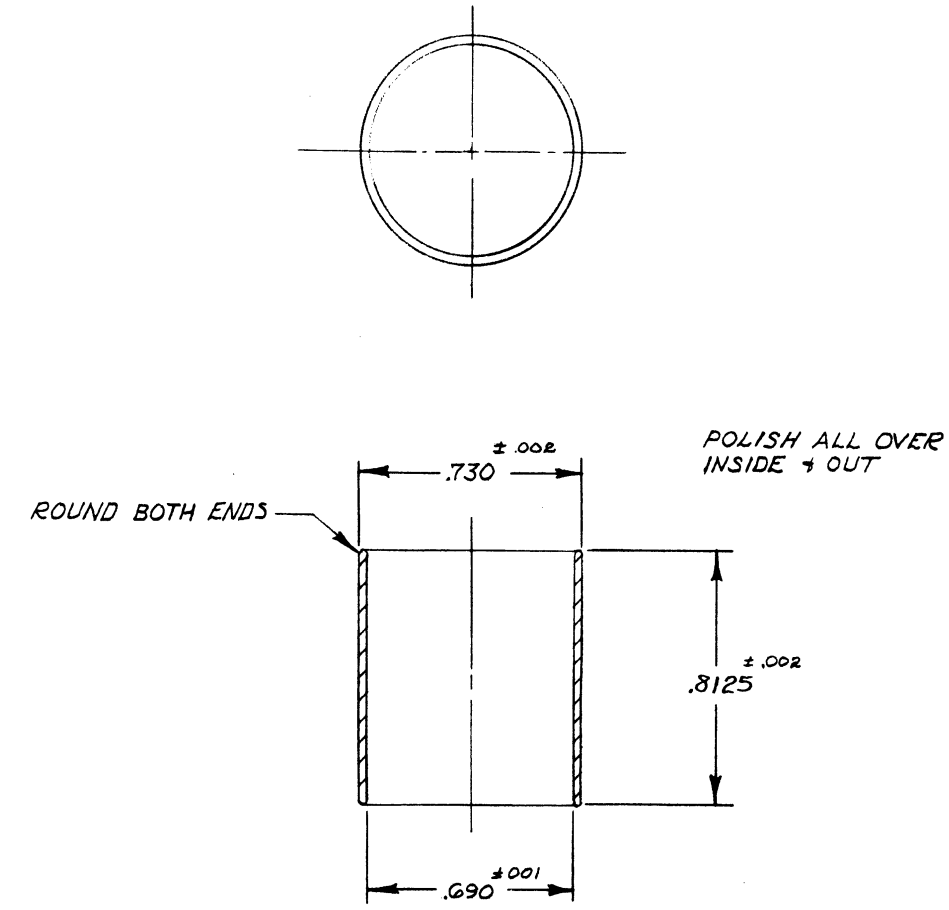

KOVAR 1 REQ'D

ALL DIMENSIONS UNLESS OTHERWISE SPECIFIED MUST BE HELD TO A TOLERANCE - FRACTIONAL ± 1/64," DECIMAL ± .005," ANGULAR ± 1/2°

ISSUE	DATE			
		ENGINEERING RESEARCH INSTITUTE UNIVERSITY OF MICHIGAN ANN ARBOR MICHIGAN	DESIGNED BY JN DRAWN BY JN CHECKED BY DRR	APPROVED BY SCALE 2X DATE 10-17-50
		PROJECT M-762	TITLE OUTER ANODE RING MODEL 9A + 9B	
		CLASSIFICATION	DWG. NO. A- 5024	

DWG. NO. A

6 VANES EQUALLY SPACED IN PLACE AFTER BRAZING

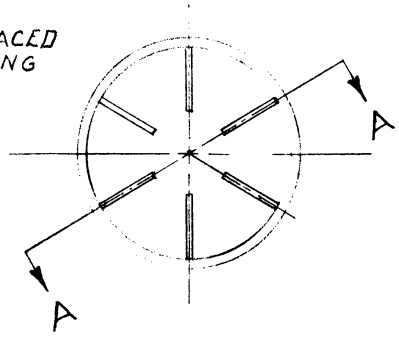

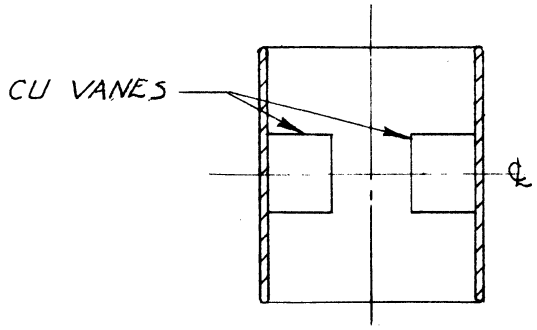

SECTION AA

ALL DIMENSIONS UNLESS OTHERWISE SPECIFIED MUST BE HELD TO A TOLERANCE - FRACTIONAL ± 1/64," DECIMAL ± .005," ANGULAR ± ½°

		ENGINEERING RESEARCH INSTITUTE UNIVERSITY OF MICHIGAN ANN ARBOR MICHIGAN	DESIGNED BY J N	APPROVED BY
			DRAWN BY NN	SCALE 2 X
			CHECKED BY [illegible]	DATE 10-17-50
		PROJECT M-762	TITLE MOD. 9B ANODE ASSEMBLY	
ISSUE	DATE	CLASSIFICATION	DWG. NO. A- 10,009A-1	

SYM	CHANGE
A	WAS 1/4

DWG. NO. A

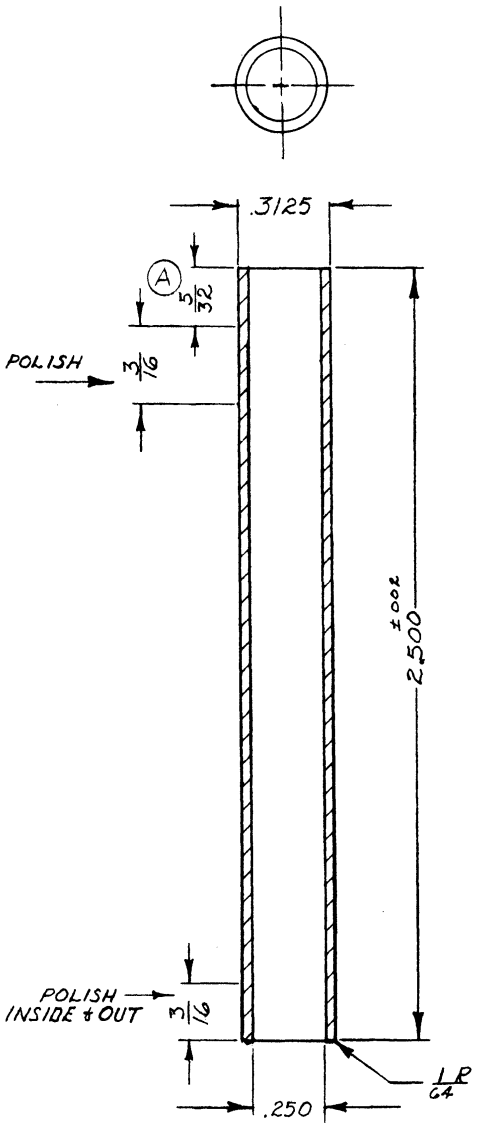

KOVAR TUBING 1 REQD

ALL DIMENSIONS UNLESS OTHERWISE SPECIFIED MUST BE HELD TO A TOLERANCE - FRACTIONAL ± 1/64," DECIMAL ± .005," ANGULAR ± ½°

ISSUE	DATE			
		ENGINEERING RESEARCH INSTITUTE UNIVERSITY OF MICHIGAN ANN ARBOR MICHIGAN	DESIGNED BY JN	APPROVED BY
			DRAWN BY MM	SCALE 2X
			CHECKED BY RTS	DATE 2-12-51
		PROJECT M-762	TITLE KOVAR CYLINDER MODEL 9A & 9B	
		CLASSIFICATION	DWG. NO. A- 9057	

DWG. NO. A

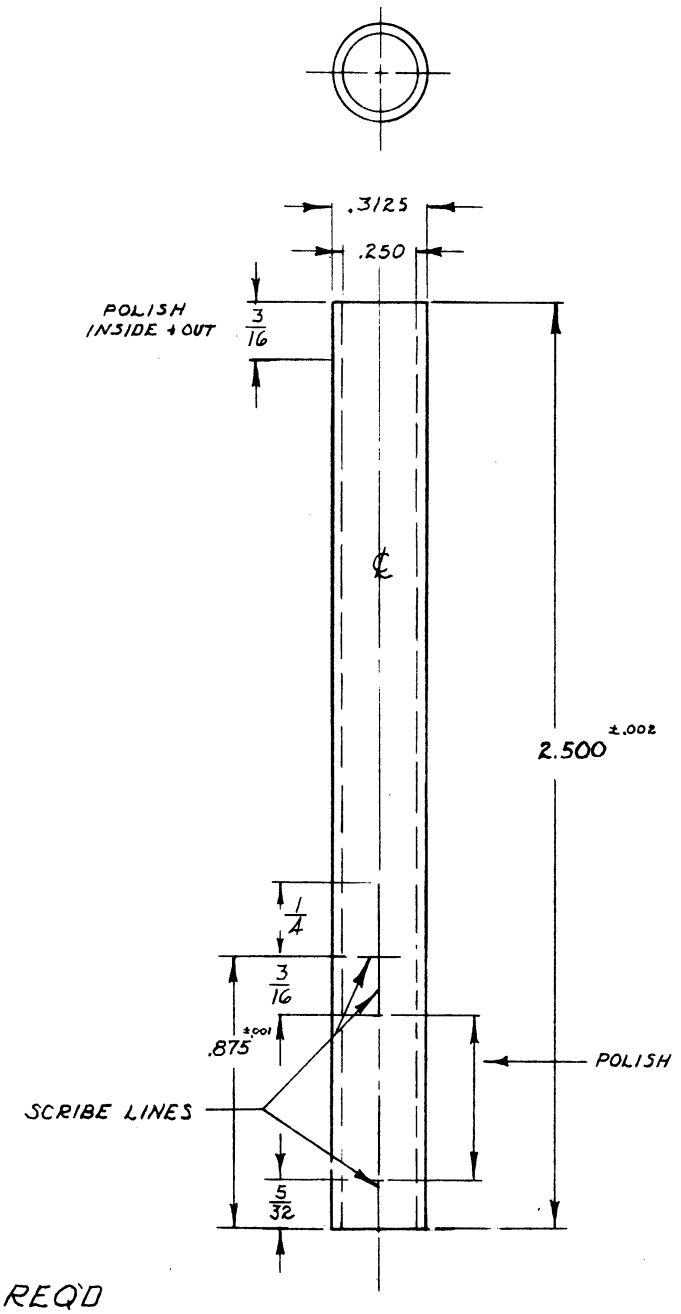

KOVAR 1 REQ'D

ALL DIMENSIONS UNLESS OTHERWISE SPECIFIED MUST BE HELD TO A TOLERANCE - FRACTIONAL ± 1/64," DECIMAL ± .005," ANGULAR ± ½°

ISSUE	DATE	ENGINEERING RESEARCH INSTITUTE UNIVERSITY OF MICHIGAN ANN ARBOR MICHIGAN	DESIGNED BY J N	APPROVED BY
			DRAWN BY M M	SCALE 2X
			CHECKED BY	DATE 11-1-50
		PROJECT M-762	TITLE KOVAR CYLINDER MODEL 9A & 9B	
		CLASSIFICATION	DWG. NO. A- 9062	

SYM	CHANGES

DWG. NO. A

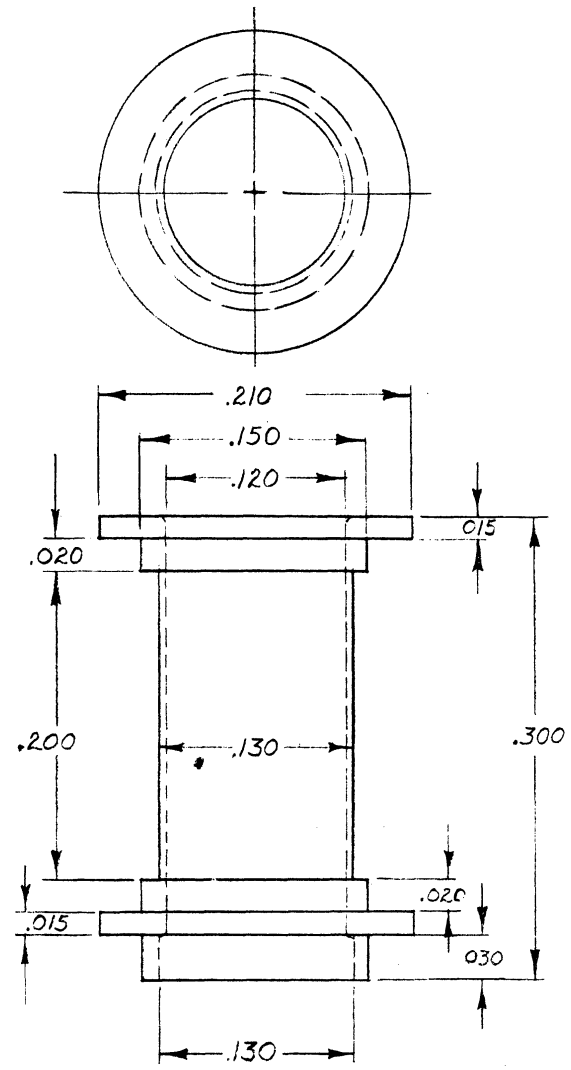

GRADE A NICKEL 1 REQ'D

ALL DIMENSIONS UNLESS OTHERWISE SPECIFIED MUST BE HELD TO A TOLERANCE - FRACTIONAL ± 1/64," DECIMAL ± .005," ANGULAR ± ½°

ISSUE	DATE	ENGINEERING RESEARCH INSTITUTE UNIVERSITY OF MICHIGAN ANN ARBOR MICHIGAN	DESIGNED BY JJO	APPROVED BY
			DRAWN BY [illegible]	SCALE 10 X
			CHECKED BY [illegible]	DATE 8-24-50
		PROJECT M-762	TITLE CATHODE BASE	
		CLASSIFICATION	DWG. NO. A- 8013-1	

DWG. NO. A

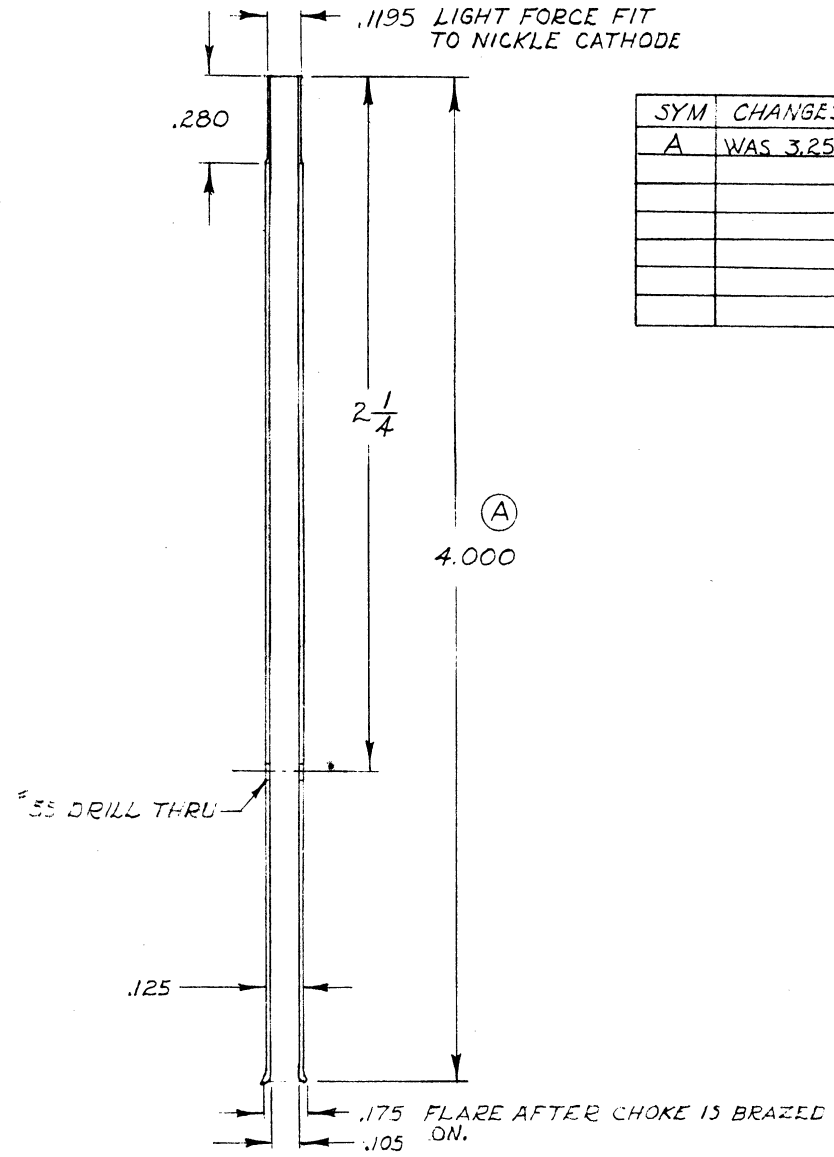

SYM	CHANGES
A	WAS 3.250

KOVAR 1 REQ'D

ALL DIMENSIONS UNLESS OTHERWISE SPECIFIED MUST BE HELD TO A TOLERANCE - FRACTIONAL ± 1/64" DECIMAL ± .005," ANGULAR ± 1/2°

		ENGINEERING RESEARCH INSTITUTE UNIVERSITY OF MICHIGAN ANN ARBOR MICHIGAN	DESIGNED BY J.N.	APPROVED BY
			DRAWN BY M.M.	SCALE 2X
			CHECKED BY [illegible]	DATE 8-23-50
		PROJECT M-762	TITLE CATHODE STEM	
2	10-21-50	CLASSIFICATION	DWG. NO. A-8013-3	
ISSUE	DATE			

SYM	CHANGES

DWG. NO. A

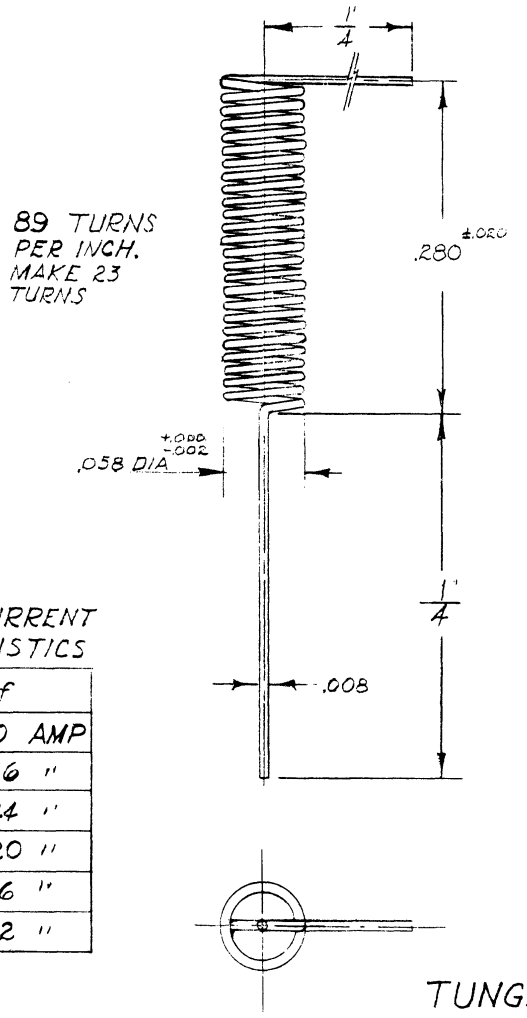

VOLTAGE CURRENT CHARACTERISTICS

Ef	If
1 VOLT	1.00 AMP
2 "	1.46 "
3 "	1.84 "
4 "	2.20 "
5 "	2.46 "
6 "	2.82 "

TUNGSTEN 1 REQD

ALL DIMENSIONS UNLESS OTHERWISE SPECIFIED MUST BE HELD TO A TOLERANCE - FRACTIONAL ± 1/64," DECIMAL ± .005," ANGULAR ± ½°

ISSUE	DATE			
		ENGINEERING RESEARCH INSTITUTE UNIVERSITY OF MICHIGAN ANN ARBOR MICHIGAN	DESIGNED BY TM	APPROVED BY
			DRAWN BY TM	SCALE 10" = 1"
			CHECKED BY [illegible]	DATE 8-21-50
		PROJECT M-762	TITLE CATHODE HEATER	
		CLASSIFICATION	DWG. NO. A- 8013-5	

SYM	CHANGES
A	WAS 3.500

DWG. NO. A

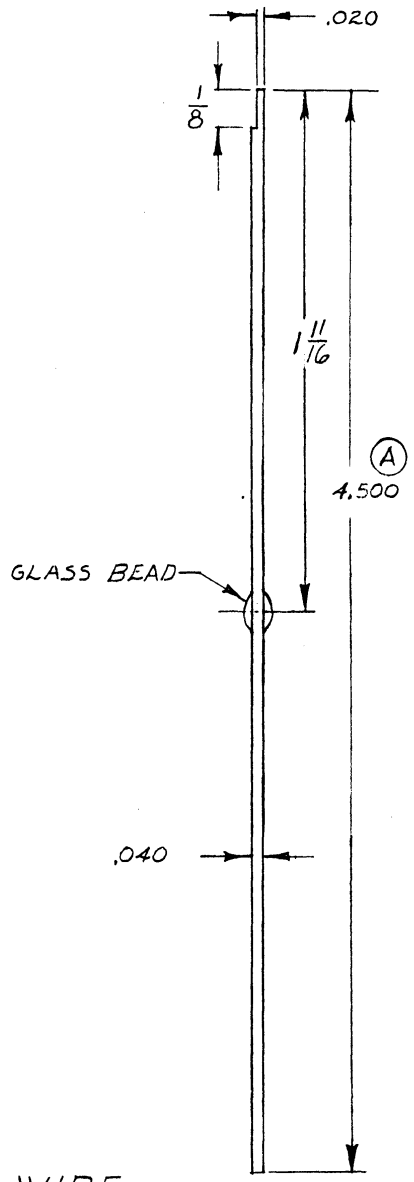

040 KOVAR WIRE

ALL DIMENSIONS UNLESS OTHERWISE SPECIFIED MUST BE HELD TO A TOLERANCE - FRACTIONAL ± 1/64," DECIMAL ± .005," ANGULAR ± 1/2°

		ENGINEERING RESEARCH INSTITUTE UNIVERSITY OF MICHIGAN ANN ARBOR MICHIGAN	DESIGNED BY JN	APPROVED BY
			DRAWN BY NN	SCALE 2X
			CHECKED BY [illegible]	DATE 8-29-50
		PROJECT M-762	TITLE KOVAR LEAD	
2	10-21-50	CLASSIFICATION	DWG. NO. A- 8013-2	
ISSUE	DATE			

APPENDIX D

CATHODE ASSEMBLY AND CATHODE BYPASS DRAWINGS

DWG. NO. A

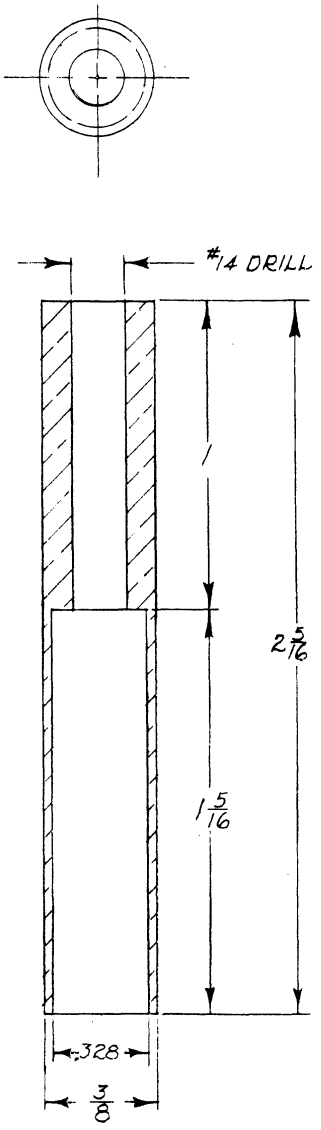

FIG. D-1

BRASS 1 REQ'D

ALL DIMENSIONS UNLESS OTHERWISE SPECIFIED MUST BE HELD TO A TOLERANCE - FRACTIONAL ± 1/64," DECIMAL ± .005," ANGULAR ± ½°

ISSUE	DATE			
		ENGINEERING RESEARCH INSTITUTE UNIVERSITY OF MICHIGAN ANN ARBOR MICHIGAN	DESIGNED BY J.S.N.	APPROVED BY
			DRAWN BY [illegible]	SCALE 2X
			CHECKED BY J.S.N	DATE 3-29-51
		PROJECT M-921	TITLE EXTERNAL BYPASS #2	
		CLASSIFICATION	DWG. NO. A-	

DWG. NO. A

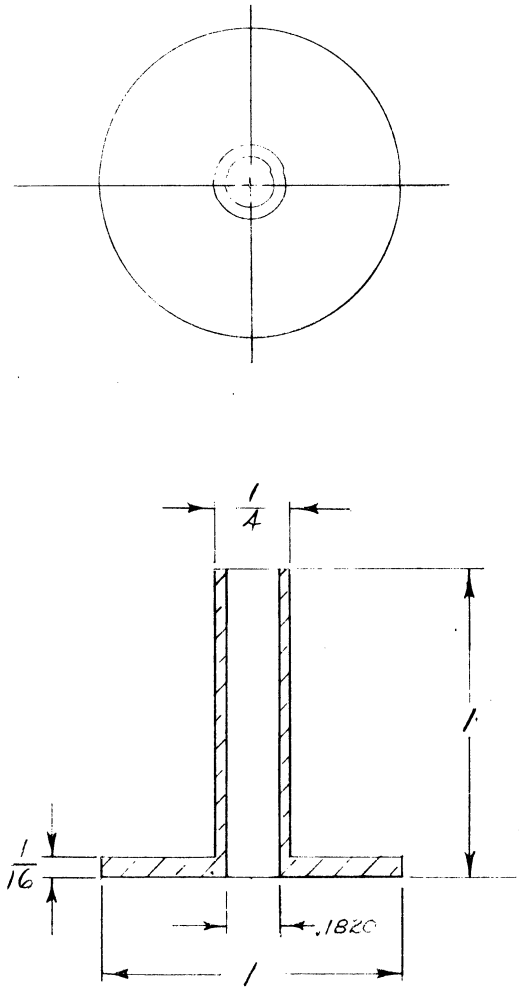

FIG. D-2

BRASS 1 REQ'D

ALL DIMENSIONS UNLESS OTHERWISE SPECIFIED MUST BE HELD TO A TOLERANCE - FRACTIONAL ± 1/64," DECIMAL ± .005," ANGULAR ± ½°

		ENGINEERING RESEARCH INSTITUTE UNIVERSITY OF MICHIGAN ANN ARBOR MICHIGAN	DESIGNED BY J. S. N.	APPROVED BY
			DRAWN BY T. N.	SCALE 2X
			CHECKED BY J. S. N.	DATE 2-2 51
		PROJECT M-921	TITLE EXTERNAL BYPASS #1	
ISSUE	DATE	CLASSIFICATION	DWG. NO. A-	

SYM	CHANGES

DWG. NO. A

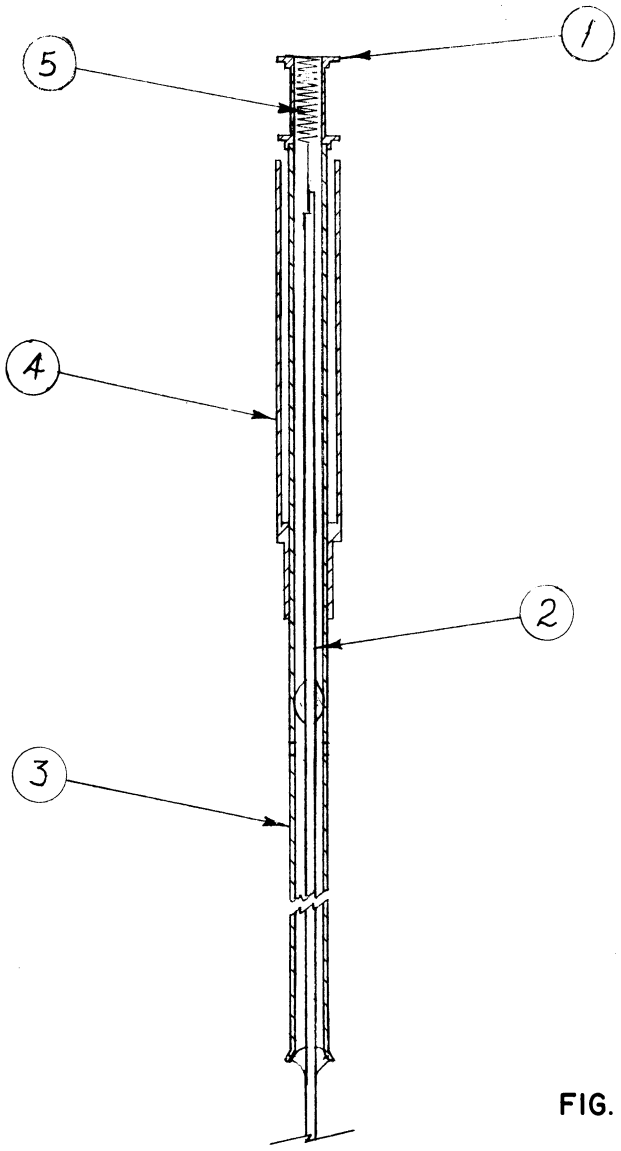

FIG. D-3

ALL DIMENSIONS UNLESS OTHERWISE SPECIFIED MUST BE HELD TO A TOLERANCE - FRACTIONAL ± 1/64," DECIMAL ± .005," ANGULAR ± ½°

ISSUE	DATE			
		ENGINEERING RESEARCH INSTITUTE UNIVERSITY OF MICHIGAN ANN ARBOR MICHIGAN	DESIGNED BY J A	APPROVED BY
			DRAWN BY [illegible]	SCALE 2X
			CHECKED BY [illegible]	DATE 8-28-50
		PROJECT M-762	TITLE OXIDE CATHODE ASSEMBLY, MOD. 9A #39	
		CLASSIFICATION	DWG. NO. A- 8013	

DWG. NO. A

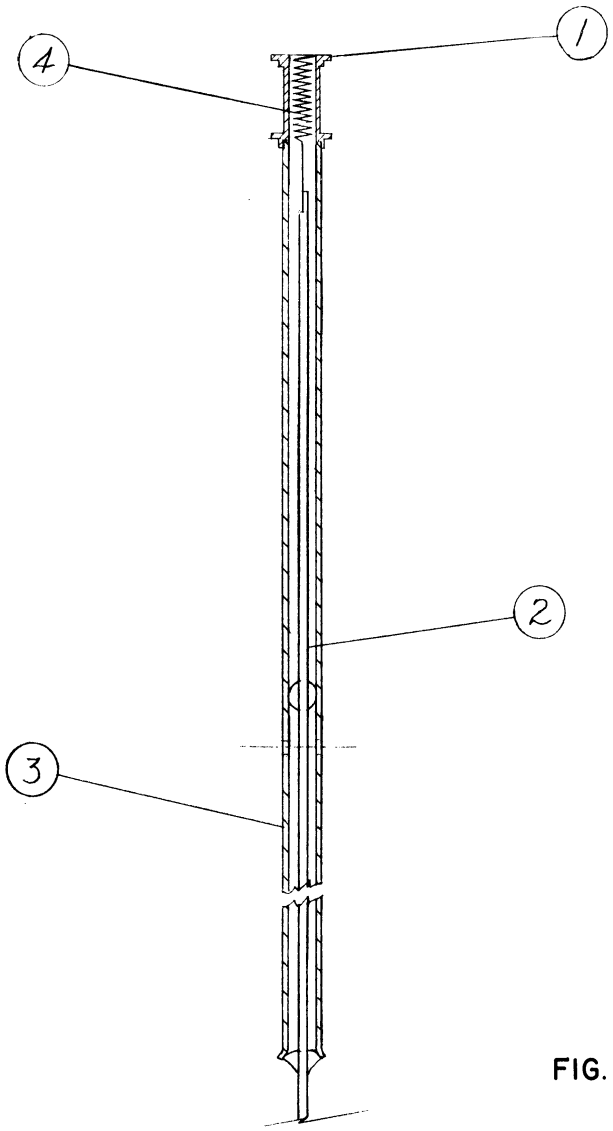

FIG. D-4

ALL DIMENSIONS UNLESS OTHERWISE SPECIFIED MUST BE HELD TO A TOLERANCE - FRACTIONAL ± 1/64," DECIMAL ± .005," ANGULAR ± 1/2°

		ENGINEERING RESEARCH INSTITUTE UNIVERSITY OF MICHIGAN ANN ARBOR MICHIGAN	DESIGNED BY	APPROVED BY
			DRAWN BY NN	SCALE 2X
			CHECKED BY	DATE
		PROJECT M-921	TITLE OXIDE CATHODE ASSEMBLY MODEL 9B #43 & 9C #48	
ISSUE	DATE	CLASSIFICATION	DWG. NO. A- 8022	

DWG. NO. A

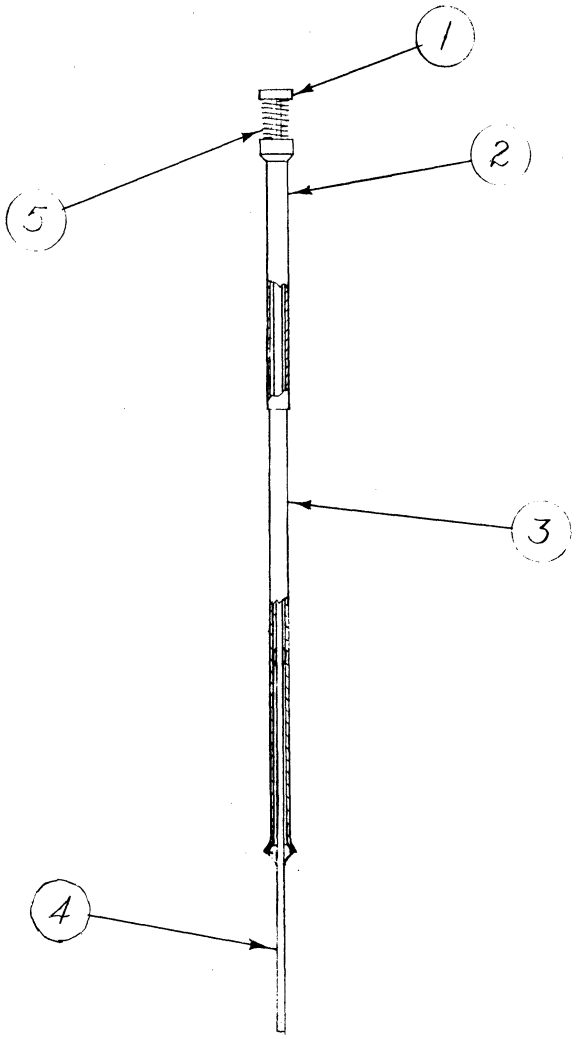

FIG. D-5

ALL DIMENSIONS UNLESS OTHERWISE SPECIFIED MUST BE HELD TO A TOLERANCE - FRACTIONAL ± 1/64," DECIMAL ± .005," ANGULAR ± 1/2°

ISSUE	DATE			
		ENGINEERING RESEARCH INSTITUTE UNIVERSITY OF MICHIGAN ANN ARBOR MICHIGAN	DESIGNED BY JSN	APPROVED BY
			DRAWN BY MM	SCALE FULL
			CHECKED BY	DATE 6-26-51
		PROJECT M-921	TITLE TUNGSTEN CATHODE MODEL 9B #49	
		CLASSIFICATION	DWG. NO. A- 8019	

BIBLIOGRAPHY

1. Hull, A.W., "Effect of a Uniform Magnetic Field on the Motion of Electrons between Coaxial Cylinders," Phys. Rev., Vol. 18, pp. 31-61, July 1921.

2. Habann, E., "The Split Anode Magnetron," Zeit. f. Hochfrequenz, Vol. 24, p. 115 and 135, 1924.

3. Kilgore, G. R., "Magnetron Oscillators for Generation of Frequencies 300-600 mc/s," Proc. I.R.E., Vol. 24, pp. 1140-1158, August 1936.

4. Záček, A., (Czech. paper reviewed in Zeit. f. Hochfrequenz, Vol. 32, p. 172, 1928).

5. Cleeton, C. E., and Williams, N. H., "The Shortest Continuous Radio Waves," Phys. Rev., Vol. 50, p. 1091, December 1936.

6. Posthumus, K., "Oscillations in a Split-Anode Magnetron, Mechanism of Generation," Wireless Engineer, Vol. 12, pp. 126-132, 1935.

7. Herringer, F. and Hülster, F., "The Oscillations of Magnetic Field Waves," Hochf. Tech. u. Elek. akus., Vol. 49, p. 123, 1937.

8. (a) Slater, J. C., Theory of the Magnetron Oscillator, Radiation Laboratory Report No. V5S (118), August 1941.

   (b) Slater, J. C., Theory of Magnetron Operation, Radiation Laboratory Report 43-28 (200), March 8, 1943.

   (c) Rieke, F. F., Analysis of Magnetron Performance, Part I: Equivalent Circuit Method, Applications, Radiation Laboratory Report 52-10 (229), September 16, 1943.

   (d) Platzman, R., Evans, J. E. and Rieke, F. F., Analysis of Magnetron Performance, Part II: Detailed Study of the Operation of a Magnetron, Radiation Laboratory Report No. 451, March 3, 1944.

9. (a) Slater, J. C., Microwave Electronics, Chapter 13: "The Magnetron Oscillator," pp. 302-367, New York, Van Nostrand, 1950.

   (b) Collins, G. B., editor, Microwave Magnetrons, Radiation Laboratory Series, Vol. 6, 1948.

10. O'Neill, G. D., "Separate Cavity Tunable Magnetron," Elect. Ind., Vol. 5, pp. 48-123, June 1946.

11. Bondley, R. J., Pat. No. 2, 450, 628 dated October 5, 1948, filed March 14, 1944.

BIBLIOGRAPHY (Con'd)

12. Needle, J. S. and Hok, G., A New Single-Cavity Resonator for a Multi-Anode Magnetron, Technical Report No. 6, Electron Tube Laboratory, Dept. of Elec. Eng., University of Michigan, Ann Arbor, January 1951.

13. Wilbur, D. A., Nelson, R. B., Peters, P. H., King, A. J., and Koller, L. R., C-W Magnetron Research, Final Report, Contract No. W-36-039 sc 32279, Research Laboratory, General Electric Company, April 1, 1950.

14. Bronwell, A. D. and Bean, R. E., Theory and Applications of Microwaves, New York, McGraw-Hill, 1947.

15. Op. Cit. 9, Slater, J. C., p. 336.

16. Hok, Gunnar, edited by Marton, L., "The Microwave Magnetron," Advances in Electronics, Vol. II, New York, Academic Press, 1950, pp. 219-249.

17. Willshaw, W. E., Rushforth, L., Stainsby, A. G., Latham, R., Balls, A. W., and King, A. H., "The High Power Pulsed Magnetron. Development and Design for Radar Applications," Jour. Inst. Elec. Eng., Pt. III-A, Vol. 93, No. 5, pp. 985-1005, 1946.

18. Doehler, O., "Sur les Propriétés des tubes á champ magnétique constant: IIe partie, Les Oscillations de resonance dans le tube á champ magnétique constant," Annales de Radioélectricité, Vol. 3, pp. 169-183, July, 1948.

19. Welch, H. W., Jr., Ruthberg, S., Batten, H. W., and Peterson, W., Analysis of Dynamic Characteristics of the Magnetron Space Charge—Preliminary Results, Technical Report No. 5, Electron Tube Laboratory, Dept. of Elec. Eng., University of Michigan, January 1951.
See also Ref. 9.

20. Op. Cit. 9b, Chapter 12.

21. Federal Telephone and Radio Corporation, Reference Data for Radio Engineers, 3rd. edition, New York, Knickerbocker Printing Corp., 1949.

22. Spangenberg, K., Vacuum Tubes, New York, McGraw-Hill, 1948.

23. Moore, A. D., Heat Transfer Notes for Electrical Engineering, Ann Arbor, Geo. Wahr, 1942.

24. Harvard University, Radio Research Laboratory Staff, Very High Frequency Techniques, Chapter 21: "Operating Characteristics of C-W Magnetrons," by Gunnar Hok, pp. 502-525, New York, McGraw-Hill, 1946.

25. Slater, J. C., Microwave Transmission, New York, McGraw-Hill, 1942, p. 36.

BIBLIOGRAPHY (Cont'd)

26. Welch, H. W., Jr., et. al., Theoretical Study, Design and Construction of C-W Magnetrons for Frequency Modulation, Quarterly Progress Report No. 2, Electron Tube Laboratory, Dept. of Elec. Eng., University of Michigan, Ann Arbor, June 1951 (A more complete study to appear shortly as Technical Report No. 12 of the University of Michigan Electron Tube Laboratory.)

27. Fisk, J. B., Hagstrum, H. D., and Hartman, P. L., "The Magnetron as a Generator of Centimeter Waves," Bell System Technical Journal, Vol. 25, No. 2, April 1946.

28. Dow, W. G., Fundamentals of Engineering Electronics, New York, John Wiley and Sons, 1937.

29. Attwood, S. S., Electric and Magnetic Fields, 3rd. ed., Chapter 7, New York, Wiley and Sons, 1949.

DISTRIBUTION LIST

22 copies — Director, Evans Signal Laboratory
Belmar, New Jersey
FOR - Chief, Thermionics Branch

12 copies — Chief, Bureau of Ships
Navy Department
Washington 25, D. C.
ATTENTION: Code 930A

12 copies — Director, Air Materiel Command
Wright Field
Dayton, Ohio
ATTENTION: Electron Tube Section

4 copies — Chief, Engineering and Technical Service
Office of the Chief Signal Officer
Washington 25, D. C.

2 copies — H. W. Welch, Jr., Research Physicist
Electron Tube Laboratory
Engineering Research Institute
University of Michigan
Ann Arbor, Michigan

1 copy — Engineering Research Institute File
University of Michigan
Ann Arbor, Michigan

W. E. Quinsey, Assistant to the Director
Engineering Research Institute
University of Michigan
Ann Arbor, Michigan

W. G. Dow, Professor
Department of Electrical Engineering
University of Michigan
Ann Arbor, Michigan

Gunnar Hok, Research Engineer
Engineering Research Institute
University of Michigan
Ann Arbor, Michigan

J. R. Black, Research Engineer
Engineering Research Institute
University of Michigan
Ann Arbor, Michigan

G. R. Brewer, Research Associate
Engineering Research Institute
University of Michigan
Ann Arbor, Michigan

J. S. Needle, Instructor
Department of Electrical Engineering
University of Michigan
Ann Arbor, Michigan

Department of Electrical Engineering
University of Minnesota
Minneapolis, Minnesota
ATTENTION: Professor W. G. Shepherd

Westinghouse Engineering Laboratories
Bloomfield, New Jersey
ATTENTION: Dr. J. H. Findlay

Columbia Radiation Laboratory
Columbia University
Department of Physics
New York 27, New York

Electron Tube Laboratory
Department of Electrical Engineering
University of Illinois
Urbana, Illinois

Department of Electrical Engineering
Stanford University
Stanford, California
ATTENTION: Dr. Karl Spangenberg

National Bureau of Standards Library
Room 203, Northwest Building
Washington 25, D. C.

Radio Corporation of America
RCA Laboratories Division
Princeton, New Jersey
ATTENTION: Mr. J. S. Donal, Jr.

Department of Electrical Engineering
The Pennsylvania State College
State College, Pennsylvania
ATTENTION: Professor A. H. Waynick

Document Office - Room 20B-221
Research Laboratory of Electronics
Massachusetts Institute of Technology
Cambridge 39, Massachusetts
ATTENTION: John H. Hewitt

Department of Electrical Engineering
Yale University
New Haven, Connecticut
ATTENTION: Dr. H. J. Reich

Department of Physics
Cornell University
Ithaca, New York
ATTENTION: Dr. L. P. Smith

Mrs. Marjorie L. Cox, Librarian
G-16, Littauer Center
Harvard University
Cambridge 38, Massachusetts

Mr. R. E. Harrell, Librarian
West Engineering Library
University of Michigan
Ann Arbor, Michigan

Mr. C. L. Cuccia
RCA Laboratories Division
Radio Corporation of America
Princeton, New Jersey

Dr. O. S. Duffendack, Director
Phillips Laboratories, Inc.
Irvington-on-Hudson, New York

Air Force Cambridge Research Laboratories
Library of Radiophysics Directorate
230 Albany Street
Cambridge, Massachusetts

Air Force Cambridge Research Laboratories
Library of Geophysics Directorate
230 Albany Street
Cambridge, Massachusetts
ATTENTION: Dr. E. W. Beth

Raytheon Manufacturing Company
Research Division
Waltham 54, Massachusetts
ATTENTION: W. M. Gottschalk

General Electric Research Laboratory
Schenectady, New York
ATTENTION: Dr. A. W. Hull

Missile and Radar Division
Raytheon Manufacturing Company
Waltham 54, Massachusetts
ATTENTION: Mr. James D. LeVan

Bell Telephone Laboratories
Murray Hill, New Jersey
ATTENTION: S. Millman

Radio Corporation of America
RCA Victor Division
415 South 5th Street
Harrison, New Jersey
Building 55
ATTENTION: Hans K. Jenny

Magnetron Development Laboratory
Power Tube Division
Raytheon Manufacturing Company
Waltham 54, Massachusetts
ATTENTION: Edward C. Dench

Vacuum Tube Department
Federal Telecommunication Laboratories, Inc.
500 Washington Avenue
Nutley 10, New Jersey
ATTENTION: A. K. Wing, Jr.

Microwave Research Laboratory
University of California
Berkeley, California
ATTENTION: Professor L. C. Marshall

General Electric Research Laboratory
Schenectady, New York
ATTENTION: P. H. Peters

Cruft Laboratory
Harvard University
Cambridge, Massachusetts
ATTENTION: Professor E. L. Chaffee

Research Laboratory of Electronics
Massachusetts Institute of Technology
Cambridge, Massachusetts
ATTENTION: Professor S. T. Martin

Collins Radio Company
Cedar Rapids, Iowa
ATTENTION: Robert M. Mitchell

Department of Electrical Engineering
University of Kentucky
Lexington, Kentucky
ATTENTION: Professor H. Alexander Romanowitz

Sperry Gyroscope Company
Library Division
Great Neck, Long Island, New York

2 copies — Mr. John Keto
Director, Aircraft Radiation Laboratory
Air Materiel Command
Wright Field
Dayton, Ohio